Microfiltration Studies Using Low Cost Ceramic Membranes

Thesis submitted in partial fulfillment of the requirements for the degree of

DOCTOR OF PHILOSOPHY

by

Sriharsha Emani

Department of Chemical Engineering

Indian Institute of Technology Guwahati

Guwahati - 781039, India

Microfiltration Studies Using Low Cost Ceramic Membranes

Sriharsha Emani

Microfiltration Studies Using Low Cost Ceramic Membranes

Thesis submitted in partial fulfillment of the requirements for the degree of

DOCTOR OF PHILOSOPHY

by

Sriharsha Emani
Roll No.: 09610726

Department of Chemical Engineering
Indian Institute of Technology Guwahati
Guwahati - 781039, India

July, 2014

Dedicated To

My Family Members

Department of Chemical Engineering
Indian Institute of Technology Guwahati
Guwahati - 781039, India

CERTIFICATE

This is to certify that the thesis entitled **"Microfiltration Studies Using Low Cost Ceramic Membranes"** being submitted by ***Sriharsha Emani*** for the award of PhD degree has been carried out under our guidance and supervision. The work documented in this thesis has not been submitted to any other University or Institute for the award of any degree or diploma.

(Dr. Ramgopal V. S. Uppaluri)
Professor
Department of Chemical Engineering
Indian Institute of Technology Guwahati
Guwahati - 781039, India.

(Dr. Mihir Kumar Purkait)
Associate Professor
Department of Chemical Engineering,
Indian Institute of Technology Guwahati
Guwahati - 781039, India.

Acknowledgements

I would like to express my gratitude to all those who helped me in different ways in completing this research work within the time span of four years and seven months directly or indirectly. First and foremost, I would like to express my deep felt gratitude to my supervisors, **Dr. Ramgopal V. S. Uppaluri** and **Dr. Mihir Kumar Purkait** for providing me continuous inspiration and guidance throughout the entire course of work. I am indebted to him for his useful suggestions and constant encouragement throughout the entire period.

I am grateful to **Dr. Ramgopal V. S. Uppaluri** for his continuous support, interesting discussions and giving me freedom in handling different issues. His uncompromising approach to complete the experimental part, data analysis, writing manuscripts as well as thesis within the stipulated time period helped me a lot in completing my research work. The numerous brain storming sessions during the project meetings with him were very useful in enriching my analytical power.

I would like to express my sincere gratitude to **Dr. Mihir Kumar Purkait** of the Department of Chemical Engineering for his valuable contribution in publishing my research work. I appreciate very much his flexibility and openness in dealing with the specific and general needs of this research work. He helped me in improving the quality of the articles and finding suitable journals for publishing my work. I thank him for his patience and helping nature. It has been a great privilege to work with him.

I must also thank my doctoral committee members **Dr. Amit Kumar, Dr. Tapas Kumar Mandal** of the Department of Chemical Engineering and **Dr. S. C. Mishra** of the Department of Mechanical Engineering, for their valuable suggestions and contribution towards the improvement of my research work.

I also thank all the faculty members of the Department of Chemical Engineering for their kind cooperation during my stay in the department. I am also thankful to all the staff members and scientific officers of the Chemical Engineering Department for their genuine help during my entire research period. I also acknowledge the financial support provided by the **DBT, New Delhi.**

I am thankful to the Central Instruments Facility of IIT Guwahati for allowing me to carry out **FESEM** analysis on my own, which has been very important in this research work. In this regard, I should acknowledge the help of **Mr. K. K. Senapati,** Scientific Officer, Central Instruments Facility, IIT Guwahati. He taught me how to use the FESEM instrument and take images at various critical conditions of the sample. I am also thankful to the **Mr. B. Choudhury** of central workshop, IIT Guwahati for helping me in the fabrication of my experimental setup which was very much essential in my research work.

I was fortunate enough to get excellent batch mates like **Rajesh, Amrita, Murali**, **Chinna Malakondaiah, Bandi Chandrasekhar, Vikranth** and **Pravallika** for their friendly support and timely assistance whenever needed. I am also thankful to **Prashant Thorat, Chola Bhargava, Saketh, Gajanand** and **Mahesh** for their friendly behavior and assistance. Special thanks to **Dr. V. K. Bulasara** for his help and co – operation in th intial stages of my research work.

Last but not the least; I would like to express my deepest sense of gratitude to my parents and family members. Their love, care, sacrifice and encouragement have made it possible for me to come so far. I appreciate the courage, understanding and dedicated support shown by all of them despite many testing times at their end.

Sriharsha Emani
(Email: 828.sriharsha@gmail.com)

Abstract

In the past two decades, significant advances in membrane technology research have been reported. Amongst various membrane applications proposed so far, microfiltration (MF) and ultrafiltration (UF) are the most significant in chemical and biochemical processes. Polymeric and ceramic membrane materials are the most relevant materials used for MF and UF membrane processes. While polymeric membranes are inexpensive and are prone to a greater degree of fouling, ceramic membranes are expensive and possess higher corrosion and mechanical resistance. Therefore, the preparation and characterization of low cost ceramic membranes is always encouraging to further the industrial cost effectiveness of membrane technology. This work presents the preparation, characterization and applications of low cost ceramic membranes suitable for MF and UF applications. Among various industrial applications of membranes, treatment of oily wastewater and MF of mosambi, orange and pine apple juice were chosen as the most important areas of research where low cost ceramic membranes can be used as an alternative to conventional fouling prone polymeric membranes. The entire work carried out in this research work is divided into five major parts:

A) *Dead end microfiltration of oil-water emulsions using low cost ceramic membranes prepared with uniaxial dry compaction method.*

This work addresses the comparative assessment of uniaxial dry compaction and paste methods for the preparation of low cost ceramic membranes. Kaolin based low cost membranes were fabricated using uniaxial dry compaction method. Fabricated membranes were characterized and used for the treatment of synthetic oily waste water solutions. It was observed that in comparison with the paste method, the membranes prepared with uniaxial dry compaction method possessed wider pore size distributions. Amongst several membranes, the membrane PM1 fabricated at a pressure of 25 Mpa provided highest flux of 24×10^{-6} $m^3/m^2.s$ and an oil rejection of 95.2 % but with a fouling index of 29.47 % at a pressure of 206.70 kPa. On the other hand, PM3 membrane provided a lower fouling index of 15.54 % at a pressure of 206.70 kPa with a membrane flux of 8×10^{-6} $m^3/m^2.s$ and a rejection of 97.9 %. For the obtained membrane morphology and chosen feed concentration, combination of pore blocking models provided best fit to represent flux decline data. High rejection values (80 – 90 %) and

good membrane flux (24×10^{-6} $m^3/m^2.s$) of the fabricated membranes was observed towards the treatment of oil water emulsions using low cost ceramic membranes.

B) *Cross flow microfiltration of oil-water emulsions using kaolin based low cost ceramic membranes.*

Emphasizing upon the need to develop and target applications of low cost ceramic membranes, this work addresses the cross flow microfiltration (MF) of oil-water emulsions. Membranes prepared using uniaxial dry compaction method and possessing higher average pore sizes (3.06 – 2.16 µm) and porosities (30.1 – 37.4 %) have been used for cross flow MF studies. Cross flow runs were conducted using a feed oil concentration of 400 mg/L of for various combinations of trans membrane pressure differentials (138 – 207 kPa) and cross flow velocities (Reynolds number = 3417 to 6835). The fitness of various fouling models indicates that combination fouling models could only represent the observed flux decline data which refers to existence of one of the pore blocking phenomena (complete/intermediate/standard pore blocking) during the first 10 minutes of experimental run followed with cake filtration for the data obtained for later time periods. Experimental investigations inferred that the membrane performance is optimal for maximum combinations of trans membrane pressure (ΔP = 207 kPa), fabrication pressure (73 MPa) and minimal cross flow velocity (Re = 3417) at which conditions, an optimal combination of fouling index, steady state flux and rejection were obtained as 11.58 %, 22.14×10^{-6} $m^3/m^2.s$ and 98.52 %, respectively.

C) *Preparation and characterization of low cost ceramic membranes for mosambi juice clarification in batch mode*

This work addresses the preparation and characterization of microfiltration membranes using low cost inorganic precursors for juice clarification. Low cost ceramic membranes have been fabricated using the uniaxial dry compaction method at various fabrication pressures (29, 39 and 49 MPa). The fabrication research has been dovetailed to identify the most critical parameters (such as fabrication pressure and particle size of the precursors) to achieve the desired membrane morphologies. The prepared membranes possessed average pore size (based on FESEM) varying from 1.85 to 0.89 µm, hydraulic pore size varying from 1.69 to 0.72 µm, porosity ranging from 35.4 to 39.4 %, flexural strength ranging from 7.81 to 11 MPa. Amongst several membranes, the MF performance of M3 membrane (fabricated at 49 MPa) for mosambi juice is highly satisfactory. The M3 membrane provided a membrane flux

of 90 to 44 × 10^{-6} m^3/m^2.s at 206.7 kPa with a permeate juice quality of negligible AIS content for the enzyme treated centrifuged juice (ETCJ). Flux decline modelling analysis indicated that enzyme treatment followed by centrifugation minimizes irreversible fouling and is highly recommended before the MF.

D) *Flux decline analysis during microfiltration of pineapple juice using low cost ceramic membranes*

For the first time, this work presents experimental investigations for the microfiltration (MF) of pineapple juice using low cost ceramic membranes fabricated with uniaxial dry compaction method. Two membranes M1 and M3 were used for the microfiltration studies with average pore sizes and porosities of 1.69 µm and 0.72 µm and 35.4 % and 39.4 % respectively. It was observed that the M3 membrane provided excellent performance for enzyme treated centrifuged juice (ETCJ). For ETCJ, the M3 membrane provided an optimal MF flux of 50 × 10^{-6} m^3/m^2.s after 30 min during dead end MF and 53 × 10^{-6} m^3/m^2.s after 20 min during cross flow MF (circulation rate of 1 LPM) at a pressure differential of 207 kPa. During cross flow microfiltration, it was evaluated that higher pressure differentials (207 kPa) and low circulation rate (1 LPM) provided maximum membrane flux. Both M1 and M3 membranes provided lowest fouling indices during cross flow MF using ETCJ but not CJ. Thus both ETCJ and cross flow MF are optimal choice for pineapple juice clarification. Amongst various fouling models, cake filtration provided the best fitness with an RMS error of 9.92 % and 6.32 % for dead end and cross flow MF, respectively.

E) *Cross flow microfiltration studies with mosambi and orange juices*

The cross flow MF study using ETCJ Mosambi and Orange juice feed samples provided significant insights with respect to the effect of membrane and operating parameters on flux and separation factors. Among all membranes, membrane M3 provided lowest fouling index and this signifies that the membrane is less susceptible for internal fouling due to its lower average pore size. For all cases considered, the optimal cases correspond to a u = 1.92 m/s, ΔP = 207 kPa for membrane M3 where a steady state flux of 33.6 × 10^{-6} m^3/m^2.s has been obtained. Similarly for ETCJ orange juice samples, for the membrane M3, the optimal case corresponds to u = 1.92 m/s, ΔP = 207 kPa where the steady state flux of 34.3 × 10^{-6} m^3/m^2.s has been obtained. All membranes provided excellent separation factors with respect to the complete removal of AIS (pectin), minimization of colour and clarity and maximum retention

of TSS, Citric acid, pH, density, viscosity and vitamin C content. In summary, the membranes fabricated provided excellent performance characteristics towards the clarification of mosambi and orange juices. While the comparative performance with respect to dead end clarification is not significantly promising, the lower fouling indices obtained and the impact of operating parameters has been extremely useful to obtain good insights with respect to the microfiltration operation. The obtained results are promising for the large scale microfiltration based clarification of enzyme treated centrifuged citrus fruit juices.

Based on the experimental as well as theoretical findings, it is herewith inferred that the prepared low cost ceramic membrane could be promising for the treatment of o/w emulsions and clarifications of mosambi, orange and pine apple juice.

Contents

Page no.

List of Tables

List of Figures

Abbreviations

AIS	alcohol insoluble solids
CPB	complete pore blocking
CF	cake filtration
CJ	centrifuged juice
ETCJ	enzyme treated centrifuged juice
FI	fouling index (dimension less)
IPB	intermediate pore blocking
MF	Microfiltration
PW_i	correspond to the pure water hydraulic permeability values for cleaned membrane
PW_f	correspond to the pure water hydraulic permeability values for fresh membrane
Re	Reynolds number
RMSE	root mean square error (dimension less)
RMS	root mean square (dimension less)
SPB	standard pore blocking
UF	ultrafiltration

Notations

ΔP	trans membrane pressure diffrential (kPa)
Δt	sampling time (min)
J	permeate flux ($m^3/m^2.s$)
V	volume of permeate (m^3)
A	effective membrane area (m^2)
C	concentration of oil in the feed (mg/L)
C_p	concentration of oil in the permeate (mg/L)
J_o	intial permeate flux ($m^3/m^2.s$)
k_b	complete pore blocking model constant (s^{-1})
J_{juice}	juice flux ($m^3/m^2.s$)
k_c	cake filtration model constant ($s.m^{-2}$)
k_i	intermediate pore blocking model constant (m^{-1})
k_s	standard pore blocking model constant ($m^{-0.5}\ s^{-0.5}$)
R^2	square of correlation coefficient (dimension less)
k_c^{CJ}	cake filtration model constant for centrifuged juice ($s.m^{-2}$)
k_c^{ETCJ}	cake filtration model constant for enzyme treated centrifuged juice ($s.m^{-2}$)
ΔP_{fab}	fabrication membrane pressure (MPa)
Q	volume of permeate (m^3)
R	rejection (dimension less)
R_t	total fouling resistance (m^2/m^3)
R_i	reversible fouling resistance (m^2/m^3)

R_m	hydraulic resistance (m^2/m^3)
R_r	irreversible fouling resistance (m^2/m^3)
R_t^{SS}	steady state total fouling resistance (m^2/m^3)
S	permeable area of membrane (m^2)
u	cross flow velocity (m/s)
W_1	dry weight of the membrane (g)
W_2	wet weight of the membrane (g)

Greek letters

ε	porosity of the membrane (dimension less)
η_w	viscosity of water (mPa S)
$\eta_{permeate}$	viscosity of permeate (mPa S)

Chapter 1:

Introduction and Literature Review

Chapter 2:

Dead end Microfiltration of Oil-Water emulsions Using Low Cost Ceramic Membranes Prepared with Uniaxial Dry Compaction Method

Chapter 3:

Cross flow Microfiltration of Oil-Water emulsions Using Kaolin based Low Cost Ceramic Membranes

Chapter 4:

Preparation and Characterization of Low Cost Ceramic Membranes for Mosambi Juice Clarification in Batch Mode

Chapter 5:

Flux Decline Analysis during Microfiltration of Pineapple Juice Using Low Cost Ceramic Membranes

Chapter 6:

Cross flow Microfiltration Studies with Mosambi and Orange Juices

Chapter 7:

Conclusions and Scope of Future Work

Appendix

List of Publications

References

Chapter 1

Introduction and Literature Review

In this chapter, after a brief orientation towards the basic principles of membrane technology, the state of the art with respect to the preparation, characterization and application of ceramic membranes has been presented. Among various applications, the focus in this work has been towards the treatment of oil/water emulsion and clarification of fruit juices (Pineapple, Mosambi and Orange Juices). Subsequently, the possible scope for further research has been elaborated. Finally, the objectives of the thesis and its organization are summarized.

1.1 Principles of membrane technology [1]

Membranes are selective barriers between two phases and drive the transport of one or more species through pressure/concentration/temperature difference. The system in which the concentration of the species are lean after leaving the membrane process is called as retentate and the stream that has higher concentration of species (in comparision to corresponding feed stream) is called as permeate stream. Membranes can be classified according to their nature as biological and synthetic membranes. While biological membranes are integral part of living beings, synthetic membranes can be extensively manufactured to cater the needs of the society.

Synthetic membranes are further classified into organic and inorganic membranes. Polymeric or liquid membranes are called organic membranes. Ceramic or metal membranes are called inorganic membranes. Based on structural classification, solid synthetic membranes

can be classified as symmetric or asymmetric membranes. Symmetric membranes consists of porous or nonporous selective barrier that are prepared as a single phase. Typically 10 to 200 µm thickness exists for symmetric membranes due to which higher mass transfer resistance exists and hence lower permeation (product) rates are achieved. To overcome this limitation, asymmetric membranes are fabricated. These comprise a top dense layer (0.1 – 0.5 µm) on a porous sub layer (50 – 150 µm). In an asymmetric membrane while the sub layer offers mechanical strength, the top layer performs desired separation.

Membrane processes with pressure difference (ΔP) as driving force are further classified as microfiltration, ultrafiltration, reverse osmosis and nanofiltration processes. Concentration driven membrane processes are classified as dialysis and membrane contactors. Electro dialysis is a classical example of a membrane process driven with potential (electrical) difference. The general membrane process classification is also based on the significant variations in the particle sizes of the solutes that are separated. The membrane pore size is appropriately similar to that of the sizes of the solutes or particles that are separated. Based on the ability to separation, driving forces such as pressure differentials across the membrane could be higher or lower. For instance, in a microfiltration process, the applied pressure is 0.1 – 2 bar which increases to 5 – 20 bar for nanofiltration and 10 – 100 bar for reverse osmosis. From the perspective of the solutes getting separated, microfiltration is capable of separating micro and macro solutes (100 – 10,000 µm). These refer to colloidal materials, bacteria and yeast cells. The operating pressure for the separation of these solutes is lower due to the higher particle size of the solutes. Since the particle sizes are high, the membrane pore size is in the range of 0.1 – 10 µm. Virus, proteins and colloidal silica having a molecular weight of 100000 – 500000 posses an average particle size of 0.01 – 0.1 µm and these separation

problems are addressed with ultrafiltration processes. Aqueous salt, metal ions and sugars have even lower particle size (0.001 – 0.1 µm) and their separation is targeted by nano-filtration, reverse osmosis etc. In summary, membranes with larger pore size can be applied for microfiltration and membranes with moderate pore size for ultrafiltration and membranes with lower pore size for reverse osmosis processes. The early research in membrane

Table 1.1: Important features of polymeric and ceramic membranes.

Polymeric	**Ceramic**
Advantages	
• Wide range of pore sizes. • Hydrophilic and hydrophobic membranes widen applicability. • Low cost. • Easy to fabricate. • Scale up.	• Corrosion resistance. • Wider pH applicability. • Wide temperature applicability. • Longer life span and less fouling. • Higher mechanical strength.
Disadvantages	
• Low solvent resistance. • Low pH and temperature range. • Lower mechanical strength. • Longer lifespan	• Limited pore size (MF and UF range). • Higher cost due to costly materials and process sintering. • Brittle in nature

technology has been extensively devoted the development and application of polymeric membranes. Polymeric membrane possess smaller pore sizes and are hence applicable for gas separation and reverse osmosis applications. On the other hand, porous ceramic membranes have been developed lately in the history of membrane technology.

A brief summary of the advantages and disadvantages are polymeric and ceramic presented in Table 1.1. It can be analyzed that ceramic membranes are restricted to MF and UF processes due to wider pore sizes. On the other hand, polymeric membranes are susceptible for fouling and therefore the development of cross linked polymers with better corrosion resistance is beneficial. Ceramic membranes are expensive and hence, reducing the sintering temperature by utilising low cost ceramic precursors would significantly reduce the cost of the ceramic membranes. This will widen the scope of their applicability. Since ceramic membranes have potential advantages in comparison with polymeric membranes for applications such as microfiltration, this thesis focuses on the state of the art associated to the preparation, characterization and applications of ceramic membranes.

1.2 Fabrication methods for ceramic membranes [2]

There exist two types of ceramic membranes namely symmetric membranes and asymmetric membranes. The symmetric membranes can be used as supports for the fabrication of asymmetric membranes. Distinct procedures are adopted for symmetric and asymmetric membrane fabrication. Among these, symmetric membrane fabrication procedures are presented in the following sub-section. Details with respect to asymmetric membrane fabrication have not been elaborated as it is beyond the scope of this thesis.

1.2.1 Symmetric ceramic membrane support fabrication

Typically, symmetric membrane is fabricated by casting inorganic precursor powder mixture into desired shape and subsequent firing or sintering. Thus, there exists three distinct steps during the fabrication of ceramic membrane namely selection of appropriate raw materials with which desired membrane morphology and porous structure can be achieved, casting the membrane in desired shape such as disc or a tube, sintering involving heat treatment. Research in these steps would facilitate the achievement of ceramic membranes with diverse and promising features such as narrow pore size distribution, high water flux, high mechanical strength etc.,

The structural density of the membrane is a function of the grain size of the raw materials used which is also the case for pore size. Also, while higher structural density provides better mechanical resistance, lower structural density provides higher permeation resistance. Therefore, the desired features of mechanical and hydraulic resistance are achieved by optimizing the composition of the inorganic raw material precursors and their grain sizes. The preparation of the green membrane prior to the sintering can be achieved with paste method. While the paste method is adopted, a binder is added to the raw materials along with the solvent to induce plastic properties to the mixture, which is a desired feature to avoid cohesion of the grains in the structure. Organic additives such as binders, plasticizers, lubricants and deflocculants facilitate the elimination of defects such as cracks during the firing and drying steps. Subsequently, mixing and pugging steps are followed that enable to achieve good dispersion and homogeneity in the desired structure. To achieve a viscous paste, the pugging step involves slow addition of water to the powder mixture. An alternative approach of the paste method is to directly utilize the powder mixture for casting purpose

without using binders. For those scenarios, the powder is grinded and thoroughly mixed in a ball mill and subsequently sieved through a suitable screen. The composition of the raw material mixture and the screen size do affect the grain sizes of the particles and hence membrane morphologies and pore size distributions.

Subsequently, green membrane is achieved from paste/powder using either extrusion or uniaxial pressing methods. The extrusion process involves keeping the paste in vacuum to avoid bubbles and eventually forcing the paste through an endless screw or piston connected to a die to achieve the green membrane in the shape of the die. Various process parameters (such as extrusion speed, geometry of cone and die, viscosity of the paste etc.,) during extrusion significantly affect the quality of membrane fabrication and there exist an optimal combination of these parameters with which a defect free membrane can be fabricated. Single channel and multichannel ceramic membrane tubes can be fabricated using the extrusion process which are famous configurations in ceramic membrane technology research and development.

On the other hand, uni-axial pressing method involves an inexpensive compaction of the powder with a suitable binder in a suitable mold at very high pressure (30 – 50 MPa) in a single (uni-axial) direction. A piston is typically used to carry out the compaction process. Apart from raw material mixture composition, the fabrication pressure is an important parameter to alter the membrane properties such as average pore size and porosity.

The final step in ceramic symmetric membrane fabrication is firing or sintering that enables the removal of water molecules and organic additives and induce phase transitions at high temperatures. Typically, thermogravimetric analysis is conducted to ensure that the desired mass variations have been achieved. At higher sintering temperatures, phase transitions and

grain growth occur which contribute enormously to the structural density of the membrane. On the other hand, pore forming agents in the raw material mixture contribute to the porosity of the membrane structure. To achieve a defect free membrane with good combinations of mechanical strength, permeation flux, narrow pore size distribution, porosity and corrosion resistance, the sintering process optimization involves the optimality of the parameters associated to heating rate, maximum sintering temperature, time of sintering temperature and cooling rate. Also, at times, it might be desired to conduct sintering in a controlled humidity environment to avoid quicker loss of water from the green membrane matrix and avoid defects such as cracks and pinholes.

1.2.2 Asymmetric ceramic membrane fabrication

The asymmetric ceramic membrane fabrication is achieved with realized symmetric membranes as supports and deposition of a top layer (skin layer) on the supports. Typically, dip coating and sol-gel methods are adopted to achieve the desired skin layer. During dip coating, the porous support is withdrawn from a dispersion by adopting either capillary colloidal filtration method or film coating methods. During sol-gel process, asymmetric membrane is fabricated using either colloidal route (that involves aqueous colloidal chemistry) or polymeric route (involving the metal organic precursor chemistry with organic solvents) is followed. Further description of these fabrication methods has not been presented as it is beyond the scope of the thesis.

1.3 Applications of ceramic membranes [1]

Symmetric ceramic membranes have been tested for the following microfiltration applications:

a) Industrial wastewater treatment for various cases such as oily wastewater, paper and pulp effluents, tannery wastewaters etc.

b) Potable water production from various contaminated natural water resources by targeting the elimination of bacteria.

c) Clarification of fruit juices such as pineapple, mosambi and orange juices.

d) Bio separation technologies such as protein recovery, milk concentration and fat separation from milk.

Among above research areas, this thesis addresses the broad areas of the treatment of oil water emulsions and fruit juice clarification as the primary targeted applications for the developed low cost ceramic membranes.

In the next section, a brief summary of the relevant state-of-the-art with respect to following areas of research have been summarized:

a) Dead end microfiltration of oil-water emulsions using ceramic membranes.

b) Cross flow microfiltration of oil-water emulsions using ceramic membranes.

c) Preparation and characterization of low cost ceramic membranes for mosambi juice clarification.

d) Dead-end and cross flow MF of pineapple juice.

e) Cross flow microfiltration of citrus fruit juices (mosambi and orange juices).

1.4 State-of-the-art

1.4.1 Dead end microfiltration of oil-water emulsions using ceramic membranes

1.4.1.1 Membrane formulation and dead end MF data

Using kaolin, pyrophyllite, feldspar, ball clay, quartz and calcium carbonate as inorganic precursors and poly vinyl alcohol (PVA) as binder, Monash *et al*. [3] prepared low cost porous ceramic membranes (membrane composition: kaolin 14.5 %, ball clay 17.6 %, feldspar 5.6 %, quartz 26.6 %, pyrophyllite 14.7 % and calcium carbonate 17.0 % on a dry basis) at a sintering temperature of 950 ^{o}C. The authors also investigated the effect of titanium dioxide on the membrane morphological parameters. Surface characterization of the membranes were carried out using thermogravimetric (TGA), particle size distribution (PSD), X - ray diffraction (XRD), N_2 adsorption - desorption and scanning electron microscopy. Membrane morphological parameters were estimated to vary from 830 – 980 nm for average pore size and 36 – 44 % for the average porosity. Additional solvent permeation studies inferred that the membrane exhibited higher permeability for the non-polar solvents. The membrane supports provided a rejection of 40 % using 100 ppm synthetic bovine serum albumin (BSA) solutions during a microfiltration run. The best membrane has an average pore size and porosity of 980 nm and 44 % respectively. During dead-end microfiltration of oil-water emulsions, with a feed concentration of 200 mg/L, the authors reported a maximum membrane flux of 1620 L/m^2.h at 350 kPa and an average rejection of 99 %.

Mittal *et al*. [4] prepared a defect free low cost hydrophilic ceramic membrane (membrane composition: clay 46.15 %, kaolin 23.08 %, sodium carbonate 3.85 %, sodium meta silicate 1.92 %, boric acid 1.92 % and water 23.08 % on a wet basis). The membranes

were fabricated using paste method. The ceramic membrane possessed an average porosity and pore diameter of 26 % and 1070 nm respectively. Subsequently, the membrane was modified with 10 % cellulose acetate solution using dip coating method. TGA, SEM, XRD analyses were carried out for the polymer-ceramic composite membrane. The composite membrane was estimated to have an average porosity and average pore size of 56 % and 28 nm respectively. Using an oil-water emulsion feed concentration of 200 mg/L, the dead end. Ultrafiltration studies conducted for the treatment of oil-water emulsions, provided a maximum membrane flux and rejection of 177 $L/m^2.h$ and 93 % respectively.

Nandi *et al*. [5, 6] reported novel inorganic precursor formulation to fabricate defect free low cost ceramic membranes (membrane composition: kaolin 29.63 %, quartz 11.11 %, calcium carbonate 18.52 %, sodium carbonate 7.40 %, boric acid 3.71 %, sodium metasilicate 3.71 % and water 25.92 % on a wet basis). The precursor formulation indicated higher content of low cost precursors (such as kaolin of about 40 %) and lower content of expensive precursors (such as quartz of about 15 %). The fabricated membranes using paste method were evaluated to have a strong morphological dependence with the sintering temperature and were evaluated to possess an average pore diameter varying from 550 – 810 nm. The membrane porosity varied from 33 to 42 %. XRD characterization study inferred that the minimum sintering temperature shall be 850 ^oC, which is lower than the sintering temperatures considered in their work (900 – 1000 ^oC). Based on SEM analysis and gas permeation experimentation, it was found that the pore size distributions are in good agreement and 20 – 30 % of the porous structure constituted pore sizes that favour Knudsen flow regime. The flexural strength of the membranes was good (3 – 8 MPa) in addition to their chemical stability (< 8 % weight loss in both acidic and basic media). For the membrane

prepared with an average pore size of 550 nm, using feed concentrations in the range of 40 – 50 mg/L, the authors obtained a membrane permeate flux of 76 L/m^2.h and rejection of 97.3 % after 30 min of experimental run at 165.47 kPa.

Vasanth *et al*. [7] used kaolin, quartz and calcium carbonate raw materials to prepare a low cost ceramic membrane for the dead end microfiltration of oil in water emulsion with a feed concentration of 250 mg/L. The prepared membrane has a porosity of 30 % and an average pore size of 2072 nm. The authors reported a maximum membrane flux of 2268 L/m^2.h at 276 kPa and an average rejection of 85 %.

Vasanth *et al*. [8] also used kaolin, quartz and calcium carbonate raw materials to prepare a low cost ceramic membrane for the oil/water emusion with a feed concentration of 200 mg/L using dead end operation. The prepared membrane has a porosity of 26 % and an average pore size of 1060 nm. The authors reported a maximum membrane flux 2340 L/m^2.h at 69 kPa and an average rejection of 96 %.

A summary of the literature data for low cost ceramic membrane fabrication and dead end MF of oil-water emulsions is presented in Tables 1.2a and 1.2b, respectively. Table 1.2a also consists of membrane fabrication data presented in the literature for applications other than oil-water emulsions. This is for comparison and reference purposes.

1.4.1.2 Literature summary

Membrane technology offers several advantages for industrial processing schemes. These include compactness, lower cost and ability to process streams with very low feed concentrations. Amongst various industrial process schemes, the treatment of oil – water emulsions is an important problem in process industries. Typically, the feed composition

Table 1.2a: A summary of literature data for low cost inorganic membranes.

S. No.	Composition	Sintering temperature (°C)	Process	Average membrane properties		Reference
				Pore size (μm)	Porosity (%)	
1.	Kaolin – 40 %, $CaCO_3$ – 25 %, quartz – 15 %, Na_2CO_3 – 10 %, boric acid – 5 % and sodium metasilicate – 5 %	850 – 1000	Paste method	0.55 – 0.81	42 - 33	[5]
2.	Kaolin – 8g, $CaCO_3$ – 5g, quartz – 3g, Na_2CO_3 – 2g, boric acid – 1g and sodium metasilicate – 1g	900	Paste method	0.55	42	[6]
3.	Kaolin – 10g, Na_2CO_3 – 2g, quartz – 3g, feldspar – 3g, boric acid – 1g and sodium metasilicate – 1g	900	Paste method	0.55	42	[9]
4.	Kaolin – 40 %, $CaCO_3$ – 25 %, quartz – 15 %, Na_2CO_3 – 10 %, boric acid – 5 % and sodium metasilicate – 5 %	900 – 1000	Uni axial dry compaction	2.60 – 4.94	40 - 22	[10]
5.	Kaolin – 50 %, $CaCO_3$ – 25 %, quartz – 25 %	900 – 1000	Uni axial dry compaction	1.30 – 2.77	30 - 22	[7]
6.	Kaolin – 50 %, $CaCO_3$ – 15 – 25 %, quartz – 25 %, TiO_2 – 3 – 10 %	900	Uni axial dry compaction	1.30 – 0.45	30 - 23	[11]
7.	Kaolin – 14.5 %, ball clay – 17.6 %, feldspar – 5.6 %, quartz – 26.6 %, $CaCO_3$ – 11 – 17 %, pyrophyllite – 14.7 %, TiO_2 – 3 - 6 %	950	Uni axial dry compaction	0.98 – 0.83	44 - 36	[3]
8.	Kaolin – 50g, $CaCO_3$ – 25g, quartz – 25g	900	Uni axial dry compaction	1.32	30	[12]

Table 1.2b: A summary of dead end MF data for the treatment of oil-water emulsions using low cost ceramic membranes.

S. No.	Feed concentration (mg/L)	Average membrane properties		Membrane Permeability after 30 min. ($m^3/m^2.s.kPa$)	Pressure differential (kPa)	Rejection (%)	Reference
		Pore size (µm)	Porosity (%)				
1.	125	1.30	30	2.21×10^{-6}	276.4	85	[7]
2.	200	0.98	44	2.31×10^{-7}	345.4	96	[3]
3.	50	0.55	42	3.28×10^{-7}	41.37	97.3	[6]
4.	200	1.06	26	2.34×10^{-6}	69.0	96	[8]

varies from 50 – 1000 mg/L of oil and it is desired to have a product stream with a maximum oil concentration of 10 – 15 mg/L [13]. Compared to other separation techniques, membrane technology is promising to process waste feed streams with low oil concentration and achieve high separation efficiency (90 – 99 %).

In the recent times, research in the fabrication of low cost ceramic membranes is getting significant attention. Low cost ceramic membranes have been fabricated using various types of clays and zeolite minerals [14 – 16]. Nandi *et al.* [6] fabricated disk shaped ceramic membranes (average pore diameter of 0.77 µm, porosity of 42 %) using a mixture of kaolin, quartz, calcium carbonate, sodium carbonate, boric acid and sodium metasilicate by paste method. The permeate flux and rejection was obtained as 15.05×10^{-6} $m^3/m^2.s$ and 98.5 % respectively, at a ΔP of 206.80 kPa and 150 mg/L feed oil concentration. Considering PVA as a binder, Monash *et al.* [3] fabricated low cost ceramic membrane using kaolin, feldspar, quartz, pyrophyllite, ball clay, calcium carbonate and titanium dioxide by adopting uniaxial dry compaction method. The fabricated membrane possessed an average pore diameter of 0.83 µm and a porosity of 36 %. For a feed oil concentration of 200 mg/L, the membrane

provided a permeate flux of 2.50 × 10^{-5} m^3/m^2.s and a rejection of 99 %. Using the same fabrication method, Vasanth *et al.* [7, 8] reported precise inorganic precursor formulations (kaolin, quartz, calcium carbonate, sodium carbonate, boric acid and sodium metasilicate) for the fabrication of ceramic membranes (pore size of 1.30 and 1.06 µm and porosity of 30 and 26 %). Amongst these membranes, the second membrane was studied for the microfiltration of oil water emulsion with a feed oil concentration of 200 mg/L to obtain a permeate flux and oil rejection of 0.65 × 10^{-4} m^3/m^2.s and 96 % respectively at a ΔP of 69 kPa. Abbasi *et al.* [17] used kaolin, clay and α – alumina powder to fabricate mullite (average pore size of 0.578 µm and porosity of 32 %) and mullite - alumina based ceramic membranes and reported a maximum membrane flux and rejection of 244 L/m^2.h and 93.8 % respectively, for the mullite membrane.

1.4.1.3 Possible scope for further research

A critical analysis of the above literatures provides the following observations. Firstly, several compositions have been presented based on trial and error approaches and a comparative assessment of two different methods namely dry compaction method and paste method for an identified precursor formulation has not been addressed. Such studies would be useful to understand the possible variation in the membrane morphology with variation in the type of fabrication method. The paste method involves the usage of water which enables flexibility in the elasticity of the green mould and can contribute significantly towards the alteration in the membrane morphological properties. On the other hand, uniaxial method involves fabrication pressure as an important parameter which can significantly influence the membrane properties and the insitu performance of the membrane for various applications.

Therefore, the comparative assessment between paste and uniaxial dry compaction methods could provide valuable information and serve as a guideline towards scale up related issues. Secondly, it has been reported only by Nandi *et al.* [6] that any standard single pore blocking models may not be able to represent the pertinent flux decline mechanism throughout the entire range of operation and combination pore blocking models need to be deployed to represent the flux decline data [6] during the MF of oil-water emulsions with feed concentrations varying from 50 – 150 mg/L. Hence, it is important to examine whether such observations have further validity and especially when the feed oil concentration is high (around 400 – 500 mg/L) and for membranes fabricated using uniaxial dry compaction method with the same composition. Thirdly, in several works [5, 6, 7, 8, 16], fouling indices have not been reported after conducting microfiltration experiments. In summary, these issues can be considered to widen the scope of research in the field of low cost ceramic membrane farbrication and dead end MF of oil-water emulsions.

1.4.2 Cross flow microfiltration of oil-water emulsions using ceramic membranes

1.4.2.1 Membrane performance

Zhou *et al*. [19] used commercial Al_2O_3 membranes for the microfiltration of oil in water emulsion prepared from 20# engine oil (1 g/L), Tween 80 (0.5 g/L), span 80 (0.5 g/L) oils in distilled water using cross flow operation. The authors reported a maximum membrane flux of 441 L /m^2 h and the trans – membrane pressure was 0.16 MPa and the cross flow velocity was 5 m/s and an average rejection of 97.8 %. The prepared membrane has the porosity of 40 %, and a mean pore diameter of 200 nm.

Using commercial tubular alumina microfiltration membranes (average pore size of 200 nm and average porosity of 40 %), Zhou *et al*. [19] prepared nano-sized zirconia-alumina composite membranes for the separation of engine oil-emulsions. The nano-sized zirconia coating was prepared using in - situ hydrolysis of $ZrCl_4$. Surface characterization studies indicated that the membrane has been developed to have more hydrophilicity by allowing the nano - zirconia deposition.

Abbasi *et al*. [17] used kaolin, clay and α – alumina powder to fabricate mullite and mullite - alumina based ceramic membrane for the cross flow microfiltration of oil in water emulsion with a feed concentration of 250 mg/L. The authors reported a maximum membrane flux of 244 L/m^2h and an average rejection 93.8 % for the mullite membrane. The prepared membrane has the porosity of 32 % and an average pore diameter of 578 nm.

Abadi *et al*. [20] used a tubular commercial ceramic α - alumina membrane for the microfiltration of oil in water using cross flow operation. The authors reported a maximum membrane flux of 290 L/m^2 h at a trans – membrane pressure of 1.25 bar, cross flow velocity of 2.25 m/s and temperature of 32.5 ^oC. The prepared membrane has a porosity of about 33 % and mean pore size of 200 nm.

Abbasi *et al*. [21] used kaolin and clay to fabricate the mullite ceramic membranes for the cross flow microfiltration of oily waste water with a feed concentration of 1000 mg/L. The authors reported a maximum membrane flux of 151 L/m^2 h at 3 bar pressure. The prepared membrane has a porosity of 32 %.

Psoch *et al*. [22] used commercial tubular alumina ceramic membrane for the microfiltration of waste oil using dead end and cross flow operations. The authors reported a

maximum membrane flux of 25 L/m^2 h at 120 – 130 kPa. The prepared membrane has an average pore size of 200 nm.

Colle *et al*. [23] fabricated alumina based tubular ceramic membranes for the microfiltration of soyabean oil in water using cross flow operation. The authors reported a maximum membrane flux of 90 L / m^2 h at 1 bar and an average rejection of 99 %. The prepared membrane has a porosity of 34.7 % and the average diameter of the membrane is 1360 nm.

Table 1.3: Summary of the literature data for the cross MF of oil-water emulsions.

S. No.	Author	Type of membrane	Average membrane properties		C mg/L	T min	Steady state flux × 10^6 ($m^3/m^2.s$)	ΔP (kPa)	Rejection (%)	Cross flow conditions
			Pore size (µm)	Porosity (%)						
1.	Vasanth et al. [11]	Low cost ceramic membrane	1.06	26	100	60	55.4	207	87	Q = 13.9 × 10^{-7} m^3/s
2.	Singh et al. [24]	Polymeric (Commercial)	1.16 µm	-	192	30	3.35	207	97.8	Re = 5769, v = 1.5 m/s
3.	Abbasi et al. [17]	Mullite – ceramic	0.57 µm	32	500	120	27.7	305.1	93.8	v = 1.5 m/s
4.	Abadi et al. [20]	α – alumina (Commercial)	0.2	> 33	92	90	69.4	127.1	95	v = 2.25 m/s .
5.	Colle et al. [23]	Alumina	1.36	34.7	-	-	-	-	99	-
6.	Psoch et al. [22]	Alumina	0.2	-	-	-	-	130	-	-

Vasanth *et al.* [11] fabricated kaolin based low cost ceramic membranes for the microfiltration of oil/water emusion using cross flow operation. The authors reported a maximum membrane flux of 1990 L/m^2 h at and an average rejection of 87 % at 207 kPa. The prepared membrane has a porosity of 26 % and the average diameter of the membrane is 1060 nm.

A summary of the literature data for cross flow microfiltration using ceramic membranes is presented in Table 1.3. The table consist of few experimental data obtained for polymeric membranes as well for comparison and reference purposes.

1.4.2.2 Literature summary

Membrane separation technology has been proven to be highly effective for the processing of feed streams characterized with multiple components and lower concentrations. In comparison with other competing technologies such as adsorption and ion exchange, biodegradation [25], flocculation [26] and sonication [27], both microfiltration and ultrafiltration membrane technologies have been opined to be important technologies for wastewater treatment operations. Compared to these technologies, membrane technology offers several advantages such as compactness, ease of operation and low cost.

Amongst various commercial and research applications of membrane technology, polymeric membranes have been substantially addressed. This is possibly due to their low cost and eases of operation. On the other hand, compared to the polymeric membranes, ceramic membranes provide better combinations of mechanical and chemical stability. Due to this reason, there has been a renewed interest towards the development and application of ceramic membranes for waste water treatment. The separation of oil water emulsions to

produce clarified water streams is a challenging task due to the maximum discharge limit of 20 mg/L oil concentration [28]. Typical feed concentrations of oil-water emulsions vary between 50 – 1000 mg/L. Using a combination of coagulation and flocculation techniques, industrial oily wastewaters above 500 mg/L can be effectively treated. However, the treatment of oily waste water streams with feed concentrations below 500 mg/L is a challenging task and advanced separation technologies such as biodegradation [25], microfiltration [29] and ultrafiltration [30] have been proposed and studied.

For the separation of oil-water emulsions, research and development in the field of membrane technology primarily addresses materials research to achieve microfiltration and ultrafiltration range membranes that provide good combinations of flux and rejection. Further, process engineering studies target upon the identification of optimal combinations of membrane (pore size and porosity) and process parameters (cross flow velocity and pressure diffrential) for a choosen feed and specific application.

Despite being efficient for the treatment of oil water emulsions, membrane technology could not address the wider applicability of ceramic membranes towards waste water treatment. This is possibly due to the high cost of alumina membranes and for about a decade, alternatives to alumina membranes were not targeted. However, recently there has been significant emphasis towards the development of low cost ceramic membranes using clay and modified clay compositions and their subsequent dead end microfiltration performance.

Till date, very few researchers have addressed cross flow microfiltration of oil-water emulsions using ceramic membranes [11, 17, 20, 24]. Vasanth *et al.* [11] studied cross flow MF of oil-water emulsions using three distinct membrane compositions and inferred that a

ceramic membrane fabricated with a simple precursor formulation (kaolin – 50 %, quartz – 25 %, calcium carbonate – 22 % and titanium oxide – 3 %) provided a steady state flux and rejection of 5.54×10^{-5} $m^3/m^2.s$ and 87 % respectively at a pressure differential and cross flow rate of 207 kPa and 13.9×10^{-7} m^3/s respectively. Similarly, for a feed concentration of 192 mg/L, Singh *et al.* [24] studied cross flow MF using commercial polymeric membrane to obtain a steady state flux of 3.35×10^{-6} $m^3/m^2.s$ at a pressure differential and cross flow velocity of 207 kPa and 1.5 m/s respectively. Abbasi *et al.* [17] reported cross flow microfiltration of oil-water emulsions using mullite ceramic membranes and obtained a steady state flux and rejection of of 2.77×10^{-5} $m^3/m^2.s$ and 93.8 % respectively at a cross flow velocity, pressure differential and feed concentration of 1.5 m/s, 305.1 kPa and 500 mg/L. On the other hand, using commercial α – alumina membranes, Abadi *et al.* [20] achieved a steady state flux of 6.94×10^{-5} $m^3/m^2.s$ using a feed of 92 mg/L total suspended solids at a cross flow velocity and transmembrane pressure differential of 2.25 m/s and ΔP = 127.1 kPa respectively.

1.4.2.3 Possible scope for further research

Based on literature summary, it is apparent that while dead end and cross flow studies have been significantly addressed for polymeric membranes, and only few studies targeted dead end MF of oil-water emulsions using alumina and kaolin based ceramic membranes [6, 8, 31]. While dead end MF could indicate upon the ability of the membrane to withstand fouling under most stringent conditions of operation, it does not represent the real time scenario where cross flow MF is adopted. Therefore, research commercialization of low cost ceramic membranes must address cross flow microfiltration performance along with the determination of fouling index. In addition, it can also be observed that there are very few literatures [11,

17] that facilitated an integrated approach of hierarchial low cost membrane development and cross flow microfiltration to systematically identify optimal combinations of membrane fabrication and microfiltration process parameters.

In other words the development and evaluation of low cost ceramic membranes for the cross flow microfiltration of oil-water emulsions has significant scope for further research an would be beneficial to widen the scope and applicability of low cost ceramic membranes for industrial processing schemes.

Table 1.4: Literature data summary for the dead end MF and UF of mosambi juice.

S. No.	Pre treatment	Membrane material	MWCO (kDa)/ pore size (µm)	Flux × 10^6 ($m^3/m^2.s$)	Pressure diffrential (kPa)	Reference
1.	Enzyme treatment + centrifugation	Kaolin	0.285	35	344.74	[9]
	Centrifugation	Kaolin	0.285	16	344.74	[9]
2.	Enzyme treatment + centrifugation	Kaolin	0.86	30	82.7	[32]
	Centrifugation	Kaolin	1.08	14	82.7	[32]
3.	Enzyme treatment + bentonite	Polyamide	50	6.4	414	[33]
4.	-	Cellulose acetate	0.2	1.9	138	[34]
	-	Polyamide	50	3.3	414	[34]

1.4.3 Preparation and characterization of ceramic membranes for the mosambi juice clarification

1.4.3.1 Promising features of membranes

The major application of membrane technology in the fruit juice industry is with respect to the clarification of the juice. The traditional method of clarification of pectin containing juice involves a number of steps. These are centrifugation to remove suspended solids, enzymatic treatment for depectinization, usage of clarifying aids such as chitosan, gelatin bentonite and polyvinyl pyridine. The use of commercial pectic enzymes is common in fruit juice processing. The technological advantages of pectic enzyme have been conveyed in several studies. These are higher membrane juice flux, higher juice yields, facilitation of filtration and greater clarity. The enzymatic hydrolysis of pectin depends on several physicochemical factors of the juice (such as incubation time, temperature, pH and enzyme concentration). The major advantages of membrane technology over traditional methods of clarification are production of clarified juice with retention of organic enzymes by the membranes, reduction in process time, elimination of usages of finer clarification aids/agents as mentioned above and their disposal. Compared to other alternate technologies, membrane technology is estimated to offer a process efficiency/yield of about 95-96 %, which is 90-92 % for the traditional techniques. For fruit juice product obtained from MF clarification, the pectin concentration (Alcohol insoluble solids) should be zero and the TDS should be as high as possible and close to the value obtained for the feed.

1.4.3.2 Membrane performance

Nandi *et al*. [9] used kaolin, quartz, calcium carbonate, sodium carbonate, boric acid and sodium metasilicate to achieve low cost ceramic membrane for the dead end microfiltration of mosambi juice. The prepared membrane has a porosity of 23.6 % and an average pore diameter of 285 nm. The authors reported a maximum membrane flux of 120 L/m^2.h for CJ (centrifuged juice) at 344.74 kPa and a membrane flux of 422 L /m^2.h for ETCJ (enzyme treated centrifuged juice) at 344.74 kPa. The prepared membrane has a porosity of 23.6 % and an average pore diameter of 285 nm.

Nandi *et al*. [32] used kaolin, quartz, calcium carbonate, sodium carbonate, boric acid and sodium metasilicate to obtain a low cost ceramic membrane for the microfiltration of mosambi juice using dead end operation. The authors reported a maximum membrane flux of 333 L /m^2.h for CJ and 669 L/m^2.h for ETCJ at 82.7 kPa. The prepared membrane has a porosity of 42 % and an average pore diameter of 1540 nm.

A summary of the literature data for dead end MF of mosambi juice using various membranes is presented in Table 1.4. The table also summarizes few experimental data obtained for polymeric membranes as well for comparison and reference purposes.

1.4.3.3 Literature summary

Amongst various ongoing research efforts, the development and application of α – alumina/zirconia/titania membranes received significant attention towards juice clarification. Jegatheesan *et al.* [35] reported the promising and optimal performance of zirconia ceramic membranes (average pore size of 0.10 µm and 35 % porosity) for the ultrafiltration of sugarcane juice. Vaillant *et al.* [36] studied Membralox membranes (alumina supported

membrane of average pore size of 0.2 µm) for the crossflow microfiltration of banana, pineapple and blackberry juices. Wang *et al.* [37] reported commercial CARBOSEP (zirconium oxide and titania with an average pore size of 0.14 µm) tubular ceramic membrane for the crossflow microfiltration of West Indian Cherry juice. On the other hand, the development and application of low cost ceramic membranes for juice clarification is gradually gaining attention in the research community. Nandi *et al.* [32] reported a ceramic composition (kaolin 40 %, quartz 15 %, calcium carbonate 25 %, sodium carbonate 10 %, boric acid 5 % and sodium metasilicate 5 %) that enabled them to prepare a membrane with an average pore size of 1.54 µm and porosity of 42 % using the paste method. The membrane provided optimal performance for the clarification of mosambi juice. Primarily, the membranes have been specified as low cost materials due to the usage of inexpensive inorganic precursors and low sintering temperature (850 – 1000 ^{o}C). Vasanth *et al.* [10] reported a ceramic precursor composition (kaolin 40 %, quartz 15 %, calcium carbonate 25 %, sodium carbonate 10 % boric acid, sodium metasilicate 5 % and 2 wt % poly vinyl alcohol) to achieve low cost ceramic membranes using uniaxial dry compaction method. The authors reported that the membrane with an average pore size of 3.45 µm, porosity of 30 % and mechanical strength of 28 MPa is suitable for various separation applications.

Various microfiltration range ceramic membranes have been studied towards the clarification of watermelon [38], hami melon [39], orange [40], mosambi [9], apple [41] and pineapple [42]. Gomes *et al.* [38] reported the MF data using a ceramic membrane possessing an average pore size of 0.1 µm. Zhang *et al.* [39] concluded that the ceramic membrane with an average pore size of 0.2 µm and an operating pressure of 2 bar is optimal for the clarification of hami melon juice. Nandi *et al.* [9, 40] reported kaolin based low cost ceramic

membrane with an average pore size of 0.285 µm for the MF of orange juice. Fukumoto *et al.* [41] reported 0.2 µm range MF ceramic membranes for apple juice clarification. de Carvalho *et al.* [42] carried out pineapple juice clarification using 0.22 µm ceramic membranes.

1.4.3.4 Possible scope for further research

Based on the ongoing research trends, it can be observed that the development of low cost ceramic membranes for juice clarification is an attractive option towards the affirmed commercialization of ceramic membrane technology. In the contemporary scenario, other than Nandi *et al.* [32], there has not been much effort with respect to the development of low cost ceramic membrane formulations that can be experimented for juice clarification. Further, it can be also noted that while Nandi *et al.* [32] adopted paste method, the uniaxial dry compaction method adopted by Vasanth *et al.* [10] is more promising due to its simplicity and ability to achieve defect free membranes. So far, there have not been efforts that addressed the fabrication of low cost ceramic membranes using uniaxial method for juice clarification. In this regard, it can be also analyzed that the membrane morphological parameters (average pore size of 3.45 µm, porosity of 30 %) reported by Vasanth *et al.* [10] are significantly high and hence may not be useful for juice clarification.

Considering the above research limitations and avenues, this work attempts to extend the research towards the identification of optimal fabrication parameters using uni-axial dry compaction method. This work focused on the compositions reported by Vasanth *et al.* [10] along with few procedural modifications (such as screen sizes and fabrication pressures) to achieve desired membrane morphologies for mosambi juice clarification**.**

1.4.4 Ceramic membrane based clarification of pineapple juice

1.4.4.1 Membrane performance

Very few literatures have investigated the ceramic membrane based clarification of pineapple juice. Multichannel monolith alumina tubes with average pore sizes of 100 and 10 nm were used by Jiraratananon *et al.* [43] for the microfiltration and ultrafiltration of dilute pineapple juice (12^{o} Brix) that was prepared from concentrated pineapple juice obtained through flash evaporation process. Resistances in series model was applied by the authors to evaluate upon the flux decline mechanisms. Cross flow microfiltration experiments were carried out with the specified membranes in the pressure differential range of 100 – 300 kPa and cross flow velocities of 1.3 – 3.95 m/s. At a pressure differential and cross flow velocity of 300 kPa and 2 m/s, steady state flux, macromolecular rejection and sugar rejection were evaluated for the MF membrane as 6×10^{-3} $m^3/m^2.h$, 84 – 87 % and 6 % respectively. Corresponding values for UF membrane have been evaluated to be 15.8×10^{-3} $m^3/m^2.h$, 91 % and 10.5 % respectively. For the MF membrane, the internal fouling resistance has been evaluated be about 70 % of the total resistance which was only 20 % for the case of the UF membrane. However, the polarized layer resistance for the UF membrane is about 60 % of the total resistance.

De Barros *et al.* [44] used alumina-titania tubular ceramic membranes with an average pore size of 10 nm for the UF of pineapple juice. Enzyme treated pineapple juice was used as a feed to the cross flow microfiltration system. The optimal operating conditions correspond to 4 bar and 50 ^{o}C at which 93 % soluble solids were recovered in the permeate stream. However, their work did not elaborate upon a systematic study with respect to the cross flow velocity variation. For the membrane, the steady state membrane flux varied from 60 – 125

kg/m^2.h for a variation in operating pressure and temperature from 40 – 50 ^oC and 2 – 6 bar respectively. The flux decline analysis was conducted using standard pore blocking models by the authors. Complete pore blocking model fit well for the flux decline trends obtained with the ceramic membrane.

Gassaye *et al.* [45] conducted pineapple juice cross flow microfiltration studies using zirconium oxide tubular membranes (80 nm average pore size) and alumina membranes (200 nm average pore size). Both enzyme treated and raw pineapple juice samples were used as feed for the experiments. For enzyme treated pineapple juice samples, at a cross flow velocity and ΔP of 4 m/s and 1 bar, the authors obtained a flux of 56.51 m^2/h for the 80 nm pore size membrane and 77.01 m^2/h for alumina membrane (200 nm average pore size).

de Carvalho *et al.* [42] conducted pineapple juice clarification using alumina based ceramic membranes (220 nm average pore size) and dilute pineapple juice (12 ^{o} Brix) prepared from concentrated pineapple juice. For the ceramic membrane at a pressure differential of 15 psi, 52 L/m^2.h was obtained which corresponds to 67.3 % recovery of the total juice fed to the membrane setup. The % recovery of Brix, pH, acidity, glucose, sucrose, total sugars, pectin, turbidity and tannins has been evaluated as 94.16 %, 100 %, 91.6 %, 90.03 %, 91.48 %, 92.42 %, 34.48 %, 1.43 % and 73.25 % respectively. Compared to the polysulfone membrane which was also tested, the ceramic membrane did not provide higher recovery rates. In summary, the ceramic membrane provided best recoveries of soluble solids, sugars and acidity.

Table 1.5: Literature data for the cross flow MF and UF of pineapple juice.

Membrane used & pore size	Geometry used	Cross flow velocity (m/s)	Flux × 10^6 ($m^3/m^2.s$)	Pressure diffrential (kPa)	Reference
Polymeric (0.20 µm)	Hollow fiber	3.4	10.27	71	[46]
Ceramic (0.1 µm)	Tubular	2.0	1.8	300	[43]
Ceramic (0.01 µm)	Tubular	2.0	4.4	300	[43]
Ceramic (0.01 µm)	Tubular	4.17	34.40	405	[44]
Polymeric (100 kDa)	Hollow fiber	1.19	12.80	20	[44]
Polymeric (50 kDa)	Plate and frame	-	4.80	590	[47]
Polymeric (100 kDa)	Plate and frame	-	4.40	590	[47]
Polymeric (30 - 80 kDa)	Tubular	-	9.90	150	[47]
Polymeric (0.10 µm)	Plate and frame	-	8.50	350	[47]
Polymeric (0.45 µm)	Plate and frame	-	5.60	300	[47]
Polymeric (0.30 µm)	Tubular	-	16.0	150	[47]
Ceramic (0.22 µm)	Tubular	-	14.4	105	[42]
Ceramic (50 kDa)	Tubular	-	13.0	390	[42]
Polymeric (50 kDa)	Plate and frame	-	6.9	500	[42]
Ceramic (0.08 µm) (enzyme treatment)	Tubular	4.0	15.7	100	[45]
Ceramic (0.08 µm) (without enzyme treatment)	Tubular	4.0	12.1	100	[45]
Ceramic (0.2 µm) (enzyme treatment)	Tubular	-	21.4	-	[45]
Ceramic (0.20 µm) (enzyme treatment)	Tubular	-	8.80	-	[45]
Polymeric (0.2 µm) (enzyme treatment)	-	-	14.9	-	[45]
	-	-	-	-	[45]

Till date, only few researchers studied pineapple juice clarification using ceramic membranes. Jiraratananon *et al.* [43] studied pineapple juice cross flow ultrafiltration using monolith alumina ceramic tubular membranes at a trans membrane pressure (ΔP) of 100 – 300 kPa and cross flow velocities of 1.3 – 3.95 m/s. The membranes provided a steady state flux of 4.4×10^{-6} $m^3/m^2.s$. The authors evaluated that the rejection of macromolecules and sugars were 84% – 87 % and 6 %, respectively. Laorko *et al.* [46] studied the effect of membrane morphology and operating conditions on the physicochemical properties and flux decline of pineapple juice using polysulfone hollow fibre membranes (0.1 – 0.2 µm). The membrane provided an average flux of 10.27×10^{-6} $m^3/m^2.s$ at a cross flow velocity and ΔP of 3.4 m/s and 71 kPa respectively. For these membranes, all physicochemical properties were evaluated to be consistent for preservation after 5 h of MF operation. Barros *et al.* [44] developed a mathematical model during the cross flow microfiltration of pineapple juice using α – Al_2O_3/ TiO_2 (average pore size of 0.01 µm). The authors obtained a flux of 34.4×10^{-6} $m^3/m^2.s$ at a ΔP of 405 kPa. The membrane provided 100 % recovery for sugars and ascorbic acid. Carvalho *et al.* [47] used α – Al_2O_3 tubular membrane (0.22 µm pore size) and obtained a permeate flux of 14.4×10^{-6} $m^3/m^2.s$ at a ΔP of 104 kPa for a feed prepared using concentrated pineapple juice. The membrane provided 65.5 % removal of pectin and recovered 90.03 % of reducing sugars.

Table 1.5 summarizes the experimental data obtained for both dead end and cross flow microfiltration of pineapple juice using both polymeric and ceramic membranes. The data for polymeric membranes has been also presented for reference and comparison purpose.

1.4.4.2 Literature summary

Among various applications for membrane technology, waste water treatment [48], bacteria separation [49], gas separation [50] and juice clarification [51] are well known. Till date, for these applications, polymeric membranes have been utilized commercially. Membrane technology research attempts to identify optimal precursor compositions (for both ceramic and polymeric membranes) and membrane morphologies to suit liquid phase separation applications. To consolidate the commercial application of membrane technology, typically, two process engineering approaches are targeted. For a specific application, while the first refers to the adaptability of developed membranes, the later refers to materials research for the development of optimal membrane morphologies. Juice clarification using membrane technology had been studied for the past 20 years. Till date, polymeric membranes have been studied with dead end and cross flow modes of operation, for the micro and ultrafiltration of mosambi [34], West Indian cherry [37], passion fruit [52], pineapple [47] and watermelon [38] juices.

Compared to the polymeric membranes, ceramic membranes possess higher fouling resistance and have been recently studied for juice processing applications. Till date several researchers studied the microfiltration and ultrafiltration performance of ceramic membranes for the clarification of juices such as sugarcane [35], mosambi [9, 18, 32], orange juices [40], pineapple [46] and pulpy fruit juices [36]. Despite providing satisfactory MF and UF performance, ceramic membranes are expensive and therefore the development of low cost ceramic membranes will be encouraging to further the commercialization of membrane technology. Thus, the major objective of membrane technology research is to target and achieve low cost membranes with excellent combinations of flux and separation

characteristics. From the perspective of durability, chemical stability and for applications involving complex industrial processing schemes, ceramic membranes perform better than polymeric membranes. From a materials perspective, alumina was extensively studied apart from zirconium and titanium. Due to the pertinent higher cost of the inorganic precursors, the module cost of ceramic membranes is significantly high and research had been initiated for the development of low cost ceramic membranes using alternative inexpensive materials [5].

Kaolin based low cost ceramic membranes were extensively studied for juice clarification such as mosambi [9, 18, 32] and orange juices [40]. On the other hand, pineapple juice clarification received limited attention from the membrane research community. This is possibly due to lower availability of pineapple juice in comparison with other citrus juices. However, pineapple juice concentrates have wider market applicability in tropical countries and hence pineapple juice clarification using membrane technology is an important area of research.

From a cost perspective, kaolin based low cost ceramic membranes were prepared using other inexpensive precursors such as quartz, calcium carbonate, sodium carbonate, boric acid and sodium meta silicate [9, 40]. The retail cost of these membranes is about 130 - 220 $\$/m^2$ [9, 40]. Another striking feature of such low cost ceramic membranes is that the maximum sintering temperature is about 900 – 1100 ^oC which is 200 – 300 ^oC lower than the sintering temperatures adopted for α-alumina membranes. Thus, in comparison with α-alumina membranes, kaolin based ceramic membranes are inexpensive due to lower combinations of materials and sintering costs.

From the literature summary, it can be observed that primarily α – alumina ceramic membranes were used within the pore size of 0.1 – 0.2 μm for the cross flow micro and

ultrafiltration of pineapple juice. In this regard, the recent emphasis on the applicability of kaolin based low cost ceramic membranes for juice clarification is promising towards further reducing cost of ceramic membranes and enhance the applicability of low cost ceramic membranes in the food process industry. It can be also observed that till date both cross flow and dead end microfiltration of pineapple juice was not investigated using low cost ceramic membranes.

1.4.4.3 Possible scope for further research

Based on the existing state of the art, the following critical issues have been identified that can be targeted in this work. Firstly, kaolin based low cost ceramic membranes were not investigated for pineapple juice clarification. Secondly, membranes fabricated with paste method have been studied for the clarification of citrus fruit juices and membranes prepared with dry compaction method also need to be evaluated for juice clarification. Thirdly, existing ceramic membrane technologies report lower membrane flux and better performance can be targeted with low cost ceramic membranes. Fourthly, a comparative assessment of dead end and cross flow microfiltration for the clarification of pineapple juice has not been investigated. Fifthly, the competence of various fouling models to represent the juice MF data has not been addressed. Such an approach could provide significant insights with respect to the reversible and irreversible fouling mechanisms. Finally, the variation of membrane fouling indices with choices of feed and operating conditions for ceramic membranes has not been investigated. Thus, there is a need to address all the above issues and widen the scope of juice processing using low cost ceramic membranes.

1.4.5 Cross flow microfiltration of mosambi and orange juices

1.4.5.1 Membrane performance

Till date there is no data with respect to the cross flow microfiltration of mosambi juice. For orange juice clarification, dead end microfiltration has been carried out by Nandi *et al.* [40] and cross flow microfiltration has been reported by Filho *et al.* [53]. Thus, it is evident that only one research group addressed cross flow microfiltration for orange juice and no research group has conducted for mosambi juice using ceramic membranes.

Filho *et al.* [53] used monotubular ceramic membranes (100, 200, 800 and 1400 nm average pore size) that were arranged in series in a tangential microfiltration setup. The 100 nm and 800 nm pore size membranes provided greater permeate fluxes in comparison with the 200 and 1400 nm membranes. The 100 nm membrane provided permeate sterility with acceptable flux of 37.5 $L/m^2.h$. Overall, the membrane clarified juice did not have better fruit flavour and odour intensity in comparison with the feed juice.

Nandi *et al.* [40] conducted dead end MF of orange juice using 285 nm average pore size kaolin based low cost ceramic membranes prepared with the paste method. After 30 minutes of experimental run, using enzyme treated orange juice and centrifuged orange juice samples respectively, the authors obtained a membrane flux of 34 and 13 $m^3/m^2.s$ at 344.74 kPa. Thus, higher membrane flux was obtained for the case where orange juice was first subjected to enzyme treatment followed with centrifugation. For the enzyme treated juice, negligible AIS content was evaluated for the permeate sample, which was not the case for the centrifuged juice. Among various pore blocking models, cake filtration model fit very well for the measured experimental data. Table 1.6 summarizes the experimental data obtained for orange

Table 1.6: Literature data for the membrane based microfiltration of orange juice.

S. No.	Pre treatment	Membrane material	Pore size (µm)	Geometry	Mode of operation	Cross flow velocity (m/s.)	Flux × 10^6 ($m^3/m^2.s$)	Pressure diffrential (kPa)	Reference
1.	Enzyme + centrifugation	Kaolin	0.285	Circular Disk	Dead end	-	34	344.74	[40]
	Centrifugation	Kaolin	0.285	Circular Disk	Dead end	-	13	344.74	[40]
2.	-	PVDF/PMMA	0.1	-	Cross flow	1.25	13.1	100	[54]
3.	-	Alumina	0.8	Monotubular	Cross flow	6.7	10.3	70	[53]

juice clarification using both dead end and cross flow MF operations. One additional data set has been also presented for polymeric membranes for comparison and reference purpose.

1.4.5.2 Scope for further research

With very limited research for cross flow microfiltration of ceramic membranes and with no literature available for the cross flow microfiltration using low cost ceramic membranes for the clarification of mosambi and orange juice, there is enough scope to conduct research in the field of cross flow microfiltration using mosambi and orange juices.

1.5 Objectives of present study

Based on the state of the art presented in sections 1.5.1 to 1.5.4, the PhD thesis targets the fulfillment of the following major objectives.

1. Dead end microfiltration of oil-water emulsions using low cost ceramic membranes prepared with uniaxial dry compaction method.

2. Cross flow microfiltration of oil-water emulsions using kaolin based low cost ceramic membranes.
3. Preparation and characterization of low cost ceramic membranes for mosambi juice clarification in batch mode.
4. Flux decline analysis during microfiltration of pineapple juice using low cost ceramic membranes.
5. Cross flow microfiltration studies with mosambi and orange juices.

1.6 Organization of the thesis

The PhD thesis is organised in seven chapters.

Chapter 1 addressed the state of the art, possible scope for further research, objectives and organisation of the thesis.

Chapter 2 addresses the comparative assessment of uniaxial dry compaction and paste methods for the preparation of low cost ceramic membranes. Kaolin based low cost membranes were fabricated using uniaxial dry compaction with the identified precursor formulation. Fabricated membranes were characterized and used for the treatment of synthetic oily waste water solutions in batch mode of operation.

Chapter 3 describes the application of the fabricated membrane for the cross flow MF of synthetic o/w emulsions. Subsequent flux decline phenomena along with the identification of suitable membrane fouling mechanism have been presented.

Chapter 4 presents results obtained from the batch MF studies of mosambi juice clarification using the prepared membranes. The effects of membrane morphological parameters on the permeate flux and juice quality was investigated. Subsequent flux decline phenomena along

with the identification of appropriate fouling mechanism have been elaborated. The fabrication research has been dovetailed to identify the most critical parameters (such as fabrication pressure and particle size of the precursors) to achieve the desired membrane morphologies.

Chapter 5 addresses the application of selected fabricated membrane for the clarification of pineapple juice using both batch and cross flow mode. Subsequently, flux decline phenomena along with the identification of suitable membrane fouling mechanism have been presented. Finally, the comparative assessment of the performance of batch and cross flow results has been summarized to identify the suitability of the membranes.

Chapter 6 summarizes results obtained from the cross flow MF studies for the clarification of mosambi and orange juice. Results obtained in cross flow mode are compared and analyzed with that of in batch mode reported in chapter 4.

Chapter 7 presents various conclusions drawn from the research work. It also provides possible directions for future work.

Dead end Microfiltration of Oil-Water emulsions Using Low Cost Ceramic Membranes Prepared with Uniaxial Dry Compaction Method

This chapter discusses the preparation and characterization of low cost ceramic microfiltration membranes for microfiltration application. For an identified inorganic precursive formulation three different fabrication pressures were used at a sintering temperature of 900 ^{o}C to achieve diverse membrane morphologies. Structural and morphological studies of the prepared membranes were carried out to evaluate the general characteristics of the membranes. Chemical stability study of the membrane was also performed to verify the corrosive resistance. The cost analysis of the prepared membranes was carried out to compare the membrane cost with the cost of other similar membranes available in literatures. The prepared membranes were evaluated for the dead end MF of oil-water emulsions.

2.1 Experimental and fouling studies

2.1.1 Ceramic membrane fabrication

Six different ceramic precursors namely kaolin (CDH, India), quartz (Research Lab Fine Chem Industry, India), calcium carbonate (Merck, India), sodium carbonate (Merck, India), boric acid (Merck, India) and sodium metasilicate (CDH, India) have been used without any further purification to fabricate porous ceramic membranes. Amongst these precursors, kaolin provides low plasticity and high refractory properties; quartz contributes to

mechanical and thermal stability; carbonates provide porous texture; sodium carbonate and boric acid act as a colloidal agent to improve dispersion properties and sodium metasilicate acts as a binder to induce higher mechanical strength to the membrane.

Membranes are prepared using the specified composition (Table 2.1) on a dry basis (40 % kaolin, 15 % quartz, 25 % calcium carbonate, 10 % sodium carbonate, 5 % boric acid and 5 % sodium metasilicate). The identified composition is based on a trial and error based on approach of Nandi *et al.* [5]. The composition of Nandi *et al.* [5] has been considered on a dry basis to evaluate the relation between membrane morphology and dry basis based composition. The initial step in the fabrication procedure involved the preparation of a membrane mould using a hydraulic press (Make: Velan Engineering, Tamilnadu, India). To obtain membranes with distinct membrane morphologies, three different fabrication pressures namely 25, 39, 73 MPa have been used and the membranes thus obtained are termed as PM1, PM2 and PM3 respectively (Table 2.1). Further procedure involves steps similar to those presented by Nandi *et al.* [5], except for the drying step. The procedure involves drying of prepared membranes (56 mm diameter and 5 mm thickness) at 150 ^{o}C for 24 h to remove adsorbed moisture and subsequent sintering at 900 ^{o}C for 4 h with a heating rate of 2 ^{o}C/min in a muffle furnace. Eventually, the membranes were allowed to cool in the furnace to 25 ^{o}C by switching the power off. The final steps in the membrane fabrication refer to polishing the membrane using C – 220 silicon carbide abrasive paper followed with cleaning using millipore water in an ultrasonic cleaning bath (Make: Elma (India, Model: T460) for 15 min.

Table 2.1: **Inorganic precursor composition and membrane nomenclature for the fabrication of low cost ceramic membranes.**

Material	Composition dry basis (Wt. %)
Kaolin	40
Quartz	15
Calcium carbonate	25
Sodium carbonate	10
Boric acid	5
Sodium metasilicate	5
Membrane	**Fabrication pressure (MPa)**
Circular disk shape for dead end	
PM1	25
PM2	39
PM3	73

2.1.2 Membrane characterization

Structural characterizations

The structural characterization of membranes involves thermogravimetric analysis (TGA), X ray diffraction analysis (XRD), morphological study using scanning electron microscope (SEM), total porosity determination, and evaluation of pore size distributions from SEM images.

Thermogravimetric analysis

TGA (*Make: Mettler Toledo, USA; Model: TGA/SDTA 851^e*) of the sample mixtures was conducted to identify the temperature regimes where predominant weight losses (and hence transformations) occur in the membrane. Thereby, an insight could be gained to analyze the effect of various temperature regimes on the porous structure, pore diameter and

mechanical strength of the membrane. TGA was carried out by heating the dry inorganic powder mixture in a α - alumina crucible from room temperature to 1000 ^{o}C at a heating rate of 10 ^{o}C per minute.

XRD analysis

XRD (XRD, Make: BRUKER, Model No. D8 Advance, Germany) analysis was conducted to evaluate the extent of different phase transformations that occurred during sintering.

Surface morphology

Membrane morphological studies were carried out using Field emission scanning electron microscopy (FESEM, Make: ZEISS, Model No ∑IGMA, USA) to analyze the presence of possible defects and estimate the membrane pore size. The estimation of average membrane pore size (d_s) and pore size distribution from FESEM micrographs was carried out using Image J software (Version 1.40). Individual pore diameters were measured for about 500 pores using the software for different pores visible in the FESEM. Since pore size distribution and average pore size distribution values are critically dependent on the sampling procedure, five FESEM pictures were evaluated using the software. These micrographs were taken randomly from the selected sections of the membranes in order to obtain pore size distributions representing the existing porous texture of the membrane. The area average pore diameter (d_s) from FESEM analysis of the membrane was evaluated by assuming cylindrical porous texture of the membrane as:

$$d_s = \left[\frac{\sum_{i=1}^{n} n_i d_i^{\,2}}{\sum_{i=1}^{n} n_i} \right]^{0.5} \qquad (2.1)$$

where, n is the number of pore, d_i is the pore diameter (μm) of i^{th} pore.

Porosity

The total porosity of the membrane was estimated using Archimedes principle. The experimental procedure involved the measurement of the volume of the wetting liquid that displaced air in a dry membrane after equilibrating the membrane with water for 12 hours. Total porosity (ε_m) of the membrane were estimated using the following equations [1]:

$$\varepsilon_m(\%) = \left[\frac{w_1 - w_2}{\rho_{water}}\right] \times \frac{100}{v_{mem}} \tag{2.2}$$

2.1.3 Permeation experiments

Experimental set up

A schematic of experimental set up used for both water permeation and batch MF experiment is presented in Figure 2.1. The set up constitutes a Teflon tubular cell (275 ml capacity) with a flat circular teflon base plate that houses the ceramic membrane. The membrane was kept in the teflon casing and sealed with epoxy resin (*Mseal, Pidilite Industries Ltd, Mumbai, India*). During water permeation experiments, the feed (de - ionized water) was filled in the cell from the top. The cell was pressurized with compressed air. Water permeate was collected in a beaker from the bottom of the cell and flux was measured using a digital weighing scale.

Liquid permeation characteristics

Permeation experiments using pure water (deionised water) were carried out for the determination of the hydraulic permeability (P_m) and hydraulic pore diameter (d_l) of the

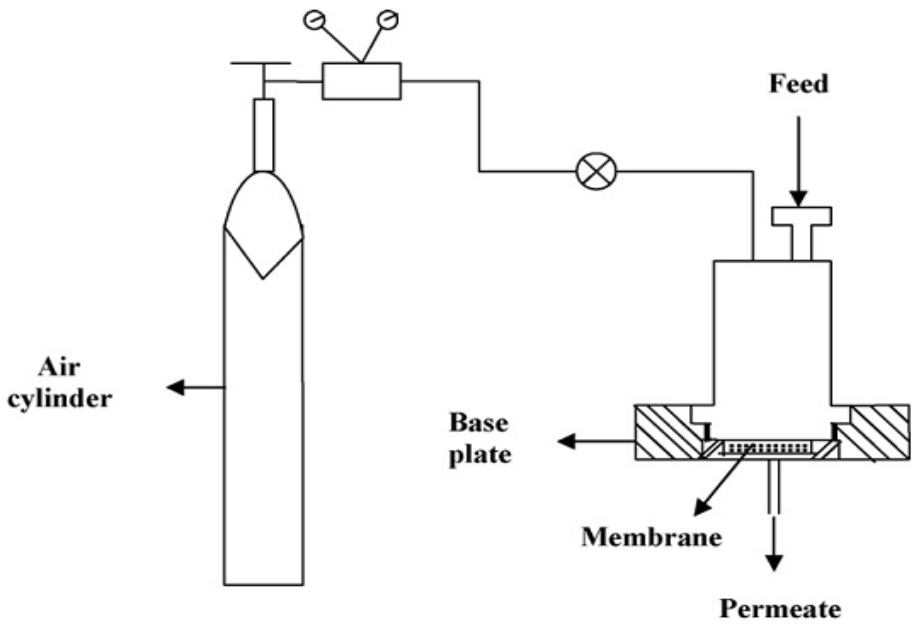

Figure 2.1: Batch experimental setup for liquid permeation and MF experiments.

membrane. The permeation tests involve the measurement of permeate liquid volume as a function of time at specific values of trans-membrane pressure drop (ΔP). The liquid flux was measured at an interval of 10 seconds to verify the variation of flux with time. After compaction, physical observations during liquid permeation tests confirmed that the flow rate did not vary during the 10 second time intervals. All permeation experiments were conducted at a temperature of 25 ^{o}C. Before conducting liquid permeation experiments, the membranes were compacted at ΔP of 310 kPa. This pressure was higher than the maximum operating pressure during MF experiments. Membrane compaction was carried out to obtain steady pure water flux through the membrane. The hydraulic permeability (P_m) and hydraulic pore radius (d_l) of the membranes were evaluated by assuming presence of cylindrical pores in the membrane matrix using the following expressions [1, 55]:

$$J_W = \frac{Q}{S.\Delta t} = \frac{\Delta P}{\mu_w}\frac{\varepsilon_m d_l^{\,2}}{32 l_m} = P_m \times \Delta P \qquad (2.3)$$

$$P_m = \frac{\varepsilon_m d_l^{\,2}}{32 \times l_m \times \mu_w} \qquad (2.4)$$

$$d_l = \left[\frac{32 \times \mu_W \times l_m \times P_m}{\varepsilon_m}\right]^{0.5} \qquad (2.5)$$

In Eq. (2.3), $\varepsilon_m d_l^{\,2}$ corresponds to effective permeable area factor that determines the actual permeable area available during filtration. It can also be analyzed that higher values of $\varepsilon_m d_l^{\,2}$ enable higher permeate fluxes and hence higher permeability of the membrane.

2.1.4 Chemical stability

All membranes were tested for their corrosion resistance using NaOH solution (pH 13) and HCl (pH 1.5). The chemical resistance of the membrane was evaluated by measuring its weight after leaving the membrane in contact with the above solutions for seven consecutive days at atmospheric conditions and determining the net weight loss after drying the membrane.

2.1.5 Microfiltration experiments

Synthetic oil - water emulsions with a concentration of 400 mg/L have been prepared using crude oil collected from Guwahati Refinery, Indian Oil Corporation Limited (IOCL), India and millipore water. The emulsification is carried out in a sonicator (Make: Elma (India); model: T460) for about 15 h without using external emulsifying agents. The prepared emulsions have been used for the MF experiments within one week. Prior to each dead end

MF experiment (Figure 2.1), the feed concentration was evaluated by measuring the absorbance using UV – Vis spectrophotometer (Spectra scan, UV 2300) at a wave length of 235 nm, where the maximum absorbance was observed. The MF experiments conducted at 25 ^{o}C involves the measurement of permeate volume at an interval of 1 min during a total run time of 30 min, after which nearly steady state flux values have been observed. Eventually, the permeate collected is also analyzed using the spectrophotometer to determine the oil concentration in the permeate stream. The time dependent concentrations in the permeate stream have been obtained by analyzing permeate samples obtained at an interval of 5 min during the MF run. For all the membranes (PM1, PM2 and PM3), the permeate flux (J, $m^3/m^2.s$) and the percent oil rejection (R) is evaluated using the expressions:

$$J = \frac{V}{A \times \Delta t} \tag{2.6}$$

$$R = (1 - \frac{C_P}{C}) \times 100 \tag{2.7}$$

where, A (m^2) is the effective membrane area, V (m^3) is the volume of permeate, Δt (s) is the sampling time, C (mg/L) and C_P (mg/L) are the concentration of oil in the feed and permeate, respectively. These are measured using UV- Visible spectro photometer.

2.1.6 Fouling studies

After each MF run, membrane cleaning is carried out by sequentially washing the membrane with tap water for 5 min. Membrane cleaning is carried out by soaking the fouled membrane in commercial detergent solution (surf excel with a concentration of 2 g/L) for 30 min; tap water washing for 5 min and back flushing; soaking the cleaned membrane in de - ionized water for 15 min and rinsing the membrane with deionized water for 5 min. Following these steps, the membrane is evaluated for its hydraulic permeability. Using the measured

hydraulic permeabilities of the fresh and cleaned membrane, the fouling index (*FI*) is calculated. *FI* for various membranes is defined as:

$$FI = \frac{PW_i - PW_f}{PW_i} \times 100 \qquad (2.8)$$

where, PW_i and PW_f correspond to the pure water hydraulic permeability values for the fresh and the cleaned membrane, respectively. Thus, higher fouling index indicates higher irreversible fouling of the membrane which could be due to pore blocking phenomena. Hence, fouling indices can be used as an additional criterion to opine upon the optimality of various fabricated membranes (PM1, PM2 and PM3) and operating pressures for the treatment of oil - water emulsion.

2.1.7 Fouling mechanism

To analyze the existent fouling mechanism during dead end MF at constant pressure, Hermia [56] proposed four different models, namely cake filtration, intermediate, standard and complete pore blocking models. During cake filtration, particles larger than the pore size of the membrane retain and enable the formation of a cake over the membrane surface. Hence the cake layer offers additional resistance to the liquid permeation. Also, as time proceeds the cake layer grows with time and is intrinsically related to flux decline. Complete, standard and intermediate pore blocking occur, when the particles enter the membrane pores, which is possible if the particle size is less than the membrane pore size. During complete pore blocking, the particles enter and block the pores, thus enabling the drastic reduction in the size of the open pores through which the liquid passes. During standard pore blocking, the permeating particles adhere on the membrane pore walls. Intermediate pore blocking is a case that corresponds to be between standard pore blocking and cake filtration where the

particles may adhere to the surface or to the pores or block the pores. Further details with respect to the derivations of flux decline models for all four cases have presented by Hermia [56] and are not presented. The linearized flux decline models for cake filtration, complete, standard and intermediate pore blocking phenomena are expressed as

(a) Complete pore blocking : $\ln(J^{-1}) = \ln(J_o^{-1}) + k_b t$ (2.9)

(b) Standard pore blocking : $J^{-0.5} = J_o^{-0.5} + k_s t$ (2.10)

(c) Intermediate pore blocking : $J^{-1} = J_o^{-1} + k_i t$ (2.11)

(d) Cake filtration : $J^{-2} = J_o^{-2} + k_c t$ (2.12)

For measured flux data, both single and combination modelling approaches have been followed. The combination models have been tested by considering the fitness of two different models to represent the short term flux decline (1 – 10 min) and the long term flux decline (11 – 30 min) of the MF data. For all cases, the coefficient of correlation (R^2) and RMS error have been used as the basis to identify the most competent model(s). Conceptually, the onset of cake filtration is beneficial from a fouling perspective, as cake filtration may correspond to maximum reversible fouling and is indicative towards longer shelf life of the membrane. In other words, the fitness of other pore blocking models is indicative towards irreversible fouling scenarios during MF, which could contribute to the shorter shelf life of the membrane and its durability.

2.2. Results and discussion

2.2.1 Membrane properties

XRD analysis

Figure 2.2 presents the XRD peaks for the unsintered raw material mixture used to fabricate PM3 membrane. It can be observed that quartz, inyoite, kaolin, nepheline peaks exist for the PM3 membrane. The obtained XRD pattern is in agreement with the XRD pattern obtained by Nandi *et al.* [5]. Thus, it is apparent that the sintering process enables the conversion of kaolinite to metakaolinite along with the appearance of nepheline phase.

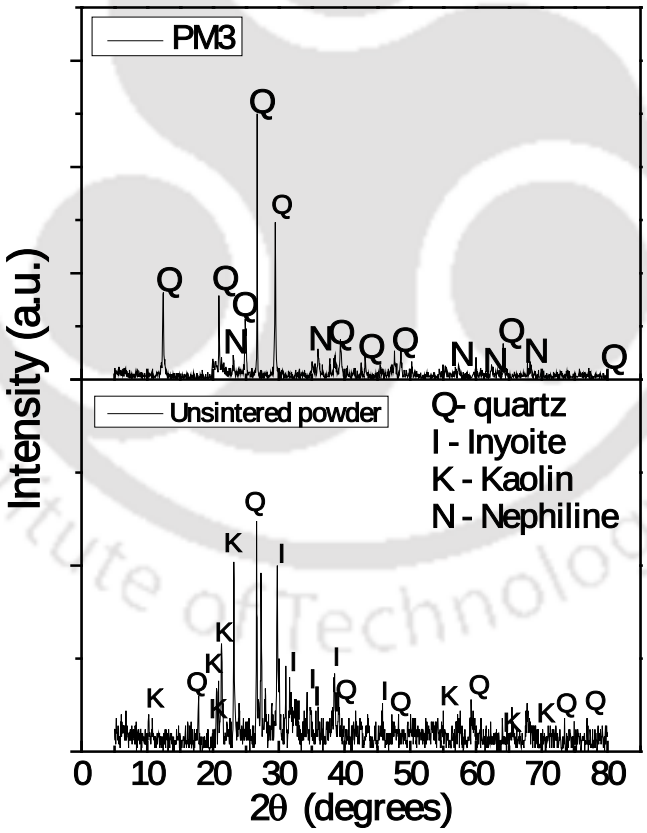

Figure 2.2: X – ray diffraction patterns of the raw material and PM3 membrane.

FESEM analysis

Figure 2.3 (a – c) illustrate the FESEM images obtained from membranes PM1 – PM3 respectively. A superficial observation of the SEM indicated that the membrane did not have any pinholes cracks and the maximum observable pore size of the surface is about 5 - 10 μm. These attributes of the membrane make it suitable for MF applications.

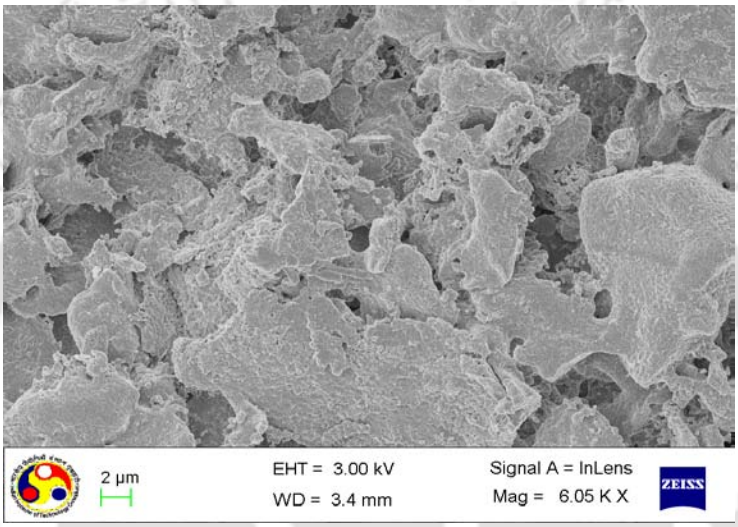

(a)

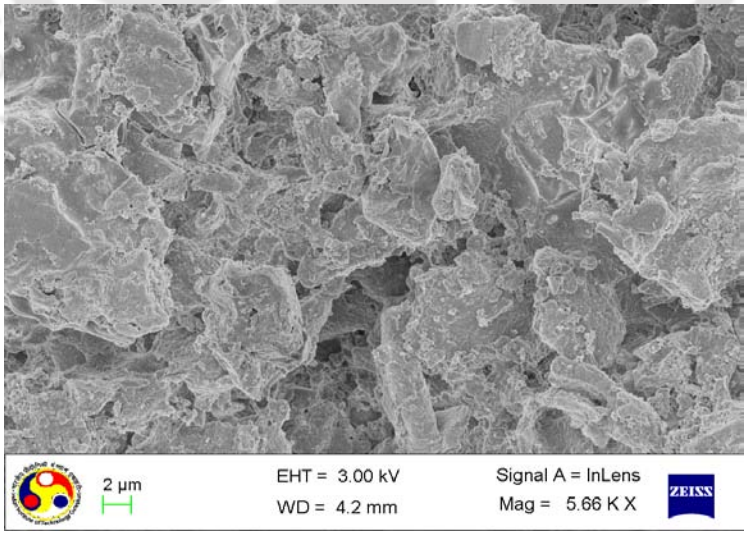

(b)

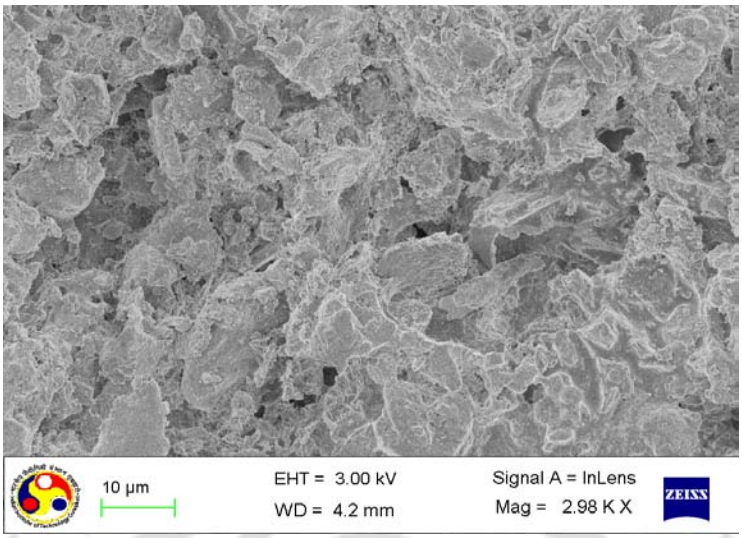

(c)

Figure 2.3: FESEM images of PM1, PM2 and PM3 membranes.

Pore size distribution

Using Image J software, the pore size distributions of various membranes PM1 – PM3 have been obtained and are presented in Figure 2.4. It can be observed that the membranes had distinct porous structure with pores ranging from 2 – 10 µm. It may also be seen from the figure that the pore size distributions involve single peak profile with wider pore size distribution for the membrane fabricated at lower pressure. Using these pore size distributions, the average pore sizes of various membranes are evaluated as 3.23 µm, 2.45 µm and 2.33 µm for PM1, PM2 and PM3 membranes, respectively. Further, it can also be observed that the maximum number of pores (%) varied significantly with fabrication pressure and are 35 %, 26 % and 20 % for PM1, PM2 and PM3 membranes, respectively. In this regard, it can be analyzed from the data trends presented by Nandi *et al.* [6] that the pore size distributions of the membranes fabricated by paste method varied from 0.1 – 3 µm with 25 %

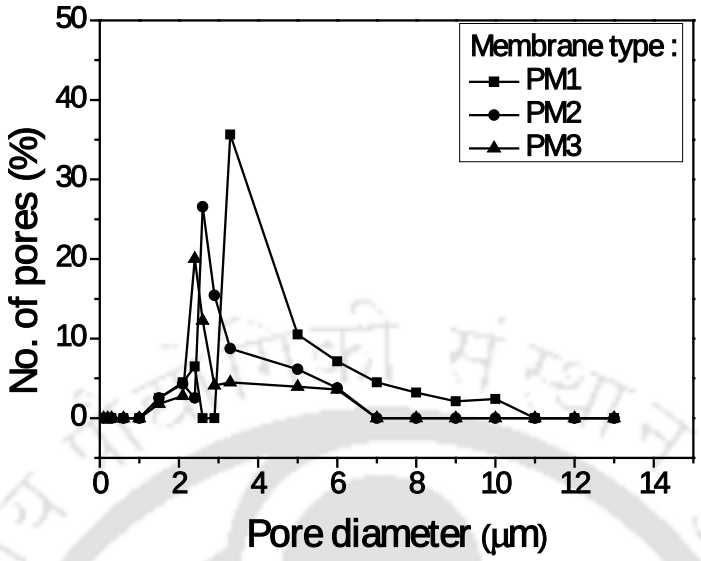

Figure 2.4: FESEM based pore size distributions of PM1, PM2 and PM3 membranes.

pores possessing a pore diameter of about 0.5 μm. The average pore size of the membrane is 0.55 μm. Thus, it is apparent that uniaxial dry compaction method provides membrane with significantly wider pore size distribution than the membrane obtained with the paste method. This is a very important observation given the fact that the presence or absence of water strongly influences plasticity of the green mould and hence membrane morphology after sintering.

Pure water flux, membrane porosity and average pore size

The pure water flux data for various membranes are presented in Figure 2.5 a. The pure water flux varied from 3.16 to 9.25 × 10^{-3}, 2.61 to 7.76 × 10^{-3} and 1.64 to 5.05 × 10^{-3} m^3/m^2.s with a variation in applied pressures from 68.9 – 206.70 kPa for PM1, PM2 and PM3 membranes, respectively. The obtained pure water flux is about 4 times higher than the pure water flux reported by Nandi *et al.* [5]. The average membrane porosity was obtained using

Archimedes principle and its variation with fabrication pressure is shown in Figure 2.5 b. It can be observed that the membrane porosity increased from 30.1 % to 37.4 % with an increase in fabrication pressure from 25 to 73 MPa. The average pore size of the membrane determined using average porosity and hydraulic permeability is also presented in Figure 2.5 b for all the membranes. The average pore size of the membranes varied from 3.06 µm to 2.16 µm, which is significantly higher than the average pore size of 0.6 µm reported by Nandi *et al.* [5] using the paste method. The enhancement in porosity with an increase in fabrication pressure is due to an enhancement in surface area brought forward with the reduction in pore size. Therefore, the utilization of water during paste method enabled finer arrangement of the precursors in the paste which is not the case for the uniaxial dry compaction method. While this is true and can be predicted even without doing the fabrication experiments, it is important to conceive technically the role of water in the paste method and the fabrication pressure in the dry compaction method to influence membrane morphology. In other words, the elimination of water as a binding agent during green mould membrane fabrication strongly enhances the membrane pore size. Thus, more research is required to relate laboratory fabrication techniques with extrusion based ceramic membrane fabrication.

2.2.2 Dead end MF of oil water emulsion

Time dependent permeate flux

Figure 2.6 a - c present the time dependent flux for membranes PM1, PM2 and PM3 respectively at various values of transmembrane pressure (ΔP) during dead end MF of oil-water emulsion. It can be observed that for all the membranes, higher ΔP provides higher flux.

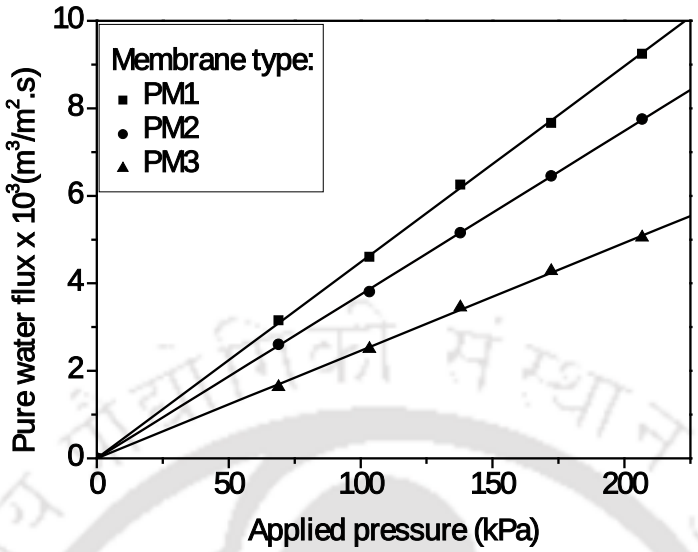

(a)

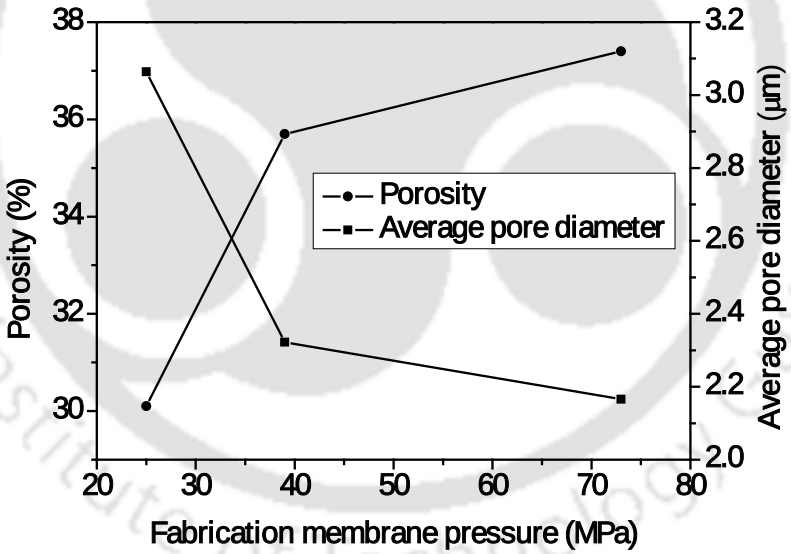

(b)

Figure 2.5: (a) Variation of pure water flux with applied pressure for PM1-PM3 membranes (b) Dependence of membrane porosity and average pore size on fabrication pressure.

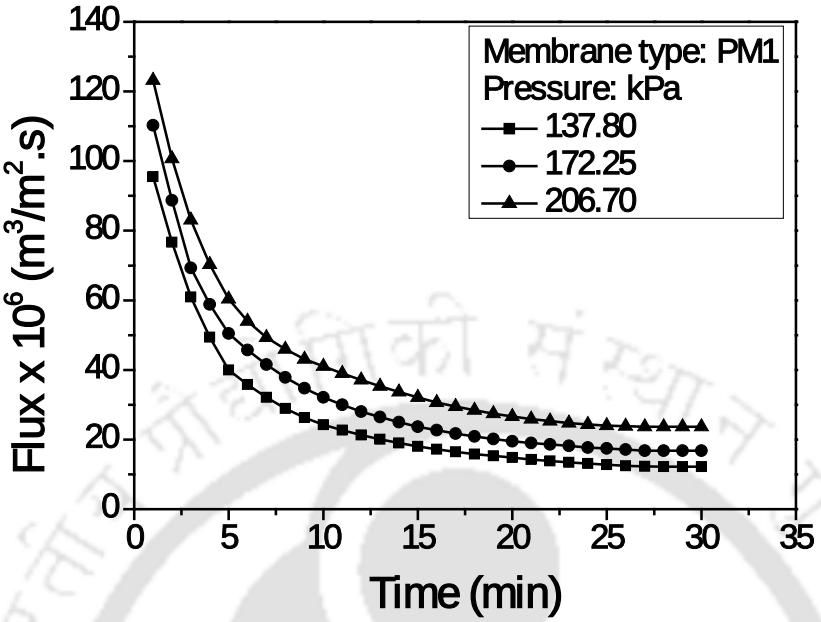
Membrane type: PM1
Pressure: kPa
137.80
172.25
206.70
Flux x 10^6 (m^3/m^2.s)
Time (min)
0
20
40
60
80
100
120
140
0
5
10
15
20
25
30
35

(a)

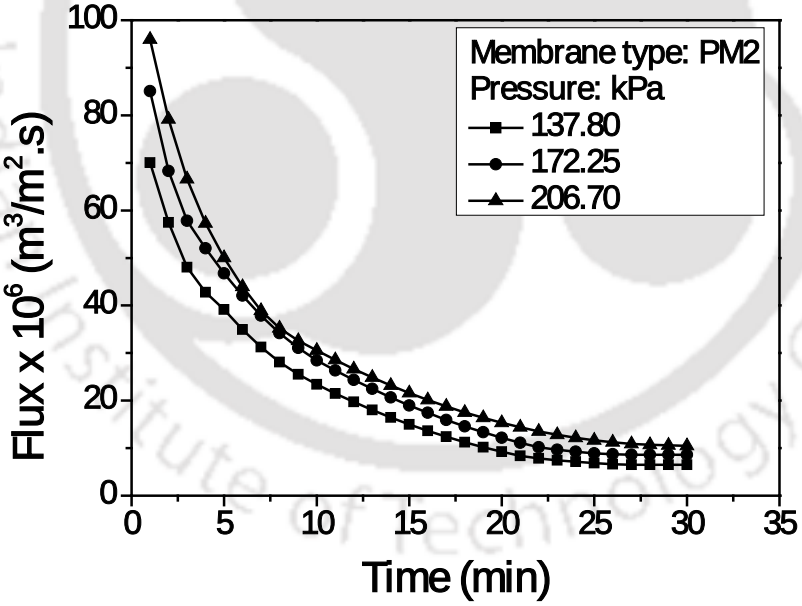
Membrane type: PM2
Pressure: kPa
137.80
172.25
206.70
Flux x 10^6 (m^3/m^2.s)
Time (min)
0
20
40
60
80
100
0
5
10
15
20
25
30
35

(b)

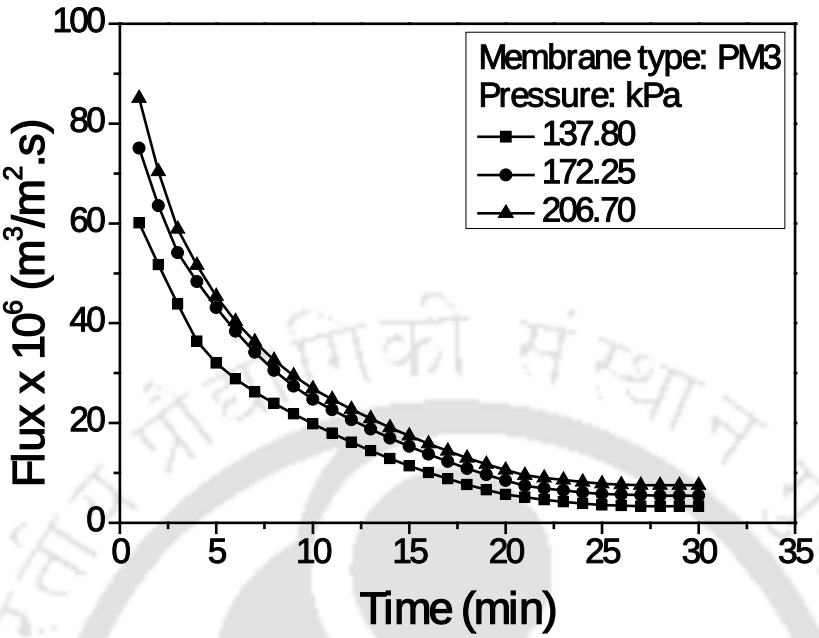

(c)

Figure 2.6: Variation of time dependent flux with pressure for (a) PM1 (b) PM2 and (c) PM3 membranes.

Further, a significant variation in the near steady state membrane flux is contributed due to the variation in membrane morphology. For instance, at an operating ΔP of 206.7 kPa, the membrane flux after 30 min of dead end MF is about 24 × 10^{-6}, 11 × 10^{-6} and 8 × 10^{-6} m^3/m^2.s for PM1, PM2 and PM3 respectively. It can also be observed that the time dependent membrane flux varied from 124 to 24 × 10^{-6}, 96 to 11 × 10^{-6}, 86 to 8 × 10^{-6} m^3/m^2.s for PM1, PM2 and PM3 respectively, at a ΔP of 206.7 kPa at the end of 30 min of operation. Therefore, it is apparent that the membrane morphology significantly influences the near steady state flux but not the intial flux. This is probably due to the reason that the membranes fabricated at lower fabricating pressures possessed wider pore size distributions and are less

susceptible for lower fouling and hence membrane PM1 is the optimal in terms of membrane flux.

Time dependent rejection

The variation in time dependent oil rejection for various membranes and at various ΔP is presented in Figure 2.7 a – c. As shown, the membrane rejection varies almost linearly for PM3 membrane with time and slightly non-linearly for the PM1 membrane. This indicates that pore blocking could be significant for the PM1 membrane, which need not be the case for PM3 membrane. It is also observed that the rejection decreases with increasing ΔP for all the membranes. This is due to the reason that higher pressures facilitate the enhancement of wetting and coalescence of oil droplets and could enable some oil droplets to pass through the membrane pores to reach the permeate stream. The enhancement in rejection with time for all the membranes is because of reduction of the pore size due to pore blocking and adsorption of

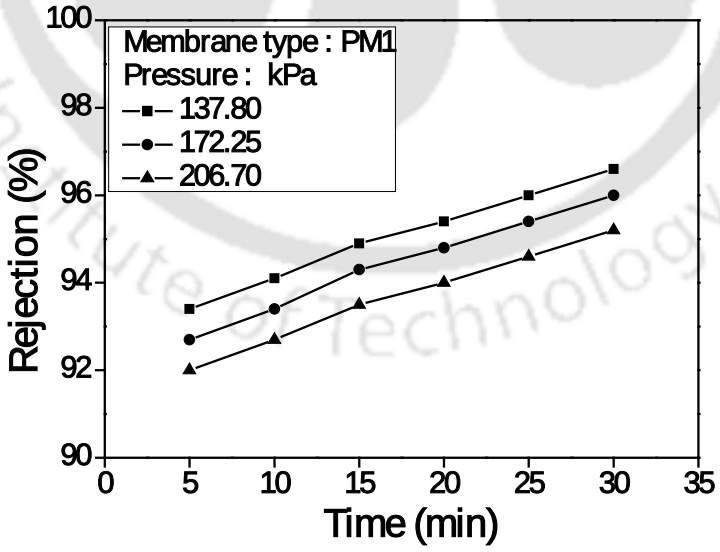

(a)

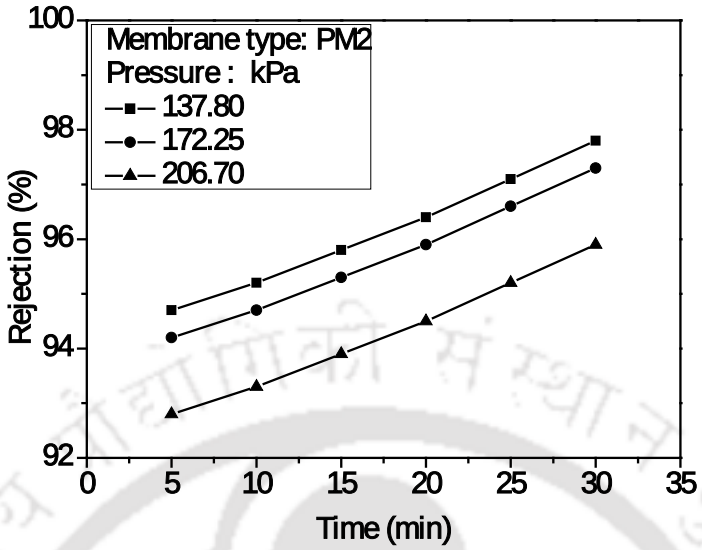

(b)

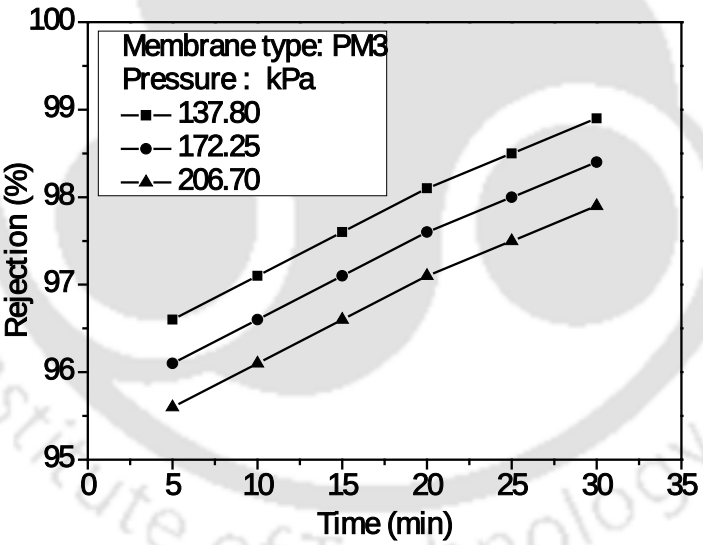

(c)

Figure 2.7: Variation of time dependent rejection (%) with pressure for (a) PM1 (b) PM2 and (c) PM3 membranes.

oil droplets onto the pores. For membrane PM1, the rejection varied from 93.4 % - 96.6 % at a ΔP of 137.80 kPa which reduced to 92 % - 95.2 % at a ΔP of 206.70 kPa. The insignificant reduction in ejection at higher ΔP during MF is indicative towards satisfactory permeation performance of the membranes.

Membrane performance in terms of flux and rejection

For a ΔP variation from 137.8 to 206.8 kPa, the fouling indices for various membranes are evaluated to vary from 40.06 % to 29.40 %, 31.73 % to 25.26 % and 25.14 % to 15.54 % for membranes PM1, PM2 and PM3 respectively. Considering fouling index as an additional criterion for the selection of membranes, the membrane PM3 at a ΔP of 206.70 kPa is the optimal choice to process the choosen feed. In other words this membrane with a fouling index of 15.54 % and a near steady state flux of 8×10^{-6} $m^3/m^2.s$ and a rejection of 97.6 % is the most suitable for the treatment of oil water emulsions. For all membranes, lower ΔP (137. 80 kPa) is not recommendable for MF operations. A comparative assessment of the obtained membrane permeability and rejection of the PM3 membrane with the data available in the literature is presented in Table 2.2. It can be observed that the obtained permeability and rejection for PM3 membrane are comparable with the values presented in the literature and the higher pore size of the membrane could process oil-water emulsion feeds with relatively higher concentration of oil (400 – 500 mg/L).

Fitness of different models

Figure 2.8 presents the linearized plots for the fitness of various pore blocking models (cake filtration, intermediate pore blocking, standard and complete pore blocking) for PM3 membrane at various values of ΔP during the dead end MF. It can be observed that even the

Table 2.2: Literature and obtained membrane performance characteristics (PM3) for the dead end MF of oil-water emulsions.

S.No.	Author	Average membrane properties		Feed concentration (mg/L)	Time (min)	Membrane Permeability ($m^3/m^2.s.kPa$)	Pressure differential (kPa)	Rejection (%)
		Pore size (µm)	Porosity (%)					
1.	Vasanth et al. [7]	1.30	30	125	30	2.21×10^{-6}	276.4	85
2.	Monash et al. [3]	0.98	44	200	30	2.31×10^{-7}	345.4	96
3.	Nandi et al. [6]	0.55	42	50	30	3.28×10^{-7}	41.37	97.3
4.	Vasanth et al. [8]	1.21	26	200	30	3.39×10^{-8}	69.0	96
5.	This work	2.16	37.4	400	30	3.65×10^{-8}	206.70	97.9

consideration of a single model in a combination based approach does not fit the flux decline data (Figure 2.8 c and Figure 2.8 d). Based on several permutations and combinations, the most competent combination of the model is identified using the correlation coefficient (R^2) values.

Table 2.3 summarizes the fitness of combination models for various membranes at a ΔP of 206.70 kPa. It can be observed that the support pore size strongly influences pore blocking phenomena. For the PM1 membrane having wider pore size distribution, cake filtration model fits well to represent the data. On the other hand the membrane provided a fouling index of 29.47 %. Hence it is concluded that the onset of cake filtration need not indicate minimal reversible fouling and therefore generalized rules of thumb are always not applicable. On the other hand, for the PM3 membrane, the combination of standard pore blocking (during 1 – 10 min) and cake filtration (during 11 – 30 min) provide the best fitness toward representing the flux decline data. It is also important to note that PM3 membrane has a minimal fouling index of 15.54 %. Therefore, while pore blocking could not be eliminating during intial stages of MF, the onset of cake filtration at a later stage is promising to give a lower fouling index of the PM3 membrane. In summary, it is apparent that MF experiments using membranes possessing wider pore size distribution, and feed stream with higher oil concentration (400 mg/L) did not indicate the flux decline phenomena to be represented with single pore blocking model. For such cases, combinational models have to be considered to represent well the flux decline phenomena.

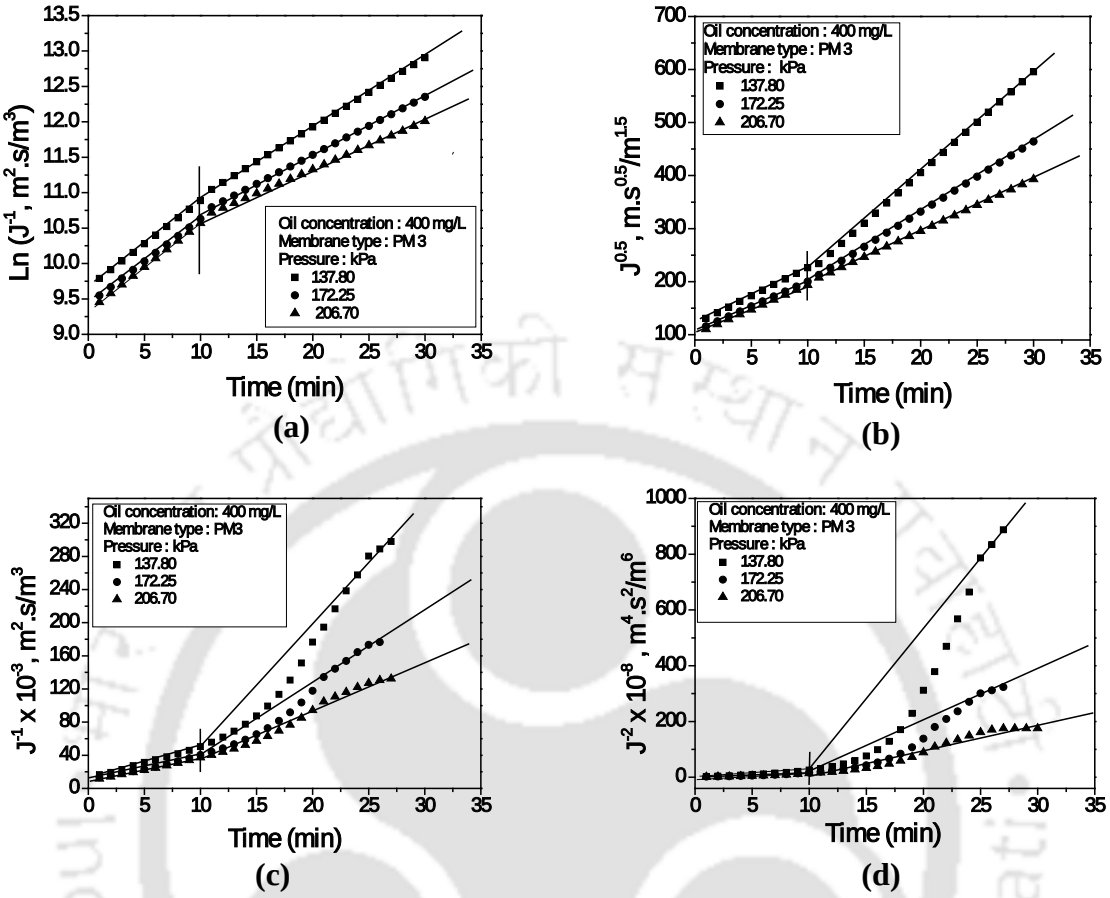

Figure 2.8: Linearized plots for the fitness of various pore blocking models to represent flux data for membrane PM3 at a ΔP of 206.70 kPa (a) complete pore blocking (b) standard pore blocking (c) intermediate pore blocking and (d) cake filtration.

Figure 2.9 summarizes the parity plot for the obtained data for two different cases namely the consideration of most competent single pore blocking and most competent combination models. It may be observed from Figure 2.9 a that for the first case significant number of data points deviated very much from the parity but for the second case (Figure 2.9 b), the deviation is minimal for the combination models. For the obtained flux decline data, single pore blocking model is considered for the first case and RMS errors were calculated. It can be

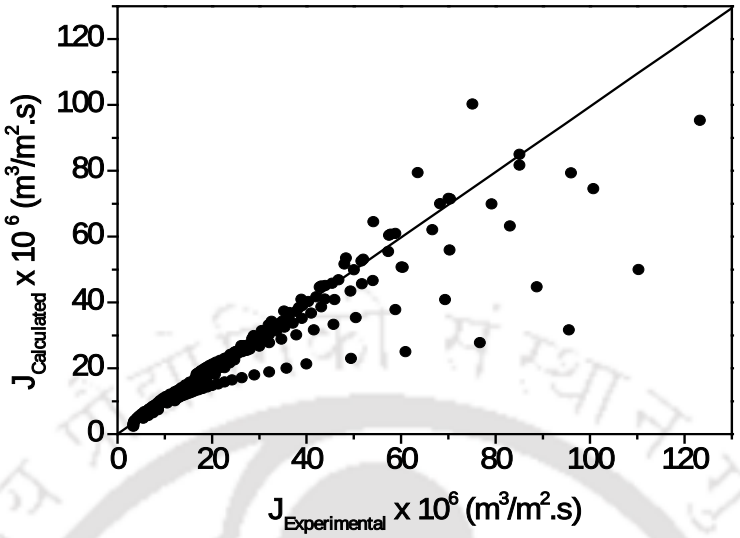

(a)

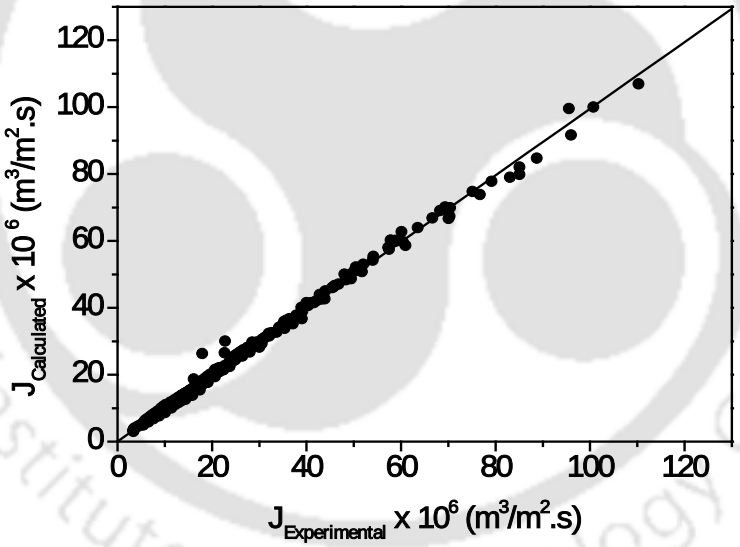

(b)

Figure 2.9: Flux parity plots for (a) most competent single pore blocking model and (b) most competent combination pore blocking models for PM1 – PM3 membranes.

Table 2.3: **Coefficient of Regression (R^2) values for the most competent combination of various pore blocking models for PM1 – PM3 membranes.**

Membrane type	Pressure (kPa)	CPB		SPB		IPB		CF	
		Intial	Final	Intial	Final	Intial	Final	Intial	Final
PM 1	137.80	0.962	0.949	0.988	0.964	0.997	0.975	0.976	0.987
	172.25	0.956	0.924	0.984	0.941	0.997	0.955	0.985	0.975
	206.70	0.950	0.906	0.976	0.919	0.991	0.931	0.994	0.950
PM 2	137.80	0.984	0.938	0.996	0.957	0.995	0.967	0.961	0.966
	172.25	0.982	0.939	0.996	0.954	0.996	0.962	0.964	0.960
	206.70	0.979	0.972	0.994	0.985	0.998	0.990	0.977	0.981
PM 3	137.80	0.980	0.949	0.995	0.968	0.998	0.970	0.972	0.943
	172.25	0.994	0.942	0.999	0.961	0.990	0.968	0.944	0.958
	206.70	0.986	0.933	0.998	0.952	0.997	0.962	0.961	0.963

seen that the RMS error varied from 36.66 – 11.06 %, 6.46 – 5.31 %, 11.73 – 6.41 %, for membranes PM1, PM2 and PM3, respectively. Also the RMS error for both the cases namely most competent single pore blocking model and most competent combination model is 30 % and 6 %, respectively.

Table 2.4a summarizes the model parameters for various membranes to represent the flux data (at ΔP of 206.7 kPa) as a combination of two most competent pore blocking models. It can also be observed from the table that the RMS error values are 3.17 – 6.39 %. Further, it is

Table 2.4a: **Summary of model parameters for the best fit combination models to represent dead end MF flux data obtained for PM1 – PM3 membranes at a ΔP of 206.7 kPa.**

Membrane type	Intial		Final		RMSE (%)
	Type of model	Parameters	Type of model	Parameters	
PM 1	Cake filtration	$J_0 = 1.58 \times 10^{-4}$ $m^3 / m^2.s$ $k_c = 2.00 \times 10^{-7}$ $s.m^{-2}$	Cake filtration	$J_0 = 3.67 \times 10^{-5}$ $m^3 / m^2.s$ $k_c = 2.15 \times 10^{-7}$ $s.m^{-2}$	5.93
PM 2	Standard pore blocking	$J_0 = 9.16 \times 10^{-4}$ $m^3 / m^2.s$ $k_s = 95.52$ $m^{-0.5} s^{-0.5}$	Intermediate pore blocking	$J_0 = 2.97 \times 10^{-5}$ $m^3 / m^2.s$ $k_i = 5159$ m^{-1}	3.17
PM 3	Standard pore blocking	$J_0 = 8.20 \times 10^{-5}$ $m^3 / m^2.s$ $k_s = 101.1$ $m^{-0.5} s^{-0.5}$	Cake filtration	$J_0 = 1.17 \times 10^{-4}$ $m^3 / m^2.s$ $k_c = 1.14 \times 10^{-7}$ $s.m^{-2}$	6.39

Table 2.4b: Summary of model parameters for the best fit combination models to represent flux data obtained for PM3 membrane at various values of ΔP.

Membrane type	Pressure (kPa)	Intial		Final		RMSE (%)
		Type of model	Parameters	Type of model	Parameters	
PM 3	137.80	Intermediate pore blocking	$J_0 = 6.27 \times 10^{-5}$ $m^3/m^2.s$ $k_i = 12170$ m^{-1}	Intermediate pore blocking	$J_0 = 2.63 \times 10^{-5}$ $m^3/m^2.s$ $k_i = 13176$ m^{-1}	6.80
	172.25	Standard pore blocking	$J_0 = 7.47 \times 10^{-5}$ $m^3/m^2.s$ $k_s = 106.3$ $m^{-0.5} s^{-0.5}$	Intermediate pore blocking	$J_0 = 2.65 \times 10^{-5}$ $m^3/m^2.s$ $k_i = 58446$ m^{-1}	6.68
	206.70	Standard pore blocking	$J_0 = 8.20 \times 10^{-5}$ $m^3/m^2.s$ $k_s = 101.1$ $m^{-0.5} s^{-0.5}$	Cake filtration	$J_0 = 1.17 \times 10^{-4}$ $m^3/m^2.s$ $k_c = 1.14 \times 10^{-7}$ $s.m^{-2}$	6.39

apparent that membrane morphology strongly influences the onset of various pore blocking phenomena. For instance, for the PM1 membrane having wider pore size distributions, the cake filtration model fits well which is the not case for PM3 membrane where standard pore blocking model fits well in initial flux regime. Also, the instantaneous flux (J_0) for these membranes are evaluated as 1.58×10^{-6}, 9.16×10^{-6} and 82×10^{-6} $m^3/m^2.s$ for PM1, PM2 and PM3 membranes respectively, which is 58.5, 8.4, 61.5 times lower than the corresponding pure water flux of these membranes. This indicates that the membrane morphology profoundly influences the instantaneous flux and also morphology of the dynamic gel layer.

The onset of cake filtration as a competent pore blocking for the PM1 membrane is possibly due to a very efficient instantaneous pore blocking that enables cake filtration to contribute to fouling later on wards. Thus, these observations definitively indicate the complexity involved in the interaction between adsorption of oil in the pores, pore blocking and associated dynamic cake filtration layer morphology.

Table 2.4b summarizes the pore blocking model parameters that were obtained using the most competent combination of two pore blocking models for the PM3 membrane. It can be observed that the RMS error for the model fitness is within 6.3 – 6.8 %. Further, it may also be observed that ΔP also influences the type of pore blocking mechanism. For instance, at a lower ΔP of 137.80 kPa, intermediate pore blocking occurred which transformed to standard pore blocking at a higher ΔP of 172.25 kPa and 206.70 kPa. For the membrane, the instantaneous flux values are varied about 55.1, 59.4 and 69.5 times lower than the corresponding pure water flux values. This indicates that ΔP insignificantly influences instantaneous membrane fouling and the dynamic gel layer morphology could be strongly

Table 2.5: Retail raw material cost based cost analysis of PM1 – PM3 membranes.

Material	Retail price (Rs./kg)	Composition (A)		
		Wt %	Amount of raw material used for preparation of one membrane (kg)	Cost of one membrane (Rs.)
Kaolin	520	40	8×10^{-3}	4.16
Quartz	358	15	3×10^{-3}	1.074
Calcium carbonate	408	25	5×10^{-3}	2.04
Sodium carbonate	660	10	2×10^{-3}	1.32
Boric acid	760	5	1×10^{-3}	0.76
Sodium metasilicate	578	5	1×10^{-3}	0.578
Total cost/ membrane (round off value)				Rs. 9.932/- Rs. 9.94/-
For the fabrication of circular disk – shaped ceramic membrane of 5 mm and 56 mm diameter = Rs. 9.94/ membrane. Raw material cost of the membrane/unit area = Rs. 4038/m^2				

affecting the rejection characteristics at higher pressure. The same is also evident from the rejection data and fouling behaviour details presented in the previous section.

2.2.3 Acid and base sustainability of membrane

It was evaluated that for the weight loss of membranes during chemical stability for acid (HCl) tests was not significant and was 6 %, 4 % and 2 % for PM1, PM2 and PM3 membranes, respectively. After corrosion test, the porosity for PM1, PM2 and PM3 membranes varied from 30.1 %, 35.7 % and 37.4 % respectively. There is no porosity change and wet loss due to base (NaOH) treatment for all the membranes.

2.2.4 Cost of membranes

Industrially competitive aspect of membrane technology lies in its cost. Table 2.5 summarized the retail prices of various inorganic precursors that were used for the fabrication of the membranes. Based on the inorganic precursor formulation, the overall cost of the membranes using retail cost indices have also been presented in the table. The retail prices of the precursors have been obtained from the manufacturers catalogs.

The materials cost of the membranes has been estimated to be Rs. 4038/m^2. The reported cost of the membrane based on raw materials costs is anticipated to be useful to provide economic benchmarks for different small scale applications such as research and pilot scale utilization of inorganic membranes. However, for large scale production the cost of raw materials will be much lower than the reported cost data. Including shipment, fabrication and other costs, the average cost of inorganic membranes using large scale production methods may vary. Contemporary elemental costs of various polymeric membranes and α-alumina ceramic symmetric membrane vary form 50 - 200 \$/m^2 [55] (Rs. 3000 – 12000/m^2) and 2000 - 4000 \$/m^2 (Rs. 12000 – 24000/m^2), respectively [57]. Therefore, it can be inferred from cost analysis that cost of the inorganic membranes based on kaolin would be closer to the cost of the polymeric membranes deployed for industrial configurations and could be slightly expensive than the modules prepared with polymeric membranes owing to the costs involved in manufacturing and bare module costs.

The reported value of the membrane cost is conceptual in nature and may vary significantly depending on the fouling characteristics, on time performance, membrane durability, long term stability and life cycle of the ceramic membrane in process applications. However, corrosion resistance data presented in this work instill confidence in the long term

performance and hence the projected membrane cost is anticipated to be close to the reported value.

Cross flow Microfiltration of Oil-Water emulsions Using Kaolin based Low Cost Ceramic Membranes

This chapter addresses three different perspectives. Firstly, this article targets the cross flow microfiltration of kaolin based low cost ceramic membranes characterized with wider pore size for the treatment of oil-water emulsions with higher feed concentrations (400 – 500 mg/L). Secondly, rectangular membrane conduits have been investigated for wide range of operating parameters (cross flow velocity/Reynolds number and transmembrane pressure differentials). Thirdly, fouling indices have been assessed systematically, as these are very important from the commercialization perspective. In summary, the effect of fabrication pressure, operating pressure and cross flow velocity (or circulation rate) on the flux and separation characteristics of kaolin based low cost ceramic membranes has been investigated to identify optimal membrane and process parameters.

3.1 Experimental and fouling mechanism

3.1.1 Membranes used

Three different membranes PM1, PM2 and PM3 respectively have been prepared using uniaxial dry compaction method (with inorganic precursor compositions presented in Table 2.1 of chapter 2) at three different fabrication pressures namely 25, 39 and 73 MPa. The membrane preparation and characterization procedures have been elaborated in chapter 2. While chapter 2 refers to circular ceramic disks, this chapter refers to the fabrication of membranes with similar morphological parameters to achieve membranes in rectangular

shape with the dimensions of 0.099 m (length) × 0.04 m (width) × 0.005 m (thickness) after sintering at a temperature of 900 ^{o}C. Thus, the fabricated membranes possess higher permeation area than those reported in chapter 2 and hence required higher fabrication forces to achieve the membranes with same morphologies, presented in chapter 2 of the thesis.

3.1.2 Microfiltration experiments

For all microfiltration experiments, synthetic oil-water emulsions with a concentration of 400 mg/L were prepared using an ultrasonic cleaning bath (make: Elma (India); model: T460) for 15 h of continuous sonication. The crude oil was collected from Guwahati Refinery, Indian Oil Corporation Limited (IOCL), India. The prepared emulsions were stable for about one week and the cross flow MF experiments were conducted within this time frame.

Figure 3.1 illustrates the cross flow microfiltration setup for all experimental investigations. As shown, the setup consists of a microfiltration filtration module that is supplemented with a reciprocating pump, stainless steel tank, rotameter, pressure gauge, valves and a weighing balance. The microfiltration membrane module consists of two rectangular stainless steel flanges that sandwich the prepared ceramic membranes using a silicon rubber gasket during the microfiltration operation. The two flanges upon tightening provided a leak proof permeation module with an effective membrane permeation area of 2.728×10^{-3} m^2 (length and width of 0.088 m and 0.031 m) and a channel height of 8×10^{-3} m for the circulation of oil - water emulsions. The experimental microfiltration run involved pumping the prepared oil - water emulsions from the stainless steel tank with a capacity of 10^{-2} m^3 using a reciprocating pump to enable controlled circulation with the two flow valves (namely the bypass valve and the flow valve located after the membrane module). Using these valves, the desired combinations of transmembrane pressure (138 – 207 kPa) and cross flow

velocity (2 – 4 liter per minute (LPM) that corresponds to a Reynolds number variation from 3417 – 6835) have been met and determined using pressure gauge and rotameter respectively. A typical microfiltration run involves the measurement of transmembrane flux using weighing balance and a glass beaker at time intervals of 1 minute during an experimental run scheduled for a total time period of 30 minutes. Thus, all experimental investigations were conducted at three different sets of ΔP (138, 172 and 207 kPa) and cross flow velocity (Re = 3417, 5126 and 6835) to evaluate upon their effect on the microfiltration, fouling and separation characteristics of the low cost ceramic membranes.

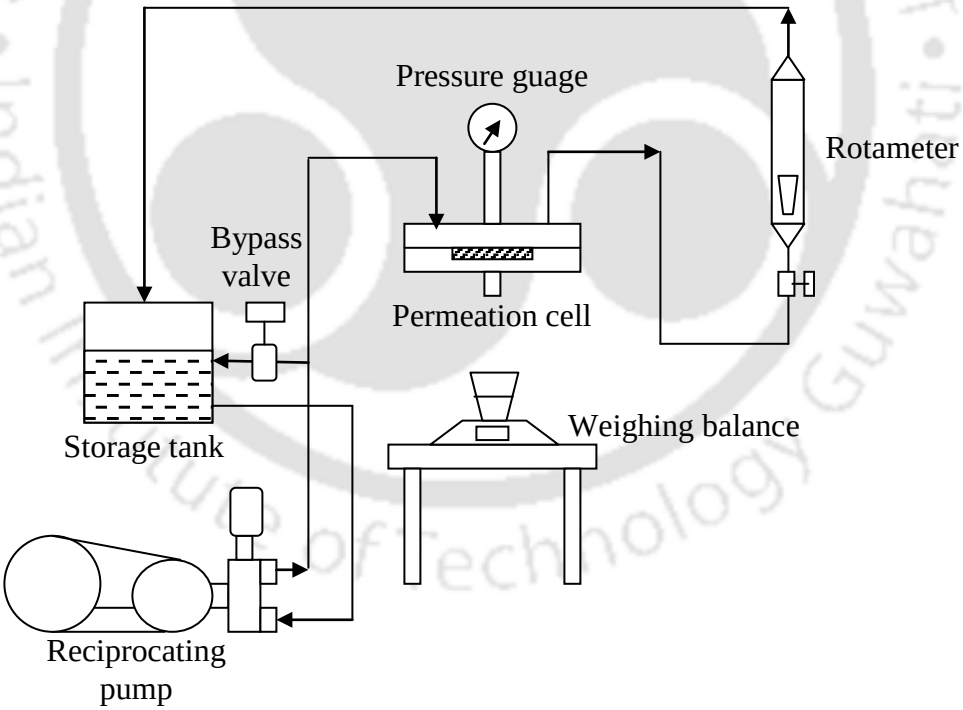

Figure 3.1: Schematic of cross flow MF setup for the treatment of oil-water emulsions.

For each MF run, the feed and permeation concentrations and permeate flux were determined. For all membranes (PM1, PM2 and PM3), permeate flux (J, $m^3/m^2.s$) and the percent oil rejection (R) were determined using the expressions reported in section 2.1.5 of the thesis.

3.1.3 Fouling studies

Fouling index (FI) is a very important measurement parameter that is often ignored during the development of low cost ceramic membranes. Higher fouling index indicates significant pore blocking and irreversible fouling and therefore, fouling index values ascertain upon the optimality of process and membrane morphological parameters. To determine the fouling index, membrane cleaning procedures were adopted as explained section 2.1.6 of the thesis.

3.1.4 Fouling models

Hermia [56] presented four different fouling models namely cake filtration (CF), intermediate (IPB), standard (SPB) and complete pore blocking (CPB) models to represent the pertinent MF flux decline data. These models are presented in section 2.1.7 of the thesis. The fitness of any one of the four models is based on the maximum value of coefficient of correlation (R^2) values coupled with positive combinations of slope and intercept values to represent either the entire or a portion of the MF permeation data. Depending upon the membrane morphology and choice of the feed and its concentration, either single or combination models have to be examined to represent the entire flux data obtained during the MF. This is also true due to the fact that the dynamic polarization and fouling layer during the MF run could have time dependent variation of morphological properties which in turn influences the time dependent flux decline. All in all, the fitness of various fouling models is

anticipated to provide significant insights with respect to the time dependent fouling characteristics and extent of irreversible fouling. A further insight in the relationship between measured fouling index and identified fouling mechanisms is also anticipated.

3.2 Results and discussion

3.2.1 Morphological parameters

Table 3.1 summarizes the morphological and cost parameters of the fabricated membranes PM1 – PM3. It can be observed that for an increasing variation in fabrication pressure from 25 (PM1 membrane) – 73 MPa (PM3 membrane), the average pore size of the membrane (based on pure water flux and porosity data) reduced from 3.06 to 2.16 µm. However, the porosity of the membranes increased from 30.1 – 37.4 %. Based on the retail cost of the inorganic precursors, the average membrane cost has been estimated to be 63 $/m^2, which is comparable with the cost of polymeric membranes [58].

3.2.2 Time dependent membrane performance

Figure 3.2 (a – c) presents the time dependent variation in permeate flux for membranes PM1 – PM3 at different values of ΔP and at Re = 3417. As shown, the membrane flux increased with increasing ΔP and has been evaluated to be maximum at ΔP = 207 kPa for

Table 3.1: M**orphological and cost parameters for PM1 – PM3 membranes.**

Membrane	Pore size (µm)	Porosity (%)	Cost ($/m^2)
PM1	3.06	30.1	63
PM2	2.32	35.7	63
PM3	2.16	37.4	63

all the membranes. At a ΔP of 207 kPa and Re of 3417, it can be observed from Figure 2 (c) that the transmembrane flux varied with time from 68.4 to 31.5, 60.7 to 28.0 and 50.0 to 22.1 $\times 10^{-6}$ $m^3/m^2.s$ for membranes PM1, PM2 and PM3 respectively. For all cases, it has been observed that distinct membrane flux profiles have been obtained for combinations of ΔP and membrane morphology. This indicates that higher membrane pore size and ΔP enhanced membrane flux and substantial enhancement in membrane fouling did not occur with the enhancement of these two parameters. Similar flux profiles have been obtained for all membranes at higher cross flow velocities (Re = 5126 and 6835).

The variation of % Rejection with time for various cases of ΔP at a Reynolds number of 3417 are presented in Figure 3.2 (d – f). At a ΔP and Re of 207 kPa and 3417 respectively, the time dependent rejection increased from 88.6 – 91.57, 96.35 – 97.56 and 97.9 – 98.2 % for membranes PM1, PM2 and PM3 respectively, which indicates that the membrane rejection increased with time and decreased with increasing average membrane pore size. The enhancement of membrane rejection with time is possibly due to the formation of dynamic concentration polarization layer and cake filtration layers on the membrane surface which further promote higher rejections with increasing time periods. Thus, the maximum rejection has been obtained for membrane PM3 (98.52 %) at a ΔP of 138 kPa. It can be also observed that the variation in rejection with a variation in membrane pore size has been insignificant for membranes PM2 and PM3 but not PM1. Thus, it is apparent that membrane PM1 with a higher average membrane pore size (3.06 μm) enabled the oil droplets to pass through the membrane and reach the permeate stream and thus provided lower rejection values (88.59 %). Similar rejection profiles have been obtained for all membranes at higher cross flow velocities. The insignificant variation of membrane rejection with deviation in membrane morphology and ΔP is indicative towards the greater role of the concentration polarization

and cake filtration layers to contribute favourably towards the separation of oil-water emulsions.

Amongst all membranes, membrane PM3 provided highest rejection (98.52 %) and lowest flux (11.5×10^{-6} $m^3/m^2.s$) after 30 minutes of MF run at Re = 3417 and ΔP of 138 kPa. Membrane PM1 provided lowest rejection (88.59 %) and highest flux (31.5×10^{-6} $m^3/m^2.s$) after 30 minutes of MF run at Re = 3417 and a ΔP of 207 kPa. At a ΔP of 207 kPa, Figure 3.3 a and 3.3 b present the time dependent flux and rejection respectively for the PM3

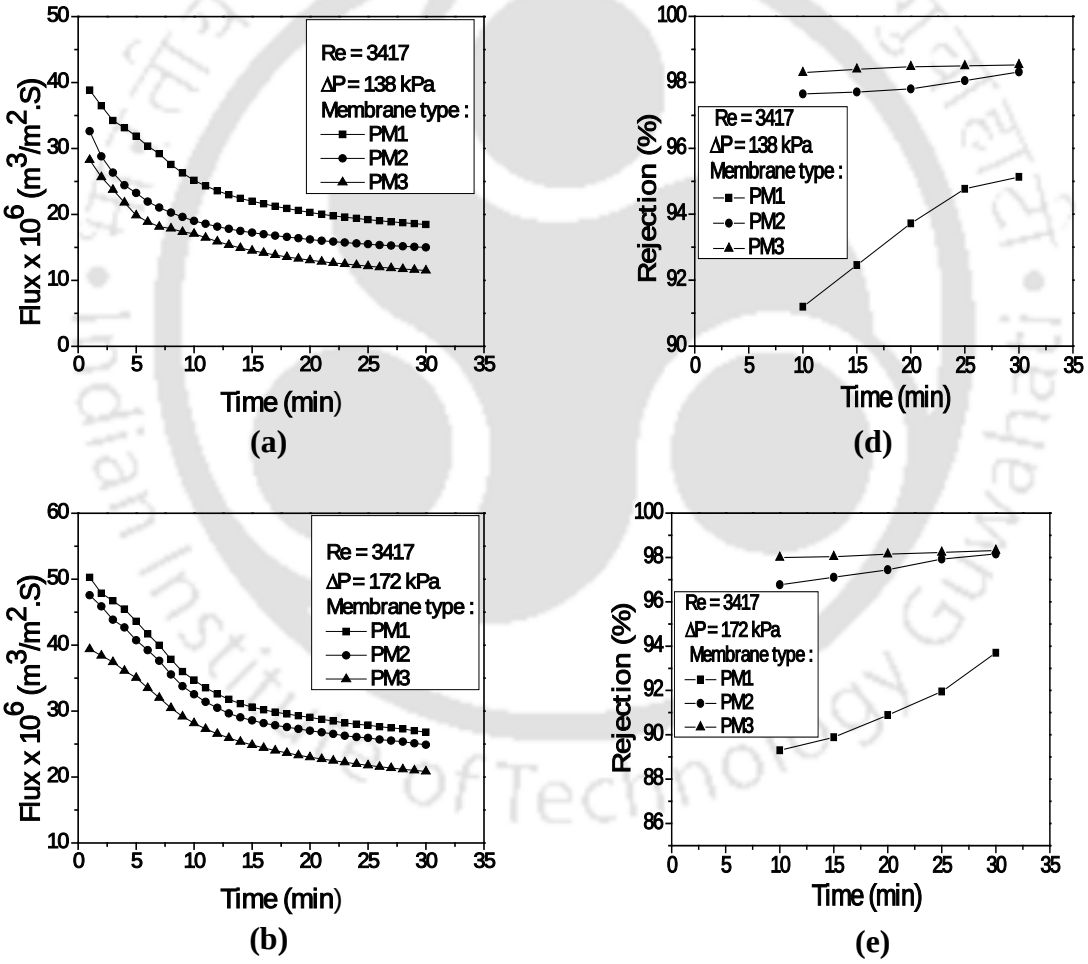

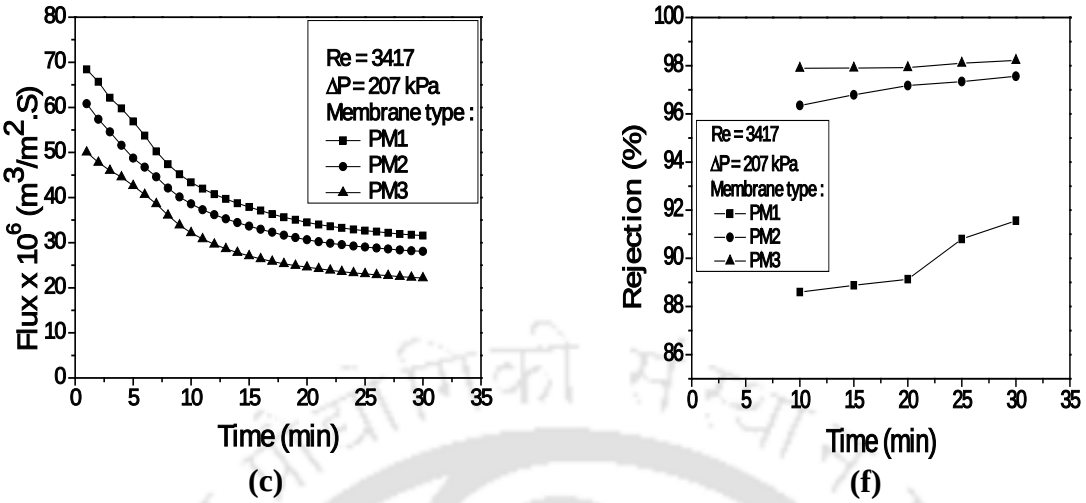

Figure 3.2: Variation of time dependent permeate flux (a – c) and rejection (d –f) with ΔP for PM1 – PM3 membranes at Re = 3417.

membrane as a function of cross flow velocity (Reynolds number). As shown, distinct flux profiles have been obtained for the PM3 membrane at various cross flow velocities. Thus, it has been observed that the fluid cross flow velocity strongly influences the flux decline which involves a short term decline of flux followed with a long term steady flux decline.

At a ΔP of 207 kPa, for the PM3 membrane, it has been observed that the steady state flux varied from 50.0 - 22.1 × 10^{-6} m^3/m^2.s at Re = 3417 which increased to 60.4 - 26.7 × 10^{-6} m^3/m^2.s at Re = 5126 and 64.4 - 29.9 × 10^{-6} m^3/m^2.s at Re = 6835 respectively. A critical observation of time dependent rejection profiles for the membrane PM3 at ΔP = 207kPa indicates that the rejection values are strongly influenced with cross flow velocity but were relatively insignificant with variation in time. For the membrane PM3, the rejection values decreased with increasing cross flow velocity (or Reynolds number), which is in agreement with the hypothesis that higher cross flow velocity increases the porosity of the dynamic cake

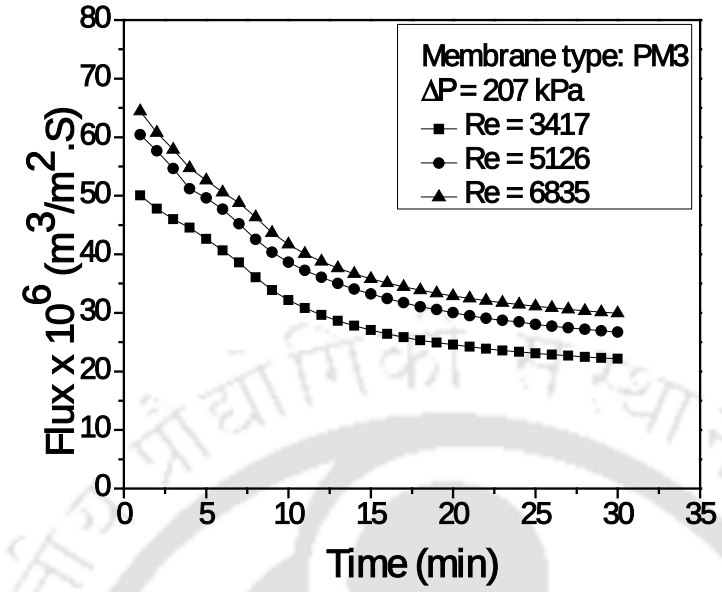

(a)

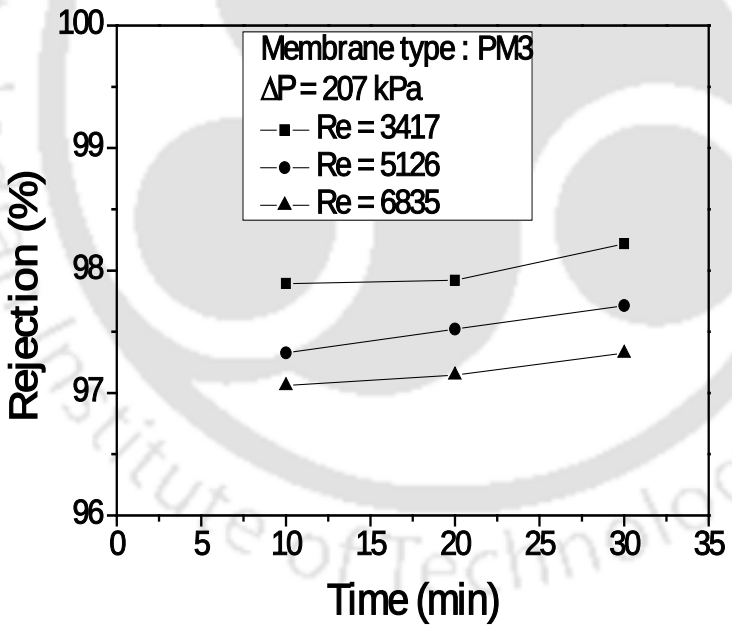

(b)

Figure 3.3: Variation of PM3 membrane time dependent (a) flux and (b) rejection for various cross flow velocities (Reynolds number = 3417, 5126 and 6835) at ΔP = 207 kPa.

filtration layer which in turn enables a reduction in the concentration of crude oil in the permeate streams. Nonetheless, the variation in rejection with variation in cross flow velocity is not above 1 % (from 97 to 98 %) for the PM3 membrane. This is possibly due to the lower average membrane pore size of the PM3 membrane, due to which the cross flow velocity could not strongly influence the morphology of the dynamic cake filtration layer during the microfiltration operation.

3.2.3 Steady state membrane performance

Figure 3.4 a and 3.4 b summarize the variation of steady state membrane flux and rejection respectively with cross flow velocity (Reynolds number) at various values of trans membrane pressure differential (ΔP) for the PM1 membrane. It can be observed that the steady state membrane flux increased and rejection decreased non-linearly with increasing cross flow velocity. This confirms that the membrane performance characteristics are strongly influenced with both cross flow velocity and trans membrane pressure drop. For instance, the steady state flux (PM1 membrane) varied from 18.4 – 31.5 × 10^{-6} $m^3/m^2.s$ at ΔP = 138 kPa, which increased to 35.7 – 44.1 × 10^{-6} $m^3/m^2.s$ at ΔP = 207 kPa for an increase in Reynolds number from 3417 - 6835. On the other hand, the steady state rejection (for PM1 membrane) reduced from 93.12 – 88.35 % at ΔP = 207 kPa, which increased to 95.13 – 91.57 % at ΔP = 138 kPa and enhanced Reynolds number from 3417 - 6835. The simultaneous enhancement in steady state flux and reduction in rejection with increasing cross flow velocity and ΔP is due to the strong influence of these parameters on the fouling characteristics during the microfiltration operation. An enhancement in cross flow velocity minimizes the role of concentration polarization and gel layer hydraulic resistance in the overall fluid transport

resistance. Thus, the observations are in good agreement with the mentioned hypothesis that elaborates upon the flux decline during the microfiltration process.

The effect of membrane fabrication pressure (PM1, PM2 and PM3 membranes) on the steady state flux at ΔP = 207 kPa and various cross flow velocities (Reynolds number) is presented in Figure 3.4 c. As shown, for all cases of cross flow velocities, the steady state membrane flux decreased with increasing membrane fabrication pressure due to the reduction in average membrane pore size. Also, significantly distinct steady state flux profiles were obtained for various sets of cross flow velocity. For instance, the steady state flux varied from 22.1 – 31.5 × 10^{-6} m^3/m^2.s at Re = 3417, which increased to 29.9 – 44.1 × 10^{-6} m^3/m^2.s at Re = 6835 for an enhancement in the membrane fabrication pressure from 25 (PM1 membrane) to 73 MPa (PM3 membrane). Similar trends have been observed for the steady state rejection profiles (Figure 3.4 d). However, the steady state rejection profiles are close to one another, which is not the case with the flux profiles. For instance, the steady state rejection varied from 88.35 – 91.57 % at Re = 3417, which increased marginally to 97.33 – 98.22 % for Re = 6835 for a variation in the membrane fabrication pressure from 25 – 73 MPa at ΔP = 207 kPa.

The enhancement in the rejection for the membranes with increasing fabrication pressure is due to the reduction in the average membrane pore size. In other words, the variation in steady state rejection is not as significant as observed for flux data with an increase in the cross flow velocity. Thus, the influence of dynamic cake filtration layer is more significant for the membrane flux but not rejection. The insignificant variation in rejection with variation in cross flow velocity is due to the greater contributions of dynamic polarization and cake filtration layer resistances towards achieving good separation characteristics.

Figure 3.4e presents the variation of steady state flux with membrane fabrication pressure (PM1, PM2 and PM3) at highest cross flow velocity (Re = 6835) and various cases of ΔP. It can be observed that the steady state flux is maximum for ΔP = 207 kPa and reduced with increasing membrane fabrication pressure. This is due to the significant reduction in average membrane pore size (from 3.06 – 2.16 µm) with increasing membrane fabrication pressure from 25 (PM1 membrane) to 73 MPa (PM3 membrane). On the other hand, the steady state rejection profiles confirmed upon increasing trends in steady state rejection values with increasing membrane fabrication pressure (Figure 3.4 f).

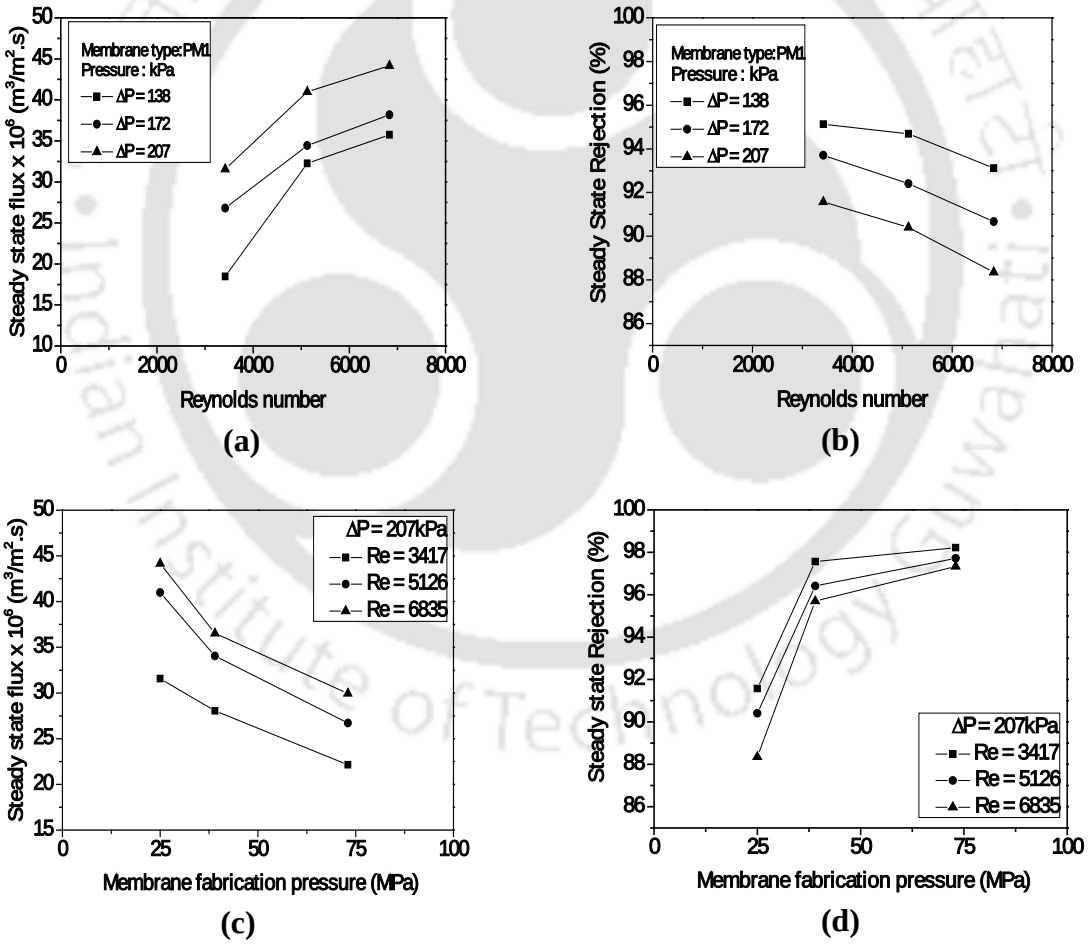

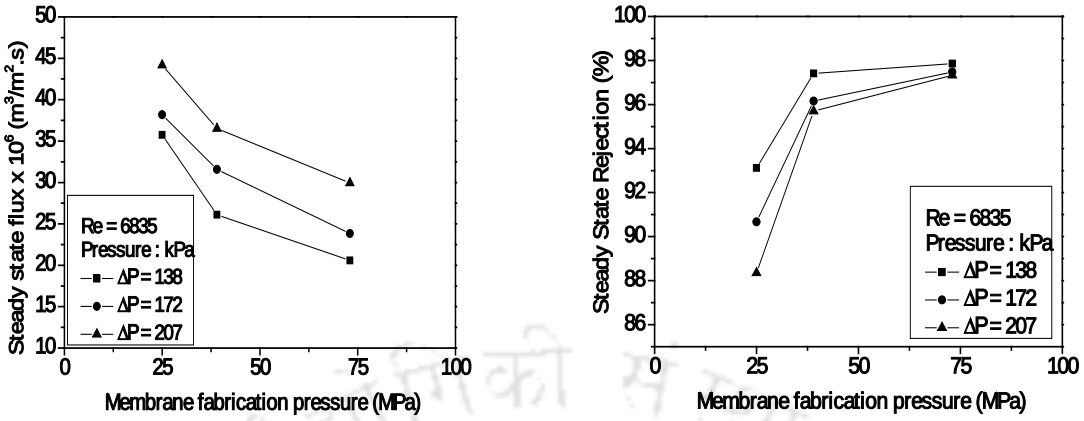

Figure 3.4: (a) Steady state flux and (b) rejection variation with cross flow velocity (Reynolds number) for PM1 membrane (c) Steady state flux and (d) rejection variation with fabrication pressure at ΔP = 207 kPa and Re = 3417 – 6835 (e) Steady state flux and (f) rejection variation with fabrication pressure at Re = 6835 and ΔP = 138 – 207 kPa.

Table 3.2 summarizes the comparative performance of the microfiltration data obtained in this work with those reported by other researchers for the cross flow microfiltration of oil-water emulsions with ceramic and polymeric membranes. It can be observed that the literature data consists of data taken at fairly different values of feed concentrations than those reported in this work. In the field of low cost ceramic membranes, the data obtained in this work is only comparable with that obtained by Abbasi *et al.* [17] and Vasanth *et al.* [11]. Further, when the feed concentrations are compared, the literature data of Abbasi *et al.* [17] can be only compared with the steady state flux and rejection data obtained in this work.

Overall, it has been observed that the obtained combinations of steady state flux and rejection values are comparable with those presented in the literature for both polymeric and

Table 3.2: A summary of obtained (PM1, PM3) and literature steady state flux and rejection data during cross flow MF of oil-water emulsions.

S.No.	Author	Type of membrane	Average membrane properties		Feed concentration (mg/L)	Time (min)	Steady state flux × 10^6 ($m^3/m^2.s$)	Pressure diffrential (kPa)	Rejection (%)	Cross flow conditions
			Pore size (µm)	Porosity (%)						
1.	Vasanth et al. [11]	Low cost ceramic membrane	1.06	26	100	60	55.4	207	87	Q = 13.9 × 10^{-7} m^3/s
2.	Singh et al. [24]	Polymeric (Commercial)	1.16	-	192	30	3.35	207	97.8	Re = 5769, v = 1.5 m/s
3.	Abbasi et al. [17]	Mullite - ceramic	0.57	32	500	120	27.7	305.1	93.8	v = 1.5 m/s
4.	Abadi et al. [20]	α – alumina (Commercial)	0.2	> 33	92	90	69.4	127.1	95	v = 2.25 m/s .
5.	This work	Low cost ceramic membrane	3.06	30.1	400	30	44.1	207	88.35	Re = 6835, v = 0.2688 m/s
6.	This work	Low cost ceramic membrane	2.16	37.4	400	30	22.14	207	98.52	Re = 3417, v = 0.1344 m/s

ceramic membranes. Further, it can be observed that the steady state flux obtained in this work corresponds to 22.1 – 44.1 × 10^{-6} $m^3/m^2.s$ at ΔP = 207 kPa, which is higher than the flux reported by Abbasi *et al.* [10] (27.7 × 10^{-6} $m^3/m^2.s$ at ΔP = 305.1 kPa). In terms of rejection, the data reported in this work varied from 88.35 – 98.52 % which is comparable with the rejections reported by Abbasi *et al.* [17], Abadi *et al.* [20] and Stack *et al.* [59]. Thus, it is apparent that the cross flow microfiltration data presented in this work is comparably better than that presented in the literature, as fairly higher fluxes at similar rejections have been obtained in this work. This is due to the fact that the fouling indices were evaluated to be insignificant which also indicates that the membrane morphologies are compatible with the particle size distributions of oil - water emulsions. Also, the comparative assessment of flux and rejection data obtained in this work indicates that the carried out research in this work could supplement as benchmark data in the field of cross flow microfiltration of oil water emulsions using low cost ceramic membranes.

A general rule of thumb for membrane separation processes is that they are highly cost effective to process wastewater streams with lower pollutant concentrations. As presented in in the previous paragraph, the results obtained in this work are comparatively better than those reported in the literature for ceramic as well as polymeric membranes in terms of flux and rejection. Thus, it is inferred that the operating cost of the low cost ceramic membrane shall be comparable to that of the polymeric membranes that have been deployed in industrial practice. Moreover, since the prepared low cost ceramic membranes possess better corrosion resistance and hence about 30 – 40 % reduction in operating cost is expected in comparison with the commercial polymeric membranes. Further, process engineering studies in this direction would be extremely beneficial to consolidate the commercialization of low cost ceramic membranes for wastewater treatment.

3.2.4 Fouling index

Figure 3.5 (a) and (b) summarize the variation of fouling indices for membranes PM1 – PM3 at various operating conditions. As shown in Figure 3.5 (a), the fouling index varied from 19.75 – 39.73 %, 17.35 – 34.65 % and 11.58 – 26.77 % for a variation in Reynolds number from 3417 - 6835 for the membranes PM1 – PM3 respectively. Minimal fouling has been obtained for the PM3 membrane. This is due to its lower average pore size (2.16 µm). This is not the case for the PM1 and PM2 membranes whose average pore size is 3.06 and 2.32 µm respectively. At Re = 6835 and ΔP = 207 kPa, the fouling index (%) for various membranes PM1 – PM3 is also shown in Figure 3.5 (a) which indicates that the fouling index of about 40 % exists for PM1 and reduces to about 25 % for the PM3 membrane. In other words, higher average membrane pore size can be analyzed to be not favourable for the cross flow MF. The effect of the variation of ΔP on the fouling index for all membranes at a Reynolds number of 6835 is presented in Figure 3.5 (b), which indicates that the fouling index for PM3 membrane is minimal at highest ΔP (207 kPa). Therefore, it is apparent that the membranes PM1 and PM2 underwent significant fouling for the chosen application and only membrane PM3 provided lowest fouling index. For comparative purposes with literature, relevant data could not be found and this work emphasized upon the relevance of fouling index for the development of low cost ceramic membranes.

3.2.5 Fitness of fouling models

A preliminary assessment of the obtained flux decline data for the developed low cost ceramic membranes indicated that either of the fouling models (namely complete pore blocking (CPB), standard pore blocking (SPB), intermediate pore blocking (IPB) and cake filtration

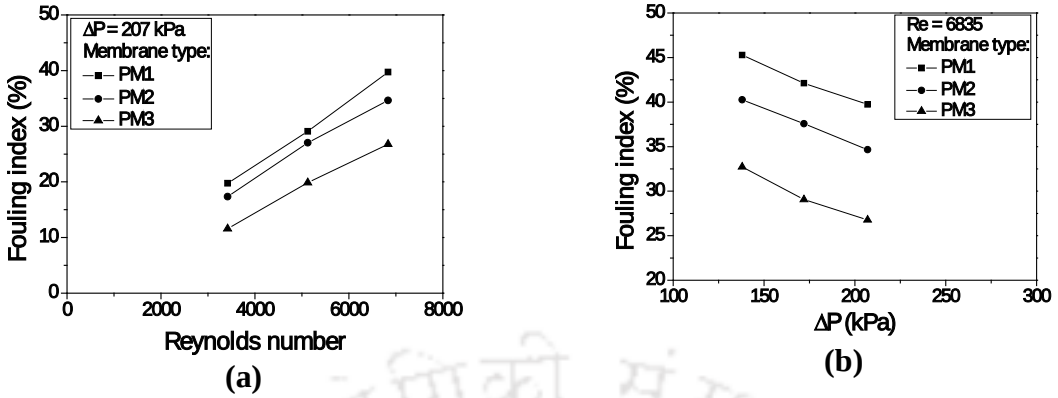

Figure 3.5: Variation of fouling index (%) with (a) cross flow velocity (Reynolds number) for PM1 – PM3 membranes at ΔP = 207kPa (b) with ΔP for PM1 – PM3 membranes at Re = 6835.

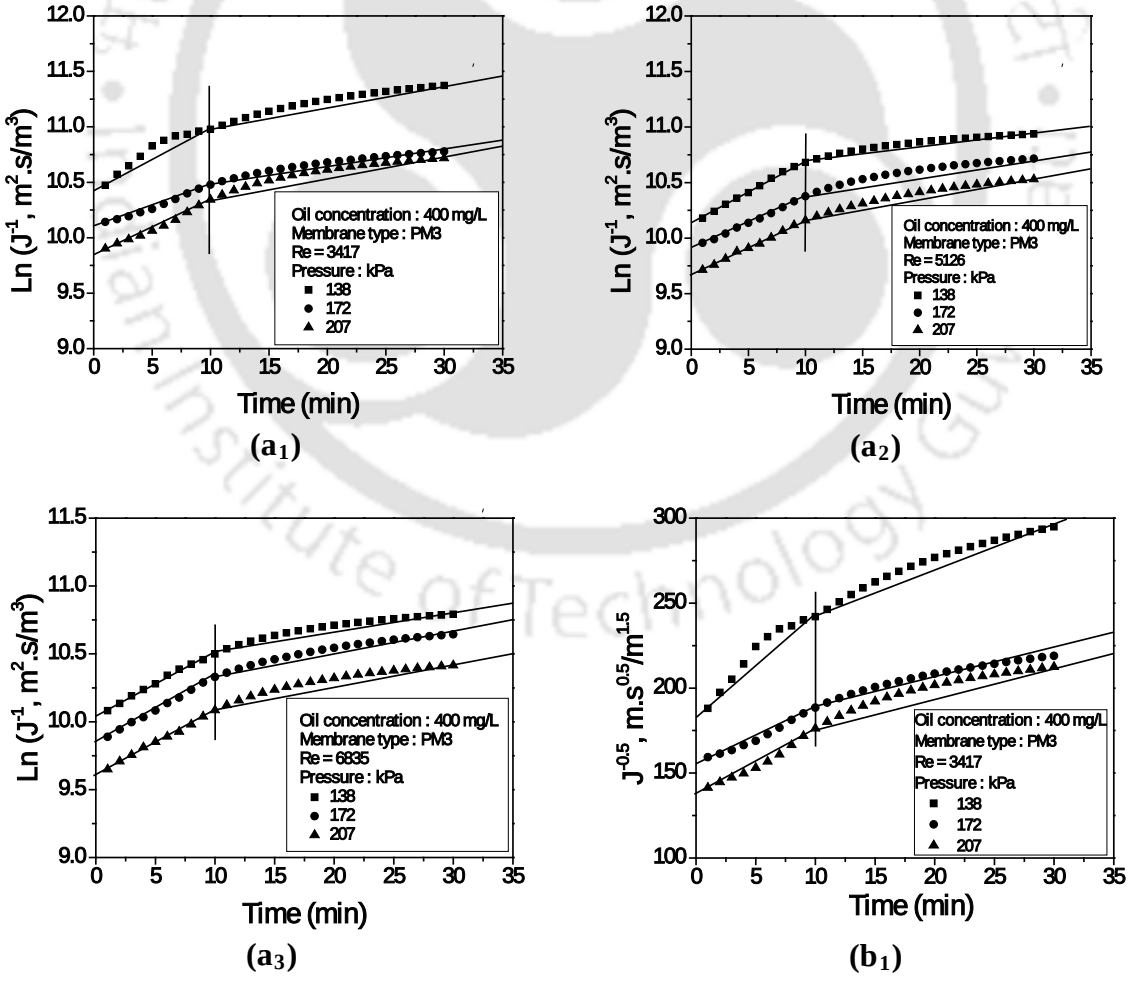

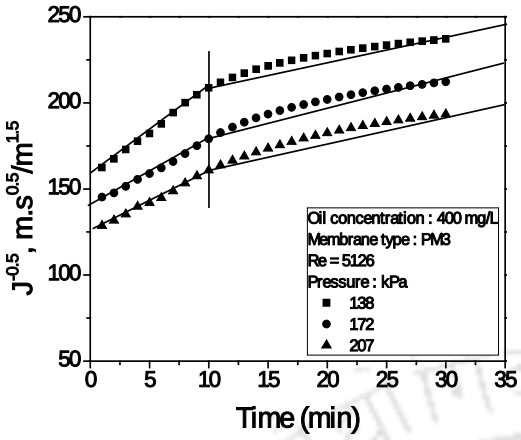

(b2)

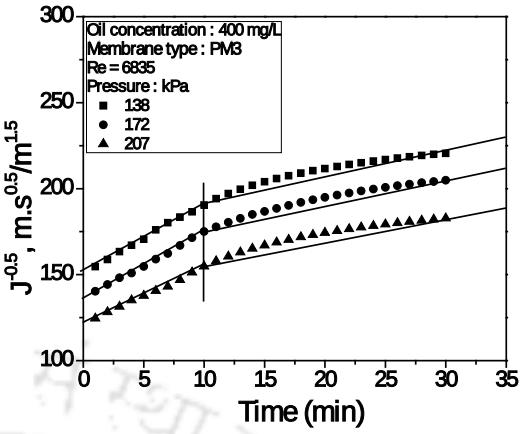

(b3)

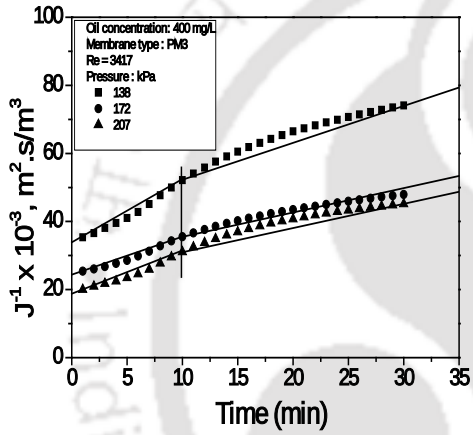

(c1)

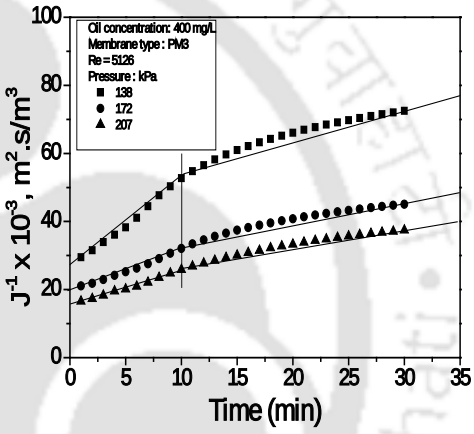

(c2)

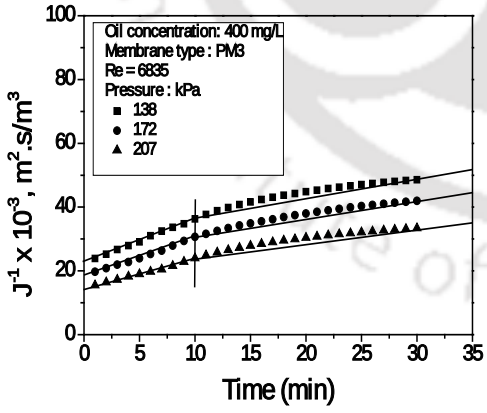

(c3)

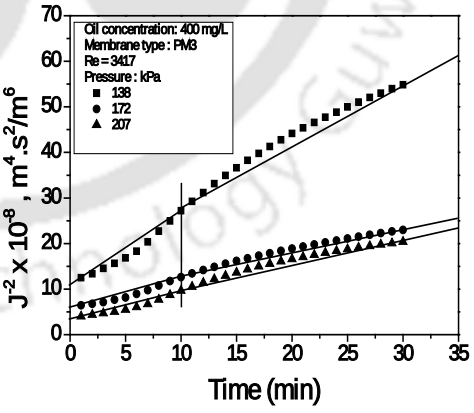

(d1)

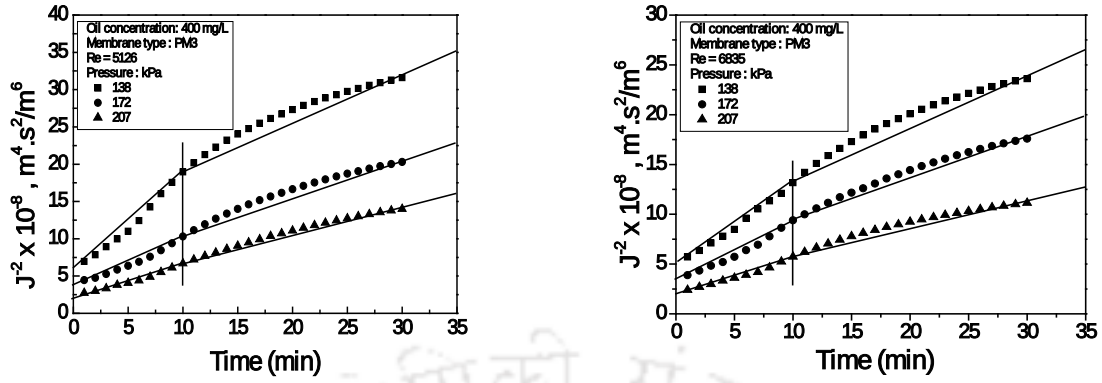

(d_2) **(d_3)**

Figure 3.6: Linearized fitness plots for various fouling models (CPB: $a_1 - a_3$; SPB: $b_1 - b_3$; IPB: $c_1 - c_3$; CF: $d_1 - d_3$) for the PM3 membranes at Re = 3417, Re = 5126 and Re = 6835.

(CF)) has not able to fit well with the data. Therefore, modelling effort has been dovetailed towards the fitness of the fouling models for two distinct combinations of the flux decline data. These correspond to the first 10 minutes of the experimental MF run and the later 11 – 30 minutes MF data. Since PM3 membrane provided lowest fouling indices values, the fitness of combination models has been illustrated in Figure 3.6 for the PM3 membrane at a Reynolds number of 3417, 5126 and 6835, respectively. Corresponding correlation coefficients (R^2) for all membranes have been presented in Table 3.3. It can be observed in Table 3.3 that for all models R^2 values are in acceptable range (0.95 – 0.99). Corresponding root mean square error (RMS error) values have been evaluated to be in the range of 0.76 – 2.12 (0.95) to 0.36 – 0.56 % (0.99). In other words, only for few best fit models, they are the lowest (R^2 = 0.99) which have been regarded to be the best fit combination models to represent the observed flux decline trends.

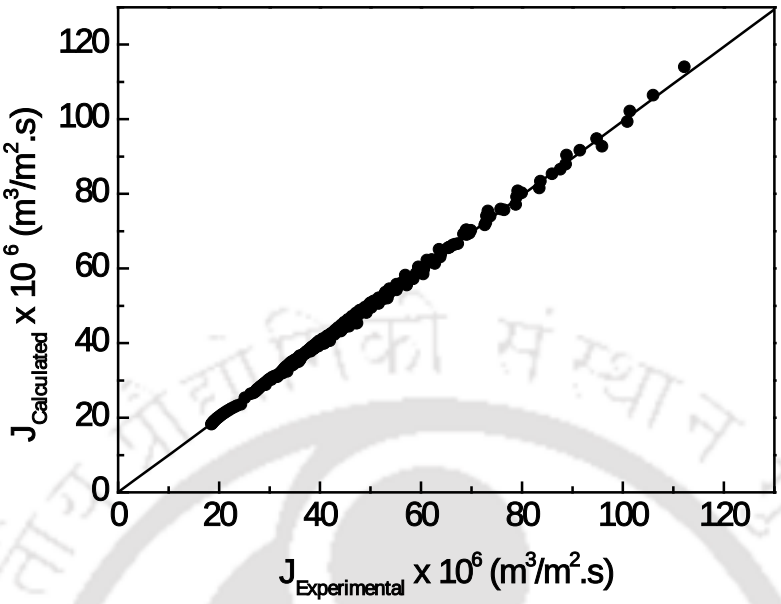
120
100
80
60
40
20
0
0
20
40
60
80
100
120
$J_{Calculated}$ x 10^6 ($m^3/m^2.s$)
$J_{Experimental}$ x 10^6 ($m^3/m^2.s$)

(a)

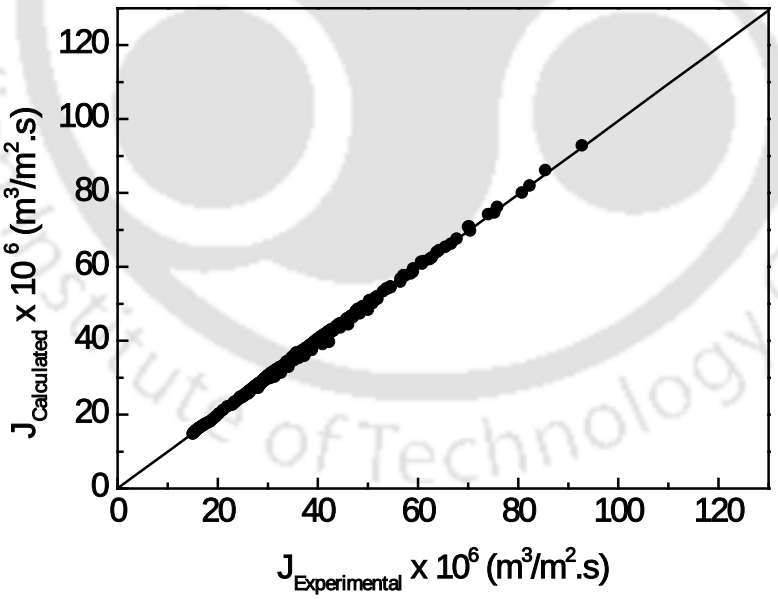
120
100
80
60
40
20
0
0
20
40
60
80
100
120
$J_{Calculated}$ x 10^6 ($m^3/m^2.s$)
$J_{Experimental}$ x 10^6 ($m^3/m^2.s$)

(b)

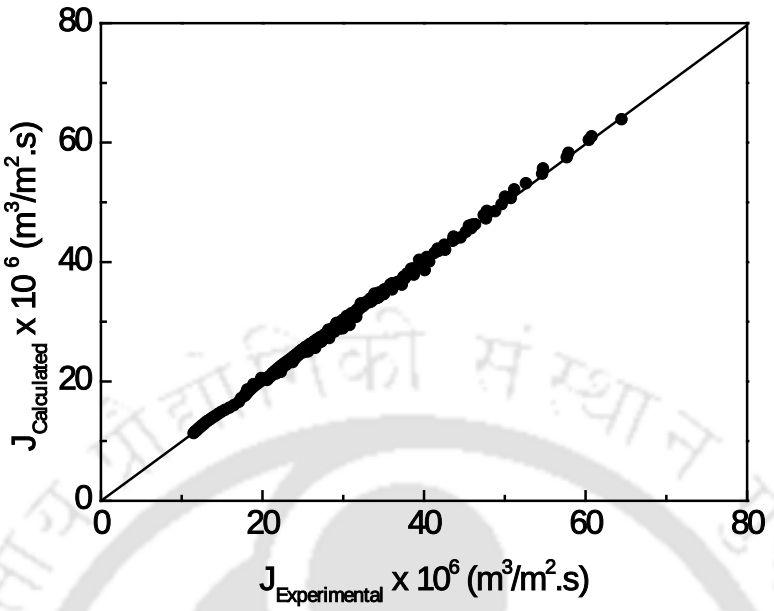

(c)

Figure 3.7: Parity plots for the fitness of various best fit combination fouling models for (a) PM1 (b) PM2 and (c) PM3 membrane.

Table 3.4 summarize the slope and intercept values for the best fit combination models to represent observed flux decline data for all membranes. It can be observed that for the membranes PM1 – PM3, the initial membrane flux (within 10 minutes of MF operation) for several cases occurred with pore blocking and only for few cases cake filtration model fit well to represent the measured flux data in the time domain. This indicates that the membranes are susceptible for pore blocking during the initial stages of microfiltration operation, which is also confirmed with the higher fouling index values obtained for the membranes. The onset of pore blocking during the initial stages of microfiltration is not a desired objective, given the fact that pore blocking significantly accounts towards irreversible membrane fouling.

Table 3.3: Evaluated correlation coefficient (R^2) values for various combination fouling models for PM1-PM3 membranes.

Membrane Name	Pressure (kPa)	Reynolds number	Complete pore blocking		Standard pore blocking		Intermediate pore blocking		Cake filtration	
			Intial	Final	Intial	Final	Intial	Final	Intial	Final
PM1	138	3417	0.99	0.95	0.99	0.96	0.99	0.97	0.98	0.98
	172		0.99	0.95	0.95	0.98	0.98	0.96	0.96	0.97
	207		0.99	0.94	0.99	0.98	0.98	0.96	0.97	0.97
	138	5126	0.99	0.97	0.99	0.98	0.98	0.98	0.97	0.99
	172		0.99	0.95	0.99	0.96	0.99	0.97	0.99	0.98
	207		0.98	0.95	0.99	0.95	0.99	0.96	0.99	0.97
	138	6835	0.99	0.93	0.99	0.94	0.99	0.95	0.98	0.96
	172		0.99	0.97	0.99	0.98	0.99	0.98	0.97	0.99
	207		0.99	0.95	0.98	0.96	0.98	0.96	0.97	0.98
PM2	138	3417	0.94	0.96	0.96	0.97	0.97	0.97	0.99	0.98
	172		0.99	0.95	0.99	0.95	0.98	0.96	0.97	0.97
	207		0.99	0.94	0.99	0.95	0.99	0.96	0.99	0.97
	138	5126	0.99	0.97	0.99	0.98	0.99	0.98	0.97	0.99
	172		0.99	0.95	0.99	0.96	0.99	0.97	0.97	0.98
	207		0.99	0.95	0.99	0.96	0.98	0.96	0.97	0.98
	138	6835	0.99	0.95	0.99	0.95	0.99	0.96	0.99	0.97
	172		0.99	0.89	0.99	0.91	0.99	0.92	0.98	0.94
	207		0.99	0.95	0.99	0.96	0.99	0.96	0.98	0.98
PM3	138	3417	0.92	0.96	0.94	0.97	0.95	0.97	0.97	0.99
	172		0.99	0.96	0.98	0.97	0.98	0.98	0.96	0.98
	207		0.98	0.94	0.98	0.95	0.97	0.96	0.95	0.97
	138	5126	0.99	0.94	0.99	0.95	0.99	0.96	0.98	0.97
	172		0.99	0.95	0.96	0.96	0.99	0.96	0.97	0.98
	207		0.99	0.96	0.99	0.97	0.99	0.97	0.98	0.98
	138	6835	0.99	0.94	0.99	0.95	0.99	0.96	0.99	0.97
	172		0.99	0.96	0.99	0.97	0.99	0.97	0.98	0.98
	207		0.99	0.94	0.99	0.95	0.99	0.96	0.98	0.97

Table 3.4: **A summary of parameters for the best fit combination models during cross flow MF of oil-water emulsions for PM1 – PM3 membranes.**

Membrane Name	Pressure (kPa)	Reynolds number	Initial			Final		
			Model	Slope	Intercept	Model	Slope	Intercept
PM1	138	3417	SPB	$k_s = 4.21\ m^{-0.5}\ s^{-0.5}$	$J^{-0.5} = 156.8$	CF	$k_c = 6.40 \times 10^{-7}\ s.m^{-2}$	$J_o^{-2} = 10.9 \times 10^8$
	172		CPB	$k_b = 0.041\ s^{-1}$	$\ln(J_o^{-1}) = 9.85$	CF	$k_c = 2.42 \times 10^{-7}\ s.m^{-2}$	$J_o^{-2} = 6.87 \times 10^8$
	207		CPB	$k_b = 0.052\ s^{-1}$	$\ln(J_o^{-1}) = 9.53$	CF	$k_c = 2.31 \times 10^{-7}\ s.m^{-2}$	$J_o^{-2} = 3.52 \times 10^8$
	138	5126	CPB	$k_b = 0.054\ s^{-1}$	$\ln(J_o^{-1}) = 9.46$	CF	$k_c = 2.34 \times 10^{-7}\ s.m^{-2}$	$J_o^{-2} = 2.79 \times 10^8$
	172		SPB	$k_s = 3.45\ m^{-0.5}\ s^{-0.5}$	$J^{-0.5} = 109.5$	CF	$k_c = 1.99 \times 10^{-7}\ s.m^{-2}$	$J_o^{-2} = 2.68 \times 10^8$
	207		CF	$k_c = 1.81 \times 10^{-7}\ s.m^{-2}$	$J_o^{-2} = 1.01 \times 10^8$	CF	$k_c = 1.57 \times 10^{-7}\ s.m^{-2}$	$J_o^{-2} = 1.52 \times 10^8$
	138	6835	SPB	$k_s = 4.32\ m^{-0.5}\ s^{-0.5}$	$J^{-0.5} = 100.9$	CF	$k_c = 1.73 \times 10^{-7}\ s.m^{-2}$	$J_o^{-2} = 2.97 \times 10^8$
	172		CPB	$k_b = 0.075\ s^{-1}$	$\ln(J_o^{-1}) = 9.12$	CF	$k_c = 1.62 \times 10^{-7}\ s.m^{-2}$	$J_o^{-2} = 2.13 \times 10^8$
	207		CPB	$k_b = 0.069\ s^{-1}$	$\ln(J_o^{-1}) = 9.01$	CF	$k_c = 1.26 \times 10^{-7}\ s.m^{-2}$	$J_o^{-2} = 1.54 \times 10^8$
PM2	138	3417	CF	$k_c = 20.1 \times 10^{-7}\ s.m^{-2}$	$J_o^{-2} = 8.19 \times 10^8$	CF	$k_c = 8.00 \times 10^{-7}\ s.m^{-2}$	$J_o^{-2} = 21.5 \times 10^8$
	172		CPB	$k_b = 0.042\ s^{-1}$	$\ln(J_o^{-1}) = 9.91$	CF	$k_c = 2.88 \times 10^{-7}\ s.m^{-2}$	$J_o^{-2} = 7.72 \times 10^8$
	207		SPB	$k_s = 3.66\ m^{-0.5}\ s^{-0.5}$	$J^{-0.5} = 124.5$	CF	$k_c = 2.92 \times 10^{-7}\ s.m^{-2}$	$J_o^{-2} = 4.46 \times 10^8$
	138	6835	IPB	$k_i = 2658\ m^{-1}$	$J_o^{-1} = 34.65 \times 10^{-3}$	CF	$k_c = 3.12 \times 10^{-7}\ s.m^{-2}$	$J_o^{-2} = 5.77 \times 10^8$
	172		SPB	$k_s = 4.13\ m^{-0.5}\ s^{-0.5}$	$J^{-0.5} = 106.3$	CF	$k_c = 2.06 \times 10^{-7}\ s.m^{-2}$	$J_o^{-2} = 4.07 \times 10^8$
	207		SPB	$k_s = 3.99\ m^{-0.5}\ s^{-0.5}$	$J^{-0.5} = 99.77$	CF	$k_c = 1.84 \times 10^{-7}\ s.m^{-2}$	$J_o^{-2} = 2.25 \times 10^8$

Membrane Name	Pressure (kPa)	Reynolds number	Initial			Final		
			Model	**Slope**	**Intercept**	**Model**	**Slope**	**Intercept**
PM3	138	3417	CF	$k_c = 25.5 \times 10^{-7}$ s.m^{-2}	$J_o^{-2} = 10.9 \times 10^8$	CF	$k_c = 20.3 \times 10^{-7}$ s.m^{-2}	$J_o^{-2} = 16.8 \times 10^8$
	172		CPB	$k_b = 0.038$ s^{-1}	$\ln(J_o^{-1}) = 10.08$	CF	$k_c = 4.94 \times 10^{-7}$ s.m^{-2}	$J_o^{-2} = 8.67 \times 10^8$
	207		CPB	$k_b = 0.048$ s^{-1}	$\ln(J_o^{-1}) = 9.84$	CF	$k_c = 5.07 \times 10^{-7}$ s.m^{-2}	$J_o^{-2} = 5.95 \times 10^8$
	138	5126	SPB	$k_s = 5.27$ m$^{-0.5}$ s$^{-0.5}$	$J^{-0.5} = 156.8$	CF	$k_c = 5.79 \times 10^{-7}$ s.m^{-2}	$J_o^{-2} = 15.1 \times 10^8$
	172		CPB	$k_b = 0.047$ s^{-1}	$\ln(J_o^{-1}) = 9.90$	CF	$k_c = 4.71 \times 10^{-7}$ s.m^{-2}	$J_o^{-2} = 6.82 \times 10^8$
	207		CPB	$k_b = 0.049$ s^{-1}	$\ln(J_o^{-1}) = 9.67$	CF	$k_c = 3.59 \times 10^{-7}$ s.m^{-2}	$J_o^{-2} = 3.68 \times 10^8$
	138	6835	IPB	$k_i = 1388$ m^{-1}	$J_o^{-1} = 22.46 \times 10^{-3}$	CF	$k_c = 4.82 \times 10^{-7}$ s.m^{-2}	$J_o^{-2} = 9.94 \times 10^8$
	172		CPB	$k_b = 0.048$ s^{-1}	$\ln(J_o^{-1}) = 9.85$	CF	$k_c = 3.99 \times 10^{-7}$ s.m^{-2}	$J_o^{-2} = 6.14 \times 10^8$
	207		CPB	$k_b = 0.046$ s^{-1}	$\ln(J_o^{-1}) = 9.62$	CF	$k_c = 2.53 \times 10^{-7}$ s.m^{-2}	$J_o^{-2} = 3.93 \times 10^8$

For all cases, cake filtration represents the measured flux during the later stages of the microfiltration operation (from 11 to 30 minutes of MF operation). The fitness of cake filtration in the later stages of microfiltration is promising. This is due to the fact that cake filtration could refer to reversible membrane fouling.

Parity plots corresponding to the fitness of various best combination models for all experimental data are illustrated in Figure 3.7 (a – c) for membranes PM1 – PM3 respectively. Corresponding RMS errors for the combination models have been evaluated as 1.22, 1.22 and 1.23 % for membranes PM1, PM2 and PM3 respectively. The best experimental MF data corresponds to the microfiltration run carried out with PM3 membrane at ΔP = 207 kPa and Re = 3417, which provided the best fitness of CPB - CF models with regression coefficient values of 0.98 (CPB) and 0.97 (CF). Based on the corresponding intercept and slope values, the modeling constants correspond to the following set of values: $k_b = 0.048\ s^{-1}$, $\ln(J_0^{-1}) = 9.84$ for the initial 10 minutes and $k_c = 5.07 \times 10^{-7}\ s.m^{-2}$, $J_0^{-2} = 5.95 \times 10^8\ s^2/m^2$ for the later 11 – 30 minutes of the MF data.

Preparation and Characterization of Low Cost Ceramic Membranes for Mosambi Juice Clarification in Batch Mode

The objective of this chapter is to develop low cost ceramic membranes with appropriate pore size and porosity to obtain clarified mosambi juice with good combinations of flux and juice quality. In other words, the clarified juice shall posses minimal pectin content (expressed in alcohol insoluble solids), higher degree of clarity and citric acid and minimal reduction in ^{o}Brix. Therefore, the microfiltration operation shall retain sugars and flavoured components and shall eliminate haze and colloidal substances that contribute to the deterioration of the juice during long term storage. The subsequent sections of this chapter elaborate upon the experimental investigations carried out to realize the membrane morphologies and juice microfiltration.

4.1 Experimental

4.1.1 Ceramic membrane fabrication and characterization

In addition to polyvinyl alcohol (PVA, M.wt. 1, 15,000, Loba Chemicals Ltd., India), six different ceramic precursors namely kaolin (CDH, India), quartz (Research Lab Fine Chem Industry, India), calcium carbonate (Merck, India), sodium carbonate (Merck, India), boric acid (Merck, India) and sodium metasilicate (CDH, India), without any further

purification have been used to fabricate the low cost porous ceramic disk shaped membranes. The membrane fabrication procedure followed the composition and methodology outlined by Vasanth *et al.* [10] and consists steps similar to their work that involved a sequential procedure of raw -material preparation, preparation of membrane mould at various fabrication pressures, drying, sintering, polishing with silicon carbide abrasive paper of the prepared membranes followed with sonication using Millipore water to remove loose particles to obtain the final membranes. This work refers to two important variations in the procedures followed Vasanth *et al.* [10]. These are the outlined as follows. Firstly, the raw-materials have been screened through a 36 mesh standard screen instead of using 30 mesh standard screen [10]. Secondly, the hydraulic press (Make: Velan Engineering, Tamilnadu, India) fabrication pressures for various membranes are 29 (M1), 39 (M2) and 49 (M3) MPa instead of using 50 MPa. Hence, the fabricated membranes M1, M2 and M3 correspond to the membranes fabricated at 29, 39 and 49 MPa fabrication pressures respectively. The characterization procedures for all membranes are same as those presented in chapter 2 of the thesis.

4.1.2 Microfiltration studies using mosambi juice

Fresh mosambi juice (FJ) was obtained using depulped mosambi fruits (sweet orange, *Citrus sinensis (L) Osbeck*) in a manually operated screw type juice extractor. Centrifuged juice (CJ) was obtained using a centrifuge (Make: SORVALL, RC 5C PLUS) and enzyme treated centrifuged juice (ETCJ) was prepared by first carrying out enzymatic pretreatment of the juice followed with centrifugation at 4000 rpm for 20 min. The enzymatic pretreatment involved heating the juice at 42 ^{o}C for 100 min. with a pectinase enzyme concentration of 0.0004 w/v% [34] followed by heating at 90 ^{o}C for 5 min to inactivate the remaining enzyme.

Following this step, the juice was cooled to ambient temperature (25 ^{o}C) to undergo centrifugation. For all membranes (M1, M2 and M3), dead end MF was carried out using CJ and ETCJ at pressure differentials (ΔP) of 68.9, 137.8 and 206.70 kPa. The effective membrane area for permeation is 1.45×10^{-3} m^2. Further details with respect to the microfiltration experimental methodology are presented in chapter 2 of the thesis.

4.1.3 Analytical methods

Various analytical techniques are used to measure relevant parameters in FJ, CJ, ETCJ and permeate juice samples. The analytical procedures involved the measurement of particle size distribution using Laser particle size analyzer (Make: Malvern; Mastersizer 2000, UK); absorbance (at 420 nm) and Transmittance (at 660 nm) using UV-Vis spectrophotometer (Make: Perkin Elmer Precisel; Model: Lambda 35, USA); total soluble solids (TSS) using Digital Refractrometer (Make: Atago; Model: DR – A1, India); pH using water and soil analysis kit (Make: VSI Electronics, Model: VSI - 06D1, India); viscosity using a rheometer (Make: Thermo Electron Corporation; Model: HAAKE Rheostress 1) and density using Pycnometer. Other analytical measurements such as Acidity (in terms of equivalent citric acid wt %) and Alcohol insoluble solids (AIS) were measured using procedures summarized in the literature [9]. All membranes were cleaned after each experiment and fouling indices (FI) were evaluated by following procedures outlined in section 2.1.6 of the thesis.

4.1.4 Theory of membrane fouling mechanism

To analyze the existent fouling mechanism during dead end MF at constant pressure, Hermia [56] models namely; cake filtration, intermediate, standard and complete pore blocking models are considered. These models are explained in section 2.1.7 of the thesis. The fitness of the flux decline data with any one of the above 4 models can be obtained by

analyzing the coefficient of correlation (R^2) values corresponding to the experimental data. The identification of most competent flux decline model will enable to examine the extent of reversible and irreversible fouling. For instance, complete pore blocking may correspond to maximum irreversible fouling and cake filtration may correspond to maximum reversible fouling and hence the onset of cake filtration during juice MF is highly appreciable to minimize fouling effect and easy restoration of flux after cleaning operation.

4.2 Results and discussion

4.2.1 Membrane characterization results

Figure 4.1 (a) presents the variation of weight loss (%) as a function of temperature for the raw material mixture. It can be observed that while sufficient weight losses existed below 800 ^{o}C, very significant weight loss existed from 900 – 1000 ^{o}C. Hence, the maximum sintering temperature of 900 ^{o}C is acceptable for the fabrication of the membranes. Also, it can be observed that weight decline up to 120 ^{o}C was due to the loss of moisture. Further, weight reduction occurred at 710 ^{o}C, where decarbonisation of carbonate salts occurs. Figure 4.1 (b) presents the XRD patterns for un sintered raw material mixture and M3 membrane sintered at 900 ^{o}C. It can be observed from the figure that kaolin related peaks disappeared in the membrane sample sintered at 900 ^{o}C, thus indicating the conversion of kaolinite and metakaolinite at the sintering temperature. The XRD patterns also indicate the existence of several nepheline and quartz peaks along with inyoite phase for the sintered membrane.

Figure 4.2 presents the FESEM images for all membranes and indicates highly porous and rough surface morphologies. The images also indicate the absence of pin holes and cracks with maximum observable pore size of 2 – 4 μm. Figure 4.3 (a) illustrates the variation of pure water flux with applied pressure for all the membranes. The pure water flux varied from

4.63 to 18.64 × 10^{-4}, 5.33 to 21.47 × 10^{-4} and 1.31 to 5.19 × 10^{-4} m^3/m^2.s with a variation in applied pressures from 68.9, 137.8, 206.7 and 276 kPa for M1, M2 and M3 membranes respectively. The variation in the average porosity of the membranes (determined using Archimedes principle) with fabrication pressure is shown in Figure 4.3 (b). With an increase in fabrication pressure from 29 to 49 MPa, the membrane porosity increased from 35.4 – 39.4 %. The increase in membrane porosity with fabrication pressure is due to the finer arrangement of the raw materials in the porous texture at increased fabrication pressure, which enabled higher surface area at lower pore sizes. Using Haigen – poiseullie equation, average porosity and hydraulic permeability, the average pore size of the membrane was evaluated to vary from 1.69 to 0.72 µm for the membranes. Vasanth *et al.* [10] reported the average pore size of 2.60 µm and porosity of 40 % at a fabrication pressure of 50 MPa. The variation in membrane morphology in this work is possibly due to reduction in particle size of the inorganic precursors.

Subsequent analysis for the pore size distribution by using Image J software (Version 1.40) was performed and the evaluated pore size distributions indicated that less than 10 % of the pores had diameters within the range of 3 – 15 µm for all the membranes (M1, M2 and M3) and distinct pore size distributions existed for the membranes within the range of 0 – 3 µm. For M1, M2 and M3 membranes, upto 45 %, 35 % and 25 % pores have been analyzed in the range of 0 – 2, 0 – 1.75 and 0 – 1 µm respectively. Based on the FESEM image analysis using Image J software, the average pore size of the membranes is 1.85, 1.78 and 0.89 µm for membranes M1, M2 and M3 respectively, which is in agreement with the pore size determined from hydraulic permeability and porosity studies.

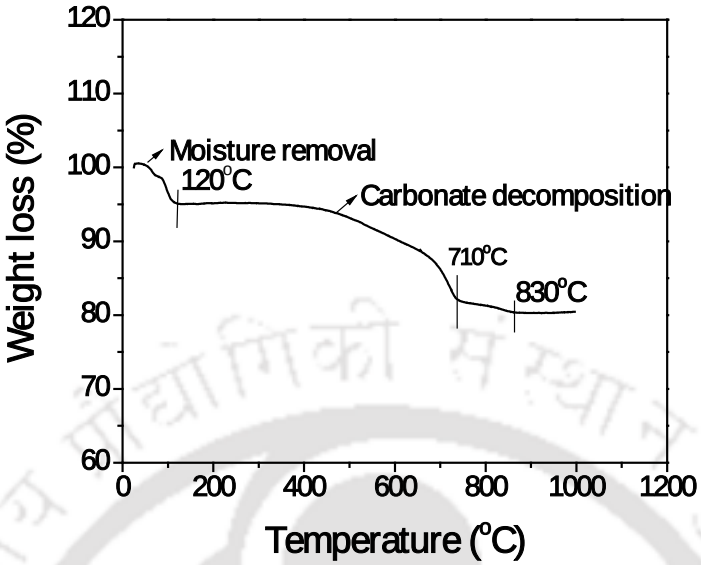

(a)

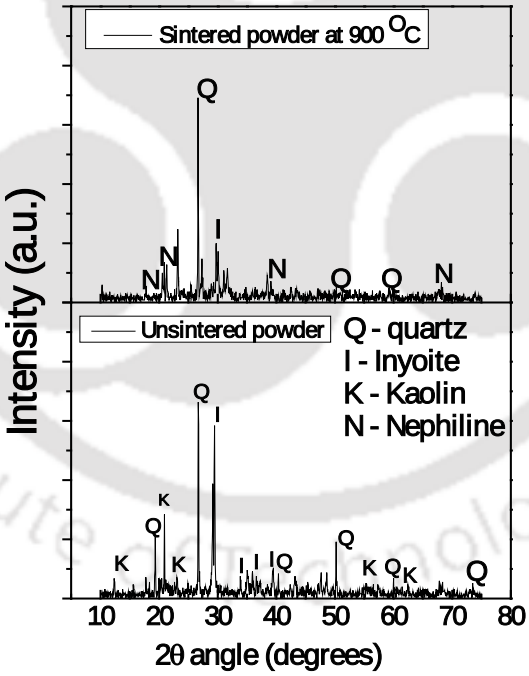

(b)

Figure 4.1: (a) Thermogravimetric analysis of the raw material mixture (b) X – ray diffraction patterns of un-sintered and sintered powder mixture (membrane M1 – M3) at 900 °C.

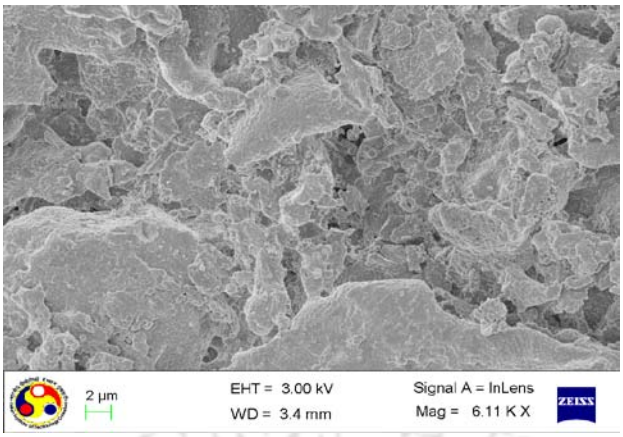

(a)

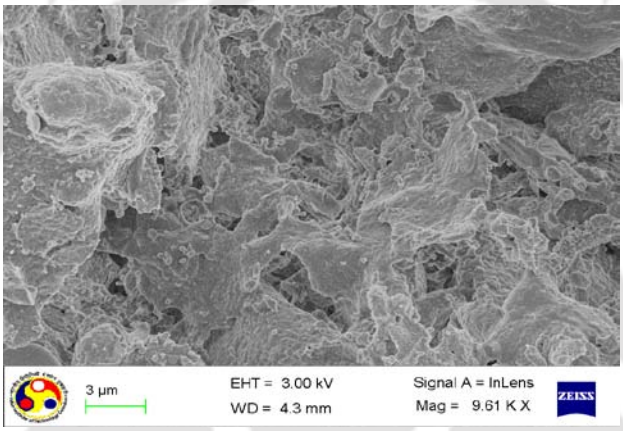

(b)

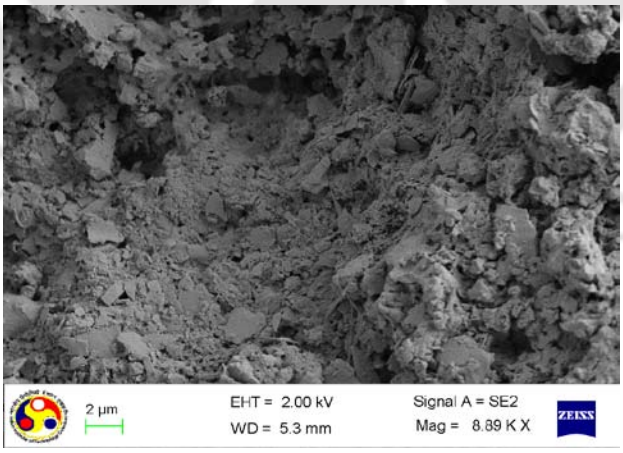

(c)

Figure 4.2: FESEM images of (a) M1, (b) M2 and (c) M3 membranes.

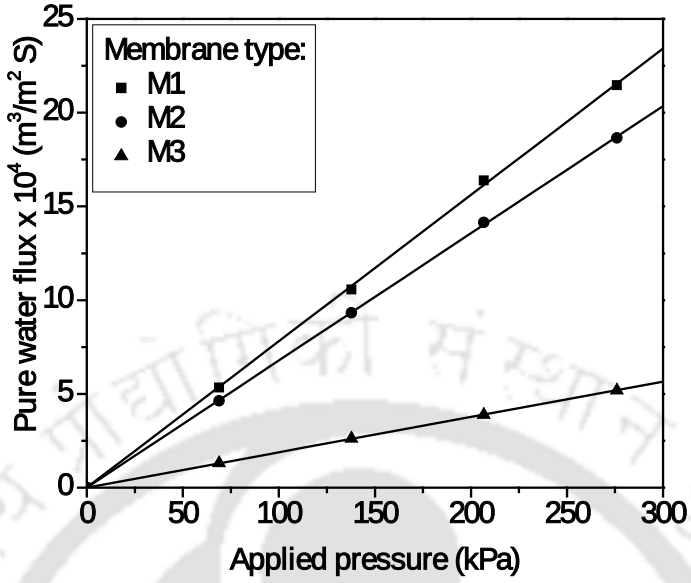

(a)

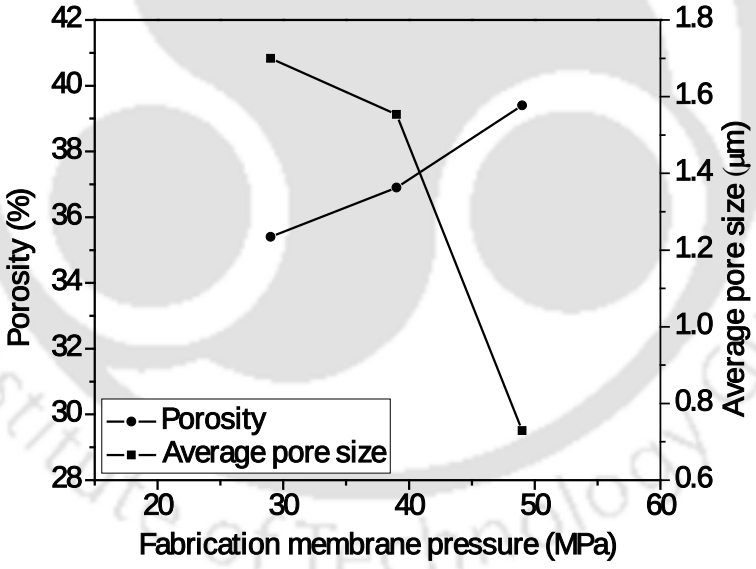

(b)

Figure 4.3: (a) Pure water flux vs applied pressure for M1 – M3 membranes (b) Variation of average porosity and pore size with membrane fabrication pressure for M1-M3 membranes.

The flexural strength values of the membranes M1 – M3 varied from 7.81 to 11 MPa, which is lower than the values reported by Vasanth *et al.* [10] (22 to 31 Mpa) and higher than the values reported by Nandi *et al.* [5] (3 to 8 MPa). This indicates that the fabricated membranes have acceptable values of flexural strength and further research is expected to enhance the flexural strength values.

4.2.2 Microfiltration of mosambi juice

The particle size distributions of FJ, CJ and ETCJ have been presented in Figure 4.4. It can be observed that FJ had unimodal particle size distribution profile ranging from 0.1 to 2000 µm. The average particle size of FJ corresponded to a value of 526 µm, which is higher than that reported by Nandi *et al.* [32]. The particle size distribution profiles for CJ and ETCJ are also shown in the Figure. As shown, for both CJ and ETCJ, the particle size distributions followed a bimodal distribution ranging from 0.1 to 600 µm. It can be also observed that larger colloidal particles are successfully eliminated by pretreatment. The average particle size of CJ and ETCJ have been determined to be about 34 and 22 µm, respectively, which is significantly higher than those reported by Nandi *et al.* [32]. Therefore, the chosen feed juice in this work is regarded to be characterized with higher concentration of larger particles, and thus pre - treatment appears to be necessary prior to the microfiltration tests. Further, it has also been observed that the maximum particle size of the CJ and ETCJ have been analyzed to be 677 and 590 µm as opposed to the original maximum particle size range of about 2000 µm. Thus, pretreatment operation can be concluded to be very important to alter the particle size distribution characteristics of the juice samples.

Table 4.1 presents the physicochemical properties of FJ, CJ and ETCJ. It can be observed that pretreatment enabled significance reduction in colour, viscosity, AIS and enhancement in the clarity of the juice. The TSS, pH and citric acid content of the juice remained fairly constant and the juice density reduced slightly after pretreatment. Therefore, it

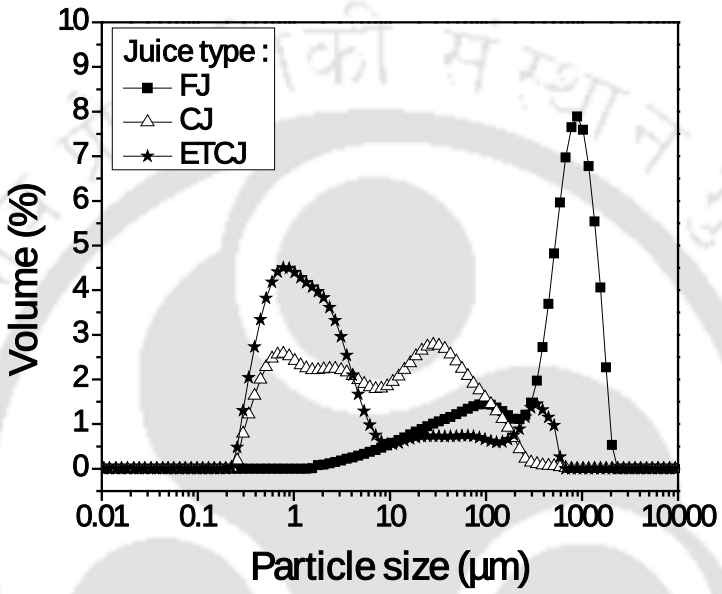

Figure 4.4: Particle size distributions for FJ, CJ and ETCJ.

Table 4.1: Physico – chemical properties of FJ, CJ and ETCJ samples.

Juice type	Colour (A_{420})	Clarity ($\%T_{660}$)	TSS (^{o} Brix)	Citricacid (wt %)	pH	Density (g/cm^3)	Viscosity (mPa S)	AIS (wt %)
FJ	4.2 – 4.3	0.14 – 0.16	9.1 - 9.2	0.83	3.8 – 3.8	1.28	3.39 – 3.41	0.8 – 0.87
CJ	0.61 – 0.67	51.52 – 58.45	9.1	0.83	3.9 – 3.9	1.27	1.49 – 1.52	0.3 – 0.37
ETCJ	0.41 – 0.48	64.45 – 72.4	9.1	0.83	3.8 – 3.9	1.20	1.49 – 1.50	0.2 – 0.24

is observed that pretreatment enabled the removal of pectic and colloidal material from the juice.

The CJ flux decline profiles for M1, M2 and M3 membranes have been presented in Figure 4.5 (a). It can be seen that the flux decline profile for M1 is located above M2 and M2 above M3. This is due to the increase in membrane pore size with fabrication pressure. For M1 membrane, the flux reduced from 80 to 20×10^{-6} $m^3/m^2.s$ with in a time period of 30 minutes at 206.7 kPa. For M3 membrane, the flux reduced from 55 to 9×10^{-6} $m^3/m^2.s$ with in a time period of 30 minutes at 206.7 kPa. Corresponding flux decline profile reported by Nandi *et al.* [32] varied from 68 to 15×10^{-6} $m^3/m^2.s$ at 165.5 kPa. Therefore, it is concluded that the best membrane performance in terms of flux decline is comparable to the literature values reported with paste method.

The ETCJ flux decline profiles for M1, M2 and M3 at 206.7 kPa are presented in Figure 4.5(b). Again, the membrane pore size contributed significantly to the flux decline performance. For M1 membrane, the flux varied from 120 to 70×10^{-6} $m^3/m^2.s$ for a time period of 30 minutes at 206.7 kPa. For M3 membrane, the flux varied from 90 to 44×10^{-6} $m^3/m^2.s$ for a time period of 30 minutes at 206.7 kPa. Flux values in the literature (Nandi *et al.* [32]) correspond to 137.5 to 50×10^{-6} $m^3/m^2.s$ at 165.5 kPa. Therefore, the performance of the membranes is comparable with those presented in the literature.

Figures 4.5 (c) and 4.5 (d) presents the variation of trans membrane flux with time for the M3 membrane at different pressures. It can be observed that for CJ the membrane flux varied from 41 to 3×10^{-6} $m^3/m^2.s$ at 68.9 kPa which increased to 55 to 9×10^{-6} $m^3/m^2.s$ at 206.7 kPa. This is due to an increase in the driving force across the membrane. On the other hand, for ETCJ the membrane flux varied from 66 to 17×10^{-6} $m^3/m^2.s$ at 68.9 kPa which

increased to 90 to 44 × 10^{-6} m^3/m^2.s at 206.7 kPa. It can be observed that the flux decline profiles are more distinctly placed for the ETCJ when compared to CJ and hence enzyme treatment is a highly promising option to increase the shelf life of the membrane.

Table 4.2 summarizes the physicochemical properties of clarified mosambi juice obtained from the MF using M1, M2 and M3 membrane. It can be observed that several juice

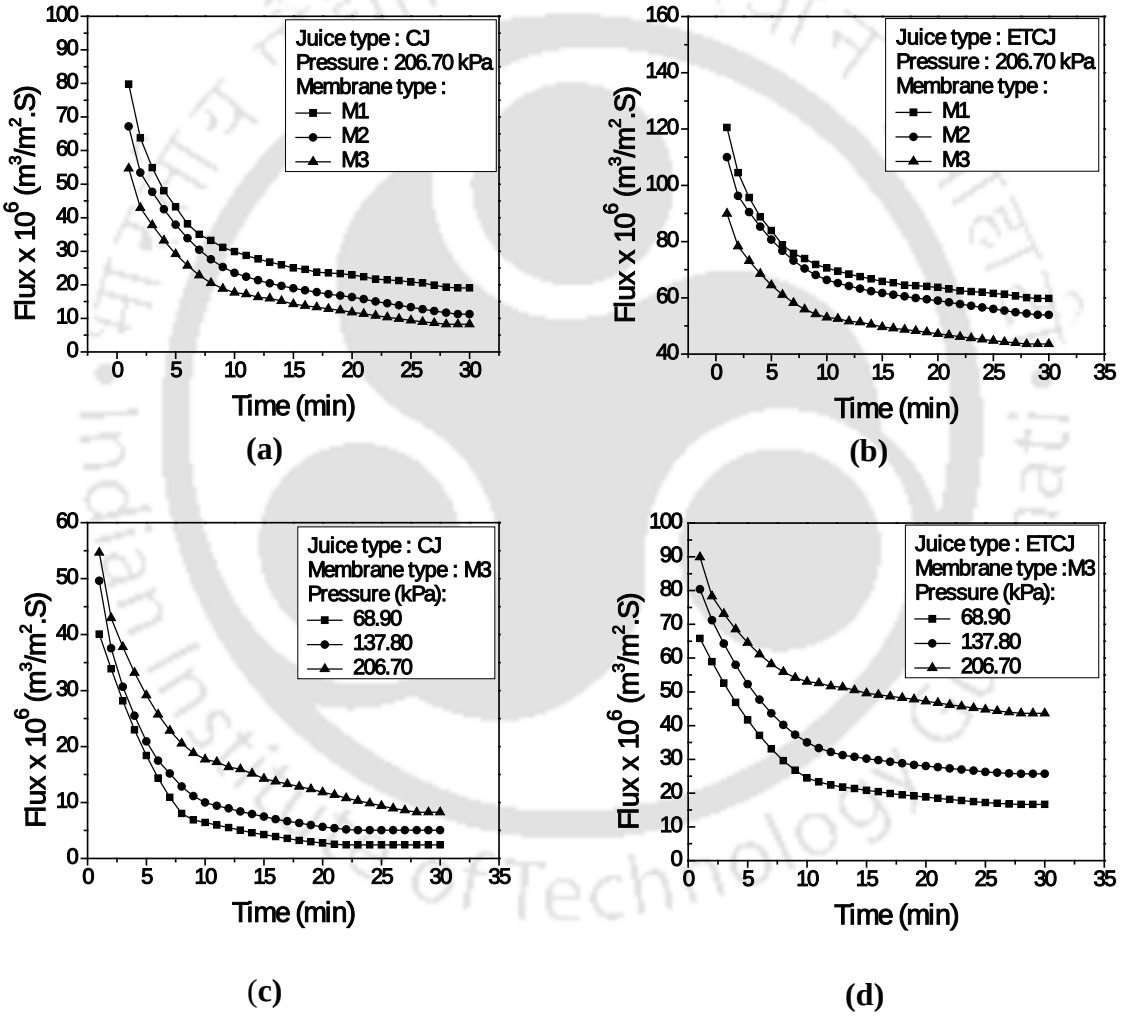

Figure 4.5: Variation of permeate flux with time for (a) membranes M1, M2 and M3 at ΔP = 206.70 for CJ (b) membranes M1, M2 and M3 at ΔP = 206.70 for ETCJ (c) membrane M3 at pressures ΔP = 68.9, 137.8 and 206.70 kPa for CJ and (d) membrane M3 at pressures ΔP = 68.9, 137.8 and 206.70 kPa for ETCJ.

Table 4.2: Physico chemical properties of mosambi juice permeate samples obtained for M1-M3 membranes at a ΔP of 206.70 kPa.

Membrane type	Juice type	Colour (A_{420})	Clarity ($\%T_{660}$)	TSS (^{o}Brix)	Citric acid (wt %)	p^{H}	Density (g/cm^3)	Viscosity (mPa S)	AIS (wt %)
M1	CJ	0.1225	96.94	9.1	0.80	3.95	1.25	1.265	0.05
	ETCJ	0.0146	97.986	9.1	0.80	3.92	1.17	1.37	Nil
M2	CJ	0.1267	97.17	9.1	0.79	3.94	1.25	1.26	0.05
	ETCJ	0.0264	98.476	9.1	0.79	3.95	1.17	1.37	Nil
M3	CJ	0.1284	97.44	9.1	0.78	3.93	1.24	1.255	0.04
	ETCJ	0.0384	98.92	9.1	0.78	3.98	1.17	1.36	Nil

properties remained similar for all membranes. The physicochemical properties of clarified mosambi juice after MF at 206.70 kPa for all membranes have been evaluated as follows: colour index of 0.12, clarity index from 0.01 to 0.03, ^{o}Brix of 9.1, citric acid wt % from 0.78 to 0.80, pH of 3.93 – 3.95, density of 1.24 to 1.25 g/cm^3, viscosity of 1.255 to 1.265 mPa.S and AIS of 0.04 - 0.05 wt % for CJ samples. For the ETCJ case, distinct properties were observed for colour index (0.01 to 0.03), density (1.17 g/cm^3) and negligible AIS content. Therefore, enzyme treatment followed with centrifugation enabled to achieve good quality feed for the microfiltration operation. The observed trends for all parameters are in good agreement with those reported by Nandi *et al.* [4].

The effect of increasing transmembrane pressure on the juice quality has also been studied for the M3 membrane. The physico-chemical properties of clarified mosambi juice after MF for M3 membrane at different pressures (68.9 – 206.7 kPa) have been evaluated as

follows: colour index of 0.11 to 0.12, clarity index ranging from 97.44 to 98.01, ^{o}Brix of 9.1, citric acid wt % from 0.77 - 0.78, pH of 3.93 – 3.95, density of 1.24 g/cm^3, viscosity of 1.255 - 1.265 mPa.S and AIS of 0.03 - 0.04 wt % for CJ samples. For the ETCJ case, distinct properties were observed for colour index (0.02 to 0.03), density (1.17 g/cm^3) and AIS (negligible). Thus, it can be observed that important parameters such as density, AIS, TSS, acidity did not vary much with variation in the pressure and confirmed that the membrane performance is satisfactory for the desired juice quality and is fairly independent of the applied pressure.

4.2.3 Fitness of fouling models

The fitness of experimental data for all membranes to represent various pore blocking models are presented in Figure 4.6 (a) and 4.6 (b) for CJ and ETCJ, respectively. It can be observed that for both CJ and ETCJ, none of the models could very closely fit to the experimental data except for M1 and CJ combination. A paradigm shift involving the onset of cake filtration after a preliminary pore blocking mechanism can be typically observed from the data presented in Figure 4.6 (b) for ETCJ. Corresponding coefficient of correlation (R^2) values along with slope and intercept values are presented in Table 4.3 for CJ and ETCJ, respectively. From Table 4.3, it is apparent that the R^2 value is not very close to 1 for any case. Consequently, it is concluded that the membrane morphology and pore size distribution favours initially pore blocking followed by cake filtration for CJ and ETCJ.

Table 4.3: Summary of various pore blocking model parameters for the M3 membrane during dead MF of mosambi juice.

Juice type	Pressure (kPa)	Complete pore blocking			Standard pore blocking			Intermediate pore blocking			Cake filtration		
		$k_b \times 10^2$	$\ln(J_0^{-1})$	R^2	k_s	$J_0^{-0.5}$	R^2	k_i	$J_0^{-1} \times 10^{-4}$	R^2	$k_c \times 10^{-7}$	$J_0^{-2} \times 10^{-8}$	R^2
CJ	68.9	9.4	10.1	0.86	18.6	157.9	0.93	16339	24.9	0.96	800	6.22	0.92
ETCJ	68.9	4.2	9.6	0.82	4.02	123.2	0.87	1568	15.1	0.91	10	2.30	0.97
CJ	137.8	7.0	9.9	0.84	10.6	141.9	0.91	6902	20.1	0.95	200	4.06	0.96
ETCJ	137.8	3.3	9.4	0.80	2.71	111.5	0.85	885.9	12.4	0.88	0.50	1.54	0.94
CJ	206.7	5.6	9.8	0.92	6.94	135.2	0.97	3536	18.2	0.99	50	3.34	0.94
ETCJ	206.7	1.9	9.3	0.81	1.28	105.4	0.85	344.6	11.1	0.88	1.00	1.23	0.93

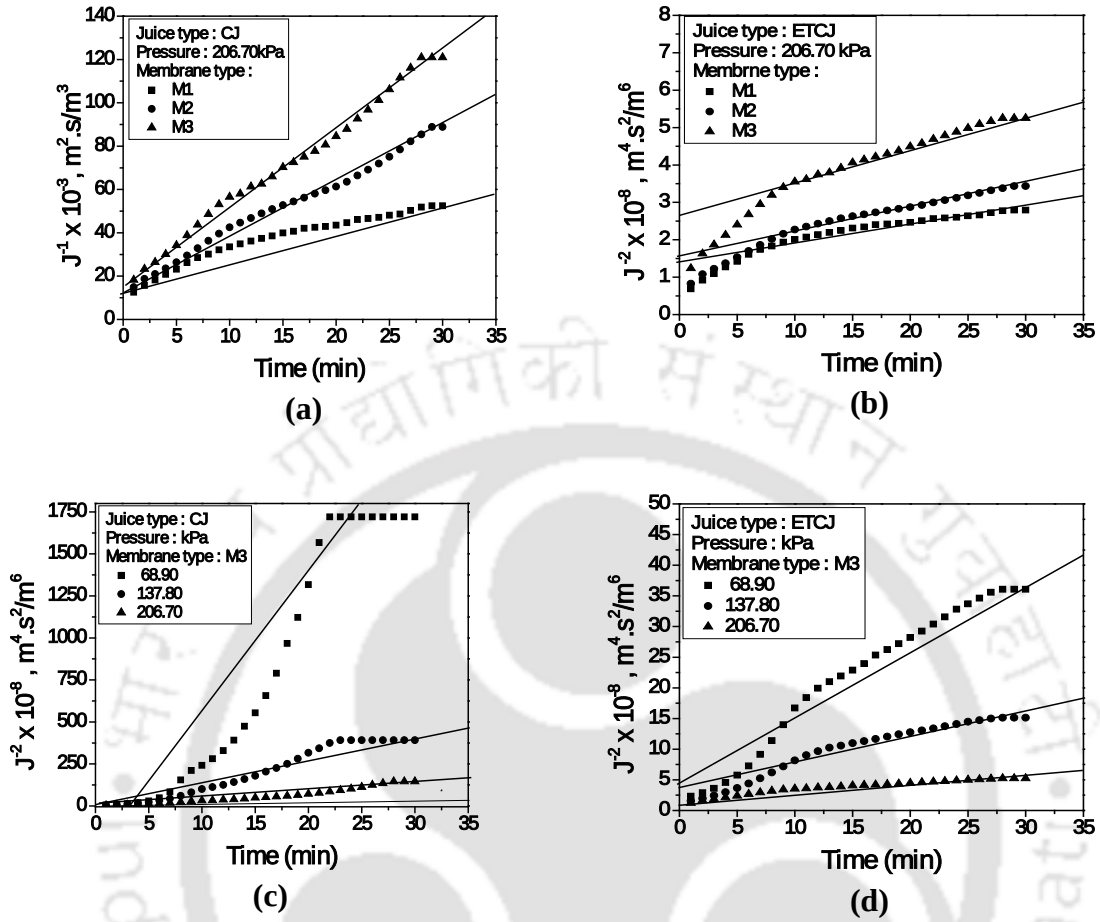

Figure 4.6: Linearized fouling model fitness plots for various cases (a) intermediate pore blocking model for M1 – M3 and CJ at ΔP = 206.70 kPa (b) intermediate pore blocking model for M1 – M3 and ETCJ at ΔP = 206.70 kPa (c) cake filtration model for M3 and CJ at ΔP = 68.7, 137.8 and 206.7 kPa and (d) cake filtration model for M3 and ETCJ at ΔP = 68.7, 137.8 and 206.7 kPa.

The fitness of M3 membrane flux data (obtained at various pressures) towards cake filtration model is presented in Figure 4.6 (c) and 4.6 (d) for CJ and ETCJ respectively. It can be observed that for ETCJ, a very good fitness of the cake filtration model exists. However, for the CJ case, the flux data obtained at 68.9 kPa did not fit well with the experimental data. On the other hand, cake filtration model fit well for the flux data obtained at 137.8 kPa and 206.7 kPa. Incidentally, the flux data at 68.9 kPa fit well with the intermediate pore blocking

model. Therefore, it is apparent that operating pressure plays an important role in defining the pertinent flux decline mechanism and lower pressures tend to maximize pore blocking and hence fouling. The same is also confirmed with the fouling index values that are also presented in this work.

The cake filtration constant (k_c) is analyzed to vary linearly with fabrication pressure. The cake filtration constant varied from $10 – 50 \times 10^{-7}$ for CJ and $0.6 – 1.0 \times 10^{-7}$ for ETCJ, respectively. Thus, it can be observed that a drastic reduction in cake filtration parameter values can be achieved by enzyme treatment followed with centrifugation. The cake filtration is suitably modelled using the expression:

$$k_C^{CJ} = 2.00 \times 10^7 \Delta P_{fab} - 5 \times 10^8, \qquad R^2 = 0.999 \tag{4.1}$$

$$k_C^{ETCJ} = 20000 \Delta P_{fab} + 20000, \qquad R^2 = 1 \tag{4.2}$$

The cake filtration constant varied from $10 - 50 \times 10^{-7}$ for CJ and $0.6 - 1.0 \times 10^{-7}$ for ETCJ, respectively. Thus it can be concluded that a drastic reduction in cake filtration constant can be achieved by enzyme treatment followed with centrifugation.

Since the MF flux decline profiles for both CJ and ETCJ could not be represented using any one of the chosen models, combination models have been analyzed to represent the flux decline data. To do so, two distinct sets of flux decline data have been subjected to the modelling analysis. These correspond to the initial flux decline profiles up to a time period of 10 minutes and the flux decline profiles from 11 – 30 minutes of the microfiltration runs. Table 4.4 summarizes the coefficient of correlation (R^2) for the combination models for both

Table 4.4: A summary of correlation coefficient parameters (R^2) for various combination pore blocking models to represent dead end MF of CJ and ETCJ using membranes M1- M3 at ΔP = 206.70 kPa.

Membrane type	Juice type	Complete pore blocking		Standard pore blocking		Intermediate pore blocking		Cake filtration	
		1 - 10	11 - 30	1 - 10	11 - 30	1 - 10	11 - 30	1 - 10	11 - 30
M1	CJ	0.952	0.984	0.975	0.989	0.990	0.991	0.996	0.991
	ETCJ	0.922	0.976	0.940	0.979	0.956	0.981	0.979	0.985
M2	CJ	0.984	0.996	0.996	0.991	0.997	0.982	0.971	0.953
	ETCJ	0.959	0.994	0.972	0.995	0.983	0.996	0.995	0.997
M3	CJ	0.982	0.993	0.996	0.993	0.997	0.987	0.971	0.965
	ETCJ	0.953	0.986	0.968	0.988	0.979	0.989	0.993	0.992

CJ and ETCJ. It can be noted that cake filtration with different combinations of parameters (initial flux (J_0) and cake filtration constant (k_c)) in both regimes suited well with the experimental data obtained using ETCJ for all the membranes. In other words, the flux data indicated the dynamic variations of cake layer morphology with time. For CJ using M1 membrane, cake filtration followed with intermediate pore blocking fit well with the data. For M2 and M3 membranes, intermediate and complete pore blocking represent the experimental data with good fitness. Thus, it can be observed that pore blocking models have been representing the CJ flux decline during the time period of 11 – 30 minutes of MF runs. This indicates the significance of irreversible fouling in the early stages of MF which is also confirmed by the fouling studies. Hence, MF of CJ can be inferred to be not suitable for the prepared membranes.

The average error of MF flux data obtained for all membranes for the combination models has been analyzed to be no more than 5 % with respect to the experimental data. Further, it has been also observed that several predicted data sets deviated significantly during the initial stages of microfiltration runs for all membranes, thus indicating that the initial pore blocking mechanism is highly complex and could not be fit with simplistic models. Nonetheless, the overall fitness of the two combination model with the experimental flux data is satisfactory.

4.2.4 Fouling index values

The fouling index for the M3 membrane has been evaluated to vary from 41.6 to 33.5 % for a variation in pressure from 68.9 to 206.7 kPa. On the other hand, for the ETCJ case, the corresponding values varied from 1.51 to 1.04 %. This indicates that enzyme treatment prior to centrifugation is highly effective towards long term usage of the ceramic membranes

for juice MF. Also, for the membranes whose MF runs carried out at 206.7 kPa, the FI values varied from 43.9 (M1) to 33.5 % (M3) for the CJ case and 1.73 (M1) to 1.04 % (M3) for the ETCJ case. This indicates that the M3 membrane is the most suitable for juice MF. This is possibly due to the early onset of pore blocking which is expected to contribute significantly towards fouling for membranes with higher pore size (M1 and M2).

4.2.5 Cost estimation

Based on retail cost of various inorganic precursors, the average cost of the membranes has been estimated. Considering the unit price of kaolin, quartz, calcium carbonate, sodium carbonate, boric acid, sodium meta silicate and poly vinyl alcohol as 520, 358, 408 660, 760, 578 and 13500 Rs./kg respectively, the total cost of the membrane has been estimated as Rs. 10.15/- per one circular disc shaped membrane. This corresponds to the membrane cost of 78 ($/m^2). Comparatively, the membrane cost reported by Vasanth *et al.* [10] is 67 ($/m^2) and that reported by Nandi *et al.* [32] is 130 ($/m^2). In other words, the cost of the membrane is comparable with the low cost membranes reported in the literature.

Chapter 5

Flux Decline Analysis during Microfiltration of Pineapple Juice Using Low Cost Ceramic Membranes

This chapter addresses the applicability of kaolin based low cost ceramic membranes for pineapple juice clarification. Low cost membranes prepared with uniaxial dry compaction method provided excellent performance during the dead end MF of enzyme treated centrifuged mosambi juice (Chapter 4). Therefore, the primary objective of this work is to address the performance of membranes M1 – M3 for pineapple juice clarification. Both dead end and cross flow microfiltration experiments were carried out with centrifuged and enzyme treated centrifuged pine apple juice. For the MF studies, with low (M3) and high (M1) average pore size were used. Further the dependence of membrane performance on enzyme treatment, centrifugation, ΔP and cross flow velocity had been also studied. Fouling indices were also evaluated to identify optimal choices of membrane and process parameters for pineapple juice MF.

5.1 Experimental

5.1.1 Low cost ceramic membranes

Laboratory fabricated low cost ceramic membranes were prepared with uniaxial dry compaction method using precursor composition and procedure reported in chapter 4. Further details with respect to the preparation and characterization of the membranes have been presented in chapter 2. Amongst various membranes, membranes M1 and M3 fabricated at a

pressure of 29 and 49 MPa have been selected for the dead end and cross flow MF of CJ and ETCJ. This is due to the fact that M1 and M3 possess an average pore size of 1.69 and 0.72 µm and correspond to high (1.69 µm) and low average pore size (0.72 µm) values. Corresponding porosities of M1 and M3 membranes have been evaluated as 35.4 and 39.4 %, respectively. Since the major objective of the MF experimentation was to identify optimal membrane morphology, a membrane with intermediate pore size was not chosen for experimental investigations.

5.1.2 Preparation of CJ and ETCJ feed samples

Fresh pineapple juice (FJ) was obtained using depulped pineapple fruits in a manually operated screw type juice extractor. Centrifuged juice (CJ) was obtained using a centrifuge (Make: SORVALL, RC 5C PLUS) and enzyme treated centrifuged juice (ETCJ) was prepared by first carrying out enzymatic pre-treatment of the juice followed with centrifugation at 4000 rpm for 20 min. The enzymatic pre-treatment involved heating the juice first at 42 ^{o}C for 100 min. with pectinase enzyme (Make: SRL Ltd., India) at a concentration of 0.0004 w/v % [34]. Subsequently, the juice was heating at 90 ^{o}C for 5 min to inactivate the remaining enzyme. Following this step, the juice was cooled to ambient temperature (25 ^{o}C) for subsequent centrifugation in an industrial centrifuge (Make: REMI K – 70, India).

5.1.3 Microfiltration of pineapple juice

Figure 5.1 illustrate the experimental setup utilized for the cross flow MF of centrifuged and enzyme treated centrifuged pineapple juice samples. The dead end microfiltration setup is the setup utilized for MF of oil water emulsions. The details of the

setup has been presented in chapter 2 of the thesis has been illustrated in Figure 2.1. As shown in Figure 5.1, the cross flow microfiltration setup (Make: S. D. Instruments and Equipments, Kolkata, India) integrated with the circular disk ceramic module unit consists of a stainless steel feed tank supplemented with chillier jacket, a variable frequency gear pump, a flow dampener, a rotameter and digital pressure measuring devices. To regulate ΔP during the MF operation, the pressure measuring devices have been located at the feed tank outlet, inlet and outlet sections of the membrane module. The variation in trans-membrane pressure differentials was brought forward by using an adjustable valve located after the rotameter and the average pressure was evaluated using inlet and outlet pressure values for the flux decline analysis. The temperature of the juice in the feed tank was controlled at 25 ± 1 ˚C during a microfiltration run using the micro processor controlled chillier unit. An auxiliary electronic weighing balance was used to measure the membrane flux as a function of the weight of the juice samples collected at various time periods during a typical cross flow microfiltration run. During microfiltration runs, different circulation rates (1 and 4 LPM) were achieved using variable frequency controller and needle valves located in the setup. The MF experimental investigations were carried out for both M1 and M3 compacted membranes using CJ and ETCJ at various combinations of ΔP (69 and 207 kPa) and circulation rates (1 and 4 LPM). The effective membrane area for permeation is 1.45×10^{-3} m^2. The feed and permeate samples after each MF run have been analyzed using various analytical techniques summarized below.

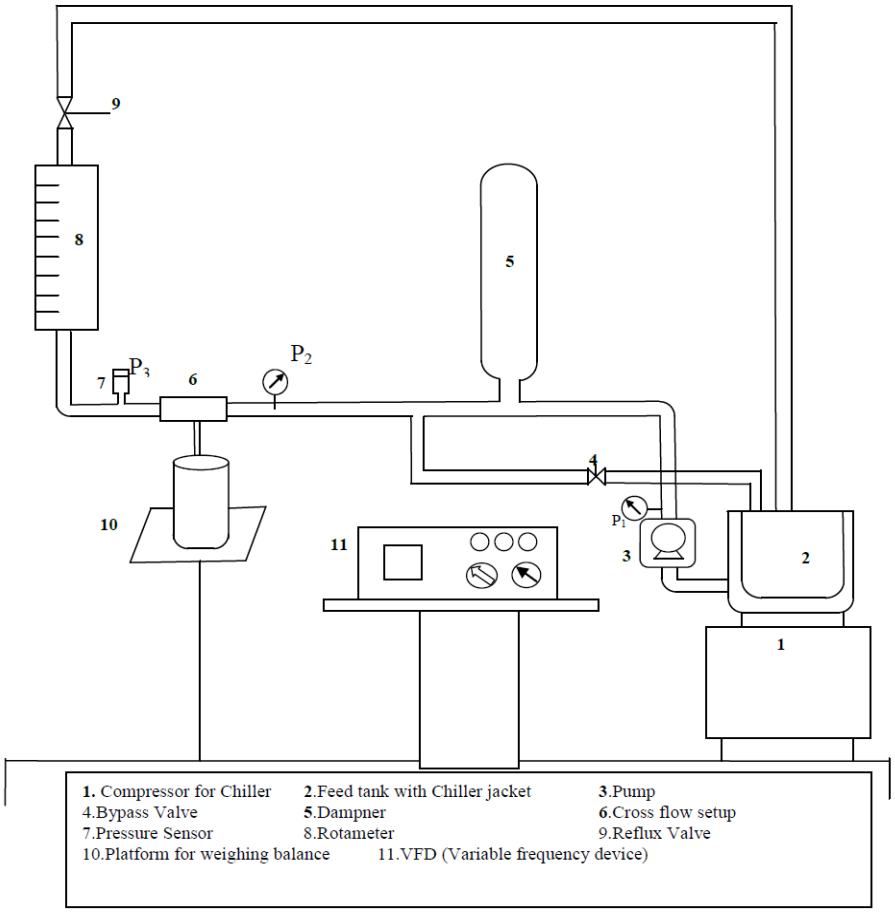

Figure 5.1: Schematic of experimental setup for the cross flow fruit juice MF using low cost ceramic membranes.

5.1.4 Measurement of juice quality and fouling studies

The analytical methods were applied to estimate various physicochemical parameters associated to CJ and ETCJ of pine apple feed and permeate samples. The analytical procedures involved are reported in, section 4.1.3 of the thesis. In addition, the vitamin C (ascorbic acid) content of the juice samples was evaluated with volumetric method [60] using 2,6 – dichlorophenol indophenol dye in oxalic acid titrating medium. The central objective of

juice MF is to reduce AIS and retain Brix and Vitamin C content in the permeate samples. Thus, analytical methods deployed will be relevant to evaluate upon the efficacy of low cost ceramic membranes for pineapple juice MF. After a MF runs, membranes were cleaned and fouling index (FI) were evaluated using the procedures mentioned in chapter 2, section 2.1.6 of the thesis.

5.1.5 Fitness of Fouling models

Four fouling models namely cake filtration, intermediate, standard and complete pore blocking models proposed by Hermia [56] have been evaluated for their fitness to represent the pertinent flux decline during the dead end and cross flow MF of both CJ and ETCJ. The linearized expressions for the fitness of these models are summarized in section 2.1.7 of the thesis. The fitness of any one of the above models was based on the coefficient of correlation (R^2) values. Further, is it important to note that while the first three models could refer to fouling within the porous structure of the membrane, the cake filtration model refers to fouling on the surface of the membrane and thus could refer to irreversible fouling. Thus, the onset of cake filtration model to represent the pertinent flux decline during the MF of CJ and ETCJ is indicative towards lower fouling index and longer shelf life of the membrane.

5.2 Results and discussion

5.2.1 Dead end MF performance

Figure 5.2 a and 5.2 b present the variation of dead end MF membrane flux with time and ΔP for M1 and M3 membranes respectively for CJ. It can be observed that for M1, the flux varied from 66 – 17 and 91 – 21 × 10^{-6} m^3/m^2.s for a ΔP of 69 and 207 kPa respectively.

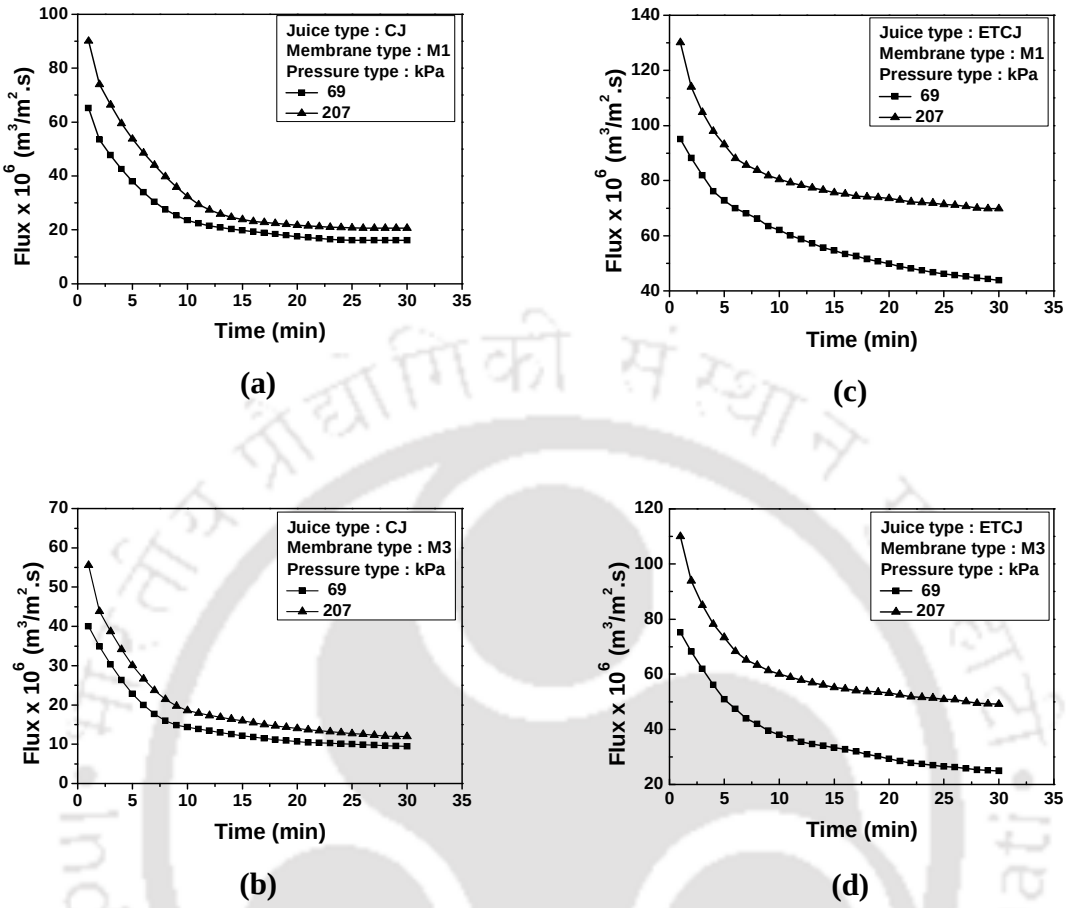

Figure 5.2: Dead end MF performance of various membranes for the clarification of pineapple juice (a) M1 membrane and CJ (b) M3 membrane and CJ (c) M1 membrane and ETCJ (d) M3 membrane and ETCJ.

On the other hand, for the M3 membrane, the time dependent dead end MF flux varied from 41 – 10 and 56 – 12 × 10^{-6} m^3/m^2.s for a ΔP of 69 and 207 kPa respectively. Thus, it can be observed that the long term flux for both membranes is significantly influenced with ΔP for M1 membrane but not M3 membrane. This is possibly due to larger fouling for the M3 membrane during the initial stages of juice permeation. Also, the insignificant enhancement in

long term flux with increasing ΔP for the M1 membrane (from 17 to 21 × 10^{-6} m^3/m^2.s with a variation in ΔP from 69 to 207 kPa) is due to the higher pectin content in the feed CJ, which contributed enormously towards the membrane pore blocking.

For ETCJ feed samples, the variation of dead end MF membrane flux with time and ΔP is presented in Figure 5.2 c and 5.2 d for M1 and M3 membranes respectively. As shown, the M1 membrane flux varied from 96 – 46 and 131 – 70 × 10^{-6} m^3/m^2.s for a ΔP of 69 and 207 kPa respectively. Similarly, for the M3 membrane, for similar values of ΔP, the dead end MF flux varied from 76 – 26 and 111 – 50 × 10^{-6} m^3/m^2.s respectively. Thus, it is apparent that for both M1 and M3 membranes, the long term membrane flux is strongly influenced with both average pore size and ΔP. Also, amongst both M1 and M3 membranes, M1 provided higher value of long term membrane flux which is due to its larger average pore size. Also, for the M1 membrane, the enhancement in the long term flux by about 52 % (from 46 – 70 × 10^{-6} m^3/m^2.s) with an increase in ΔP from 69 - 207 kPa is indicative towards its promising capabilities for pineapple juice clarification. Compared to the CJ, the ETCJ long term flux for the M1 membrane is about two to three times higher than that obtained with the CJ. Thus, the relevance of higher pectin content in the feed juice to influence significantly the permeation characteristics of the low cost ceramic membranes is evident from the dead end MF experimental investigations.

5.2.2 Cross - flow MF performance

Figure 5.3 a and 5.3 b present the variation of cross flow MF membrane flux with time and ΔP for M1 and M3 membranes respectively for CJ at a cross flow velocity of 1.92 m/s (circulation rate of 1 LPM). It can be observed that for M1 the cross flow flux varied from 42 – 24 and 51 – 31 × 10^{-6} m^3/m^2.s for a ΔP of 69 and 207 kPa respectively. On the other hand,

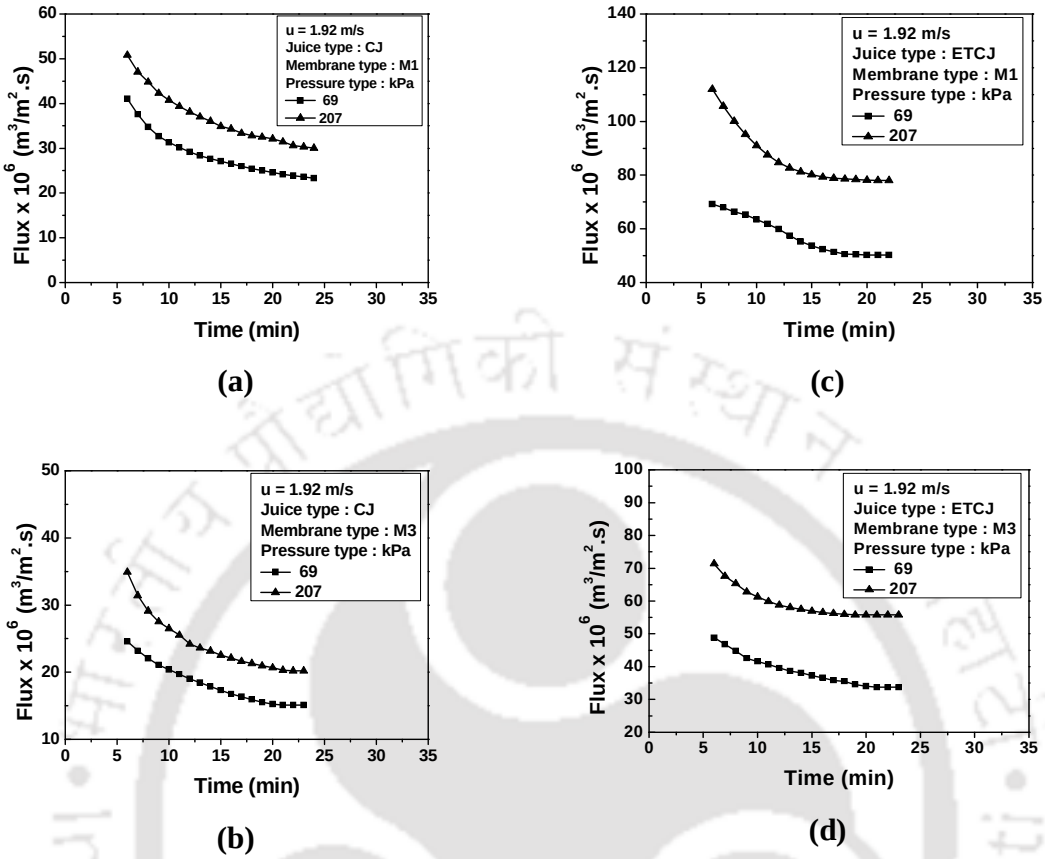

Figure 5.3: Cross flow microfiltration performance of various membranes at a circulation rate of 1 LPM (cross flow velocity of 1.92 m/s) (a) M1 membrane and CJ (b) M3 membrane and CJ (c) M1 membrane and ETCJ (d) M3 membrane and ETCJ.

for the M3 membrane, the time dependent cross flow MF flux varied from 25 – 16 and 35 – 21 × 10^{-6} m^3/m^2.s for a ΔP of 69 and 207 kPa respectively. Thus, it can be observed that the flux profiles did not significantly vary with variation in ΔP for the CJ case for both M1 and M3 membranes. This is due to the dominance of pectin content in the CJ which significantly affects pore blocking and provides additional permeation resistance towards the transport.

For the CJ case, it can be observed that an increase in ΔP from 69 to 207 kPa enhanced the steady state flux by only 20.8 – 31.2 % respectively for membranes M1 and M3.

For the M1 membrane and ETCJ feed samples, at a cross velocity of 1.92 m/s (circulation rate of 1 LPM), the time dependent variation of cross flow MF membrane flux varied from 70 – 51 and 112 – 79 × 10^{-6} m^3/m^2.s (Figure 5.3 c) at a ΔP of 69 and 207 kPa respectively. For similar values of ΔP, the time dependent flux of the M3 membrane varied from 49 – 34 and 72 – 56 × 10^{-6} m^3/m^2.s (Figure 5.3 d) at a ΔP of 69 and 207 kPa respectively. Thus, it can be concluded that the variation in ΔP significantly altered the time dependent ETCJ flux profiles which is due to the lower pectin content in the ETCJ in comparison with the CJ. For all cases, it can be observed that the flux decline exists upto a maximum time period of 20 min during the cross flow operation after which the steady state flux was achieved. For the ETCJ case, the steady state membrane flux increased by about 55 % with variation in ΔP from 69 to 207 kPa. Thus, it is apparent that the ΔP profoundly enhances the transmembrane flux for the ETCJ case which was not the case for the CJ case.

The effect of cross flow velocity (or circulation rate) on the steady state flux of M3 membrane at a ΔP of 207 kPa is presented in Figure 5.4. The flux decline profiles for this case followed trends similar to that presented in the earlier paragraphs of this sub - section. It can be observed from Figure 5.4 that the steady state flux for the M3 membrane varied from 21 to 26 × 10^{-6} m^3/m^2.s for CJ and 53 to 60 × 10^{-6} m^3/m^2.s for ETCJ case for an enhancement in the cross flow velocity from 1.92 to 7.68 m/s. This corresponds to an increase of about 23.8 and 13.2 % for membrane flux with an increase in cross flow velocity from 1.92 to 7.68 m/s for CJ and ETCJ cases respectively. Thus, only marginal enhancement in permeate flux was achieved through the enhancement in the circulation rate in comparison with ΔP for the ETCJ

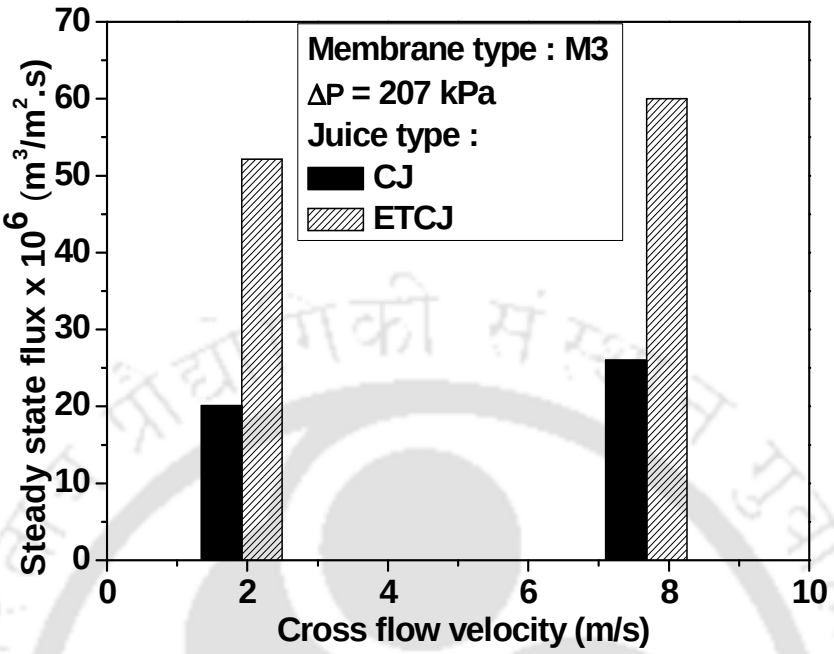

Figure 5.4: Variation of CJ and ETCJ steady state flux with cross flow velocity for M3 membrane at a ΔP of 207 kPa.

case and this is indicative of better feed juice quality for the ETCJ case in comparison with the CJ.

A comparative assessment of the transmembrane flux obtained after 30 min of dead end MF and 20 min of cross flow operation (at a circulation rate of 1 LPM) during the juice MF is presented in Table 5.1 for both M1 and M3 membranes. As presented, compared to the dead end MF flux, steady state cross flow MF was enhanced by 59.2 – 35.7 and 60.1 – 68.3 % for M1 and M3 membranes respectively and CJ feed samples. On the other hand, for ETCJ case, in comparison with the dead end MF, the enhancement in the steady state membrane flux was about 10.5 – 11.6 for M1 and 28.2 – 22.4 % for M3 membranes. These observations convey that the M3 membrane provided maximum enhancement in the flux for ETCJ during

cross flow MF and significant fouling could have occurred during the dead - end MF for both M1 and M3 membranes. The same has been confirmed with the measured fouling indices which will be elaborated in the next subsequent sections.

A comparative assessment of the transmembrane flux obtained for various relevant cases in this work with those presented in the literature for pineapple juice clarification is presented in Table 5.2. It can be observed that while few articles addressed pineapple juice MF, the membrane M3 performance is comparatively better than that presented by Gassaye *et al.* [45] who carried out membrane microfiltration using 0.08 µm ceramic membrane. While Gassaye *et al.* [45] reported a steady state flux of 12.1×10^{-6} $m^3/m^2.s$ at a ΔP of 100 kPa, membrane M3 provided a steady state flux of 55.1×10^{-6} $m^3/m^2.s$ at a ΔP of 207 kPa for lower cross flow velocities. All other membrane data presented in Table 5.2 refers to lower values of flux in comparison with the measured flux values in this work. Thus it is inferred that the low cost ceramic membrane M3 provided best cross flow MF performance and is highly relevant for pineapple juice clarification.

Table 5.1: A summary of dead end membrane flux measured after 30 min and cross flow membrane flux (measured at a cross flow velocity of 1.92 m/s) after 20 min.

		Batch flux × 10^{-6} ($m^3/m^2.s$)		**Cross flow flux × 10^{-6} ($m^3/m^2.s$)**		**Increasing flux in cross flow (%)**	
Membrane name	**Juice type**	**69 kPa**	**207 kPa**	**69 kPa**	**207 kPa**	**69 kPa**	**207 kPa**
M1	CJ	14.46	20.66	23.03	28.05	59.27	35.77
	ETCJ	45.47	69.92	50.25	78.03	10.52	11.60
M3	CJ	9.41	11.94	15.07	20.10	60.15	68.35
	ETCJ	25.03	45.02	32.10	55.13	28.25	22.46

Table 5.2: A summary of obtained (M3 membrane) and literature steady state MF flux data during pineapple juice clarification.

Membrane filtration	Membrane used & pore size	Geometry used	Mode of operation	Cross flow velocity (m/s)	Flux × 10^6 ($m^3/m^2.s$)	Pressure diffrential (kPa)	Reference
MF	Polymeric (0.20 µm)	Hollow fiber	Cross flow	3.4	10.27	71	[46]
UF	Ceramic (0.1 µm)	Tubular	Cross flow	2.0	1.8	300	[43]
	Ceramic (0.01 µm)	Tubular	Cross flow	2.0	4.4	300	
UF	Ceramic (0.01 µm)	Tubular	Cross flow	4.17	34.40	405	[44]
	Polymeric (100 kDa)	Hollow fiber	Cross flow	1.19	12.80	20	[44]
UF	Polymeric (50 kDa)	Plate and	Cross flow	-	4.80	590	[47]
	Polymeric (100 kDa)	frame	Cross flow	-	4.40	590	[47]
	Polymeric (30 - 80 kDa)	Plate and frame Tubular	Cross flow	-	9.90	150	[47]
MF	Polymeric (0.10 µm)	Plate and	Cross flow	-	8.50	350	[47]
	Polymeric (0.45 µm)	frame	Cross flow	-	5.60	300	[47]
	Polymeric (0.30 µm)	Plate and frame Tubular	Cross flow	-	16.0	150	[47]
MF	Ceramic (0.22 µm)	Tubular	Cross flow	-	14.4	105	[42]
	Ceramic (50 kDa)	Tubular	Cross flow	-	13.0	390	[42]
UF	Polymeric (50 kDa)	Plate and frame	Cross flow	-	6.9	500	[42]

Membrane filtration	Membrane used & pore size	Geometry used	Mode of operation	Cross flow velocity (m/s)	Flux × 10^6 ($m^3/m^2.s$)	Pressure diffrential (kPa)	Reference
MF	Ceramic (0.08 µm) (enzyme treatment)	Tubular	Cross flow	4.0	15.7	100	[45]
	Ceramic (0.08 µm) (without enzyme treatment)	Tubular	Cross flow	4.0	12.1	100	[45]
	Ceramic (0.2 µm) (enzyme treatment)	Tubular	Cross flow	-	21.4	-	[45]
	Ceramic (0.20 µm) (enzyme treatment)	Tubular	Cross flow	-	8.80	-	[45]
	Polymeric (0.2 µm) (enzyme treatment)	-	-	-	14.9	-	[45]
MF	**Ceramic (0.72 µm)**	**Circular disk**	**Dead end (CJ)**	**-**	**11.94**	**207**	**This work**
MF	**Ceramic (0.72 µm)**	**Circular disk**	**Dead end (ETCJ)**	**-**	**45.02**	**207**	**This work**
MF	**Ceramic (0.72 µm)**	**Circular disk**	**Cross flow (CJ)**	**1.92**	**20.10**	**207**	**This work**
MF	**Ceramic (0.72 µm)**	**Circular disk**	**Cross flow (ETCJ)**	**1.92**	**55.13**	**207**	**This work**

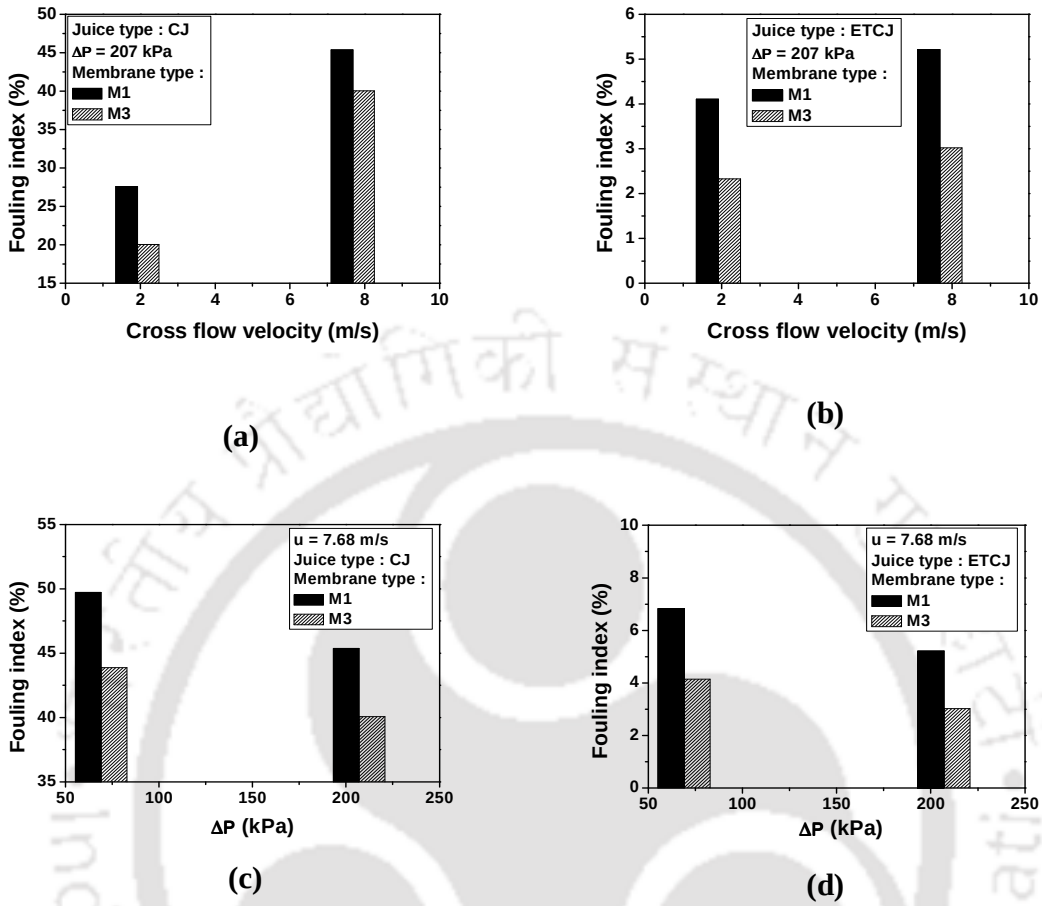

Figure 5.5: Effect of various operational parameters on M1 and M3 membrane fouling index: (a) CJ circulation rate at a ΔP of 207 kPa; (b) ETCJ circulation rate at a ΔP of 207 kPa; (c) ΔP at a CJ cross flow velocity of 7.68 m/s and (d) ΔP at a ETCJ cross flow velocity of 7.68m/s.

5.2.3 Fouling indices

The fouling indices for membranes M1 – M3 during the dead end microfiltration runs was evaluated to vary from 30.47 – 24.72 for CJ and 3.89 – 3.38 % for ETCJ respectively at a ΔP of 207 kPa. For membrane M3, lowest fouling indices have been evaluated for all dead end MF runs. This indicates that pore blocking enhanced with increasing average pore size of

the membranes. For the M3 membrane, for a variation in ΔP from 69 to 207 kPa, the fouling indices varied from 27.06 – 24.72 for CJ and 4.32 – 3.38 % for ETCJ. Thus it can be observed that ΔP did not significantly influence the fouling indices for the M3 membrane and hence M3 membrane possesses optimal membrane morphologies for the clarification of pineapple juice. ETCJ is the ideal feed for the MF of pineapple juice using M3 membrane.

The variation of membrane fouling index with cross flow velocity for membranes M1 and M3 has been presented in Figure 5.5 a and 5.5 b for CJ and ETCJ respectively. As shown in Figure 5.5 a, for CJ, at a ΔP of 207 kPa, the fouling index varied from 27.59 – 45.38 for M1 and 20.06 – 40.06 % for M3 membranes with increasing cross flow velocities from 1.92 – 7.68 m/s. On the other hand, as shown in Figure 5.5 b, corresponding fouling indices for ETCJ varied from 4.11 – 5.21 and 2.33 – 3.02 % for M1 and M3 membranes respectively. Thus, it can be inferred that substantial fouling occurred for the CJ case even for cross flow microfiltration. This was not the case for ETCJ. Thus, enzyme treatment followed with centrifugation has been identified to be a very important step to enhance the shelf life of low cost ceramic membranes. Also, an enhancement in cross flow velocity resulted in an enhancement in the fouling indices for both CJ and ETCJ cases. This indicates that higher turbulence promoted pore blocking. However, the enhancement in the fouling index is not significant for the ETCJ case. This is due to lower pectin content in the ETCJ feed samples.

The variation of membrane fouling index with ΔP for maximum cross flow velocity case (7.68 m/s) is illustrated in Figure 5.5 c and 5.5 d for CJ and ETCJ respectively. As shown in Figure 5.5 c, for a ΔP variation from 69 – 207 kPa, the fouling indices varied from 49.72 – 45.38 for M1 and 43.87 – 40.06 % for M3 membrane and CJ feed samples. This indicates that

Table 5.3 a: Physico - chemical properties of CJ and ETCJ (pineapple juice) feed samples.

Juice type	Colour (A_{420})	Clarity (T_{660})	TSS (^{o}Brix)	Citric acid (wt %)	pH	Density (g/cm^3)	Viscosity (mPa.S)	AIS (wt %)	Vitamin C (mg/100 ml)
CJ (dead end MF)	0.735 – 0.764	71.22 – 73.25	13.56	0.79	3.53 – 3.54	1.02	2.055 – 2.081	0.28	27.51 – 27.62
ETCJ (dead end MF)	0.547 – 0.558	85.88 – 88.67	13.57	0.79	3.53 – 3.54	1.02	2.051 – 2.061	0.15	25.64 – 25.65
CJ (cross flow MF)	0.744 – 0.864	72.22 – 79.25	13.56	0.79	3.53 – 3.57	1.02 – 1.03	2.145 – 2.301	0.25 – 0.28	25.39 – 25.62
ETCJ (cross flow MF)	0.548 – 0.658	86.88 – 91.67	13.57	0.79	3.55 – 3.59	1.02 – 1.03	2.1 – 2.150	0.13 – 0.15	23.44 – 23.65

*Range of values are shown for various experiments.

Table 5.3 b: Physico - chemical properties of CJ and ETCJ permeate samples obtained for M1 - M3 membranes during pineapple juice clarification.

Juice type	Colour (A_{420})	Clarity (T_{660})	TSS (^{o}Brix)	Citric acid (wt %)	pH	Density (g/cm^3)	Viscosity (mPa.S)	AIS (wt %)	Vitamin C (mg/100 ml)
CJ (dead end MF)	0.1657 – 0.1714	83.75 – 90.12	13	0.75 – 0.76	3.56 – 3.57	1.02	1.981 – 2.011	0.16	27.37 – 27.56
ETCJ (dead end MF)	0.0326 – 0.0457	92.14 – 95.57	13	0.75 – 0.76	3.57 – 3.58	1.02	2.025 – 2.032	Nil	25.14 – 25.53
CJ (cross flow MF)	0.1907 – 0.2014	85.75 – 92.12	13.4 – 13.5	0.77 – 0.79	3.54 – 3.58	1.02 – 1.03	2.031 – 2.161	0.15 – 0.17	25.27 – 25.56
ETCJ (cross flow MF)	0.0356 – 0.0557	92.14 – 97.57	13.4 – 13.5	0.76 – 0.78	3.55 – 3.6	1.02 – 1.03	1.891 – 2.051	Nil	22.94 – 23.53

*Range of values are shown for various experimental conditions.

higher ΔP reduced membrane fouling. This is possibly due to the alteration of pore blocking phenomena and dynamic cake filtration layer characteristics with variations in ΔP. On the other hand, as shown in Figure 5.5 d, for a variation of ΔP from 69 – 207 kPa, the fouling indices varied from 6.83 – 5.21 for M1 membrane and 4.14 – 3.02 % for M3 membrane respectively using ETCJ. Once again, it can be confirmed that higher ΔP and enzyme treatment are most favourable choices to maximize the shelf life of the developed low cost ceramic membranes. Similar fouling indices were evaluated at lower cross flow velocities and have not been discussed in this section.

5.2.4 Separation characteristics

Tables 5.3 a and 5.3 b respectively present the physicochemical properties (such as colour, clarity, TSS, citric acid, pH, density, viscosity, AIS and vitamin C) of CJ, ETCJ feed samples and permeate samples. It can be observed that for both cases of dead end and cross flow MF, the performance of M1 and M3 membranes has been excellent to retain vitamins and reduce AIS with a significant reduction in colour index. In this regard, it is important to note that the pH (3.55 – 3.6), density (1.02 – 1.03), citric acid content (0.75 – 0.79) remained fairly constant and clarity (from 71.22 – 91.67 of feed to 83.75 – 97.57 for permeate sample) increased marginally. Amongst both dead end and cross flow MF, cross flow provided better performance in terms of clarity (83.75 – 95.57 for dead end and 85.75 – 92.12 for cross flow MF) and viscosity (1.981 – 2.032 for dead end and 1.891 – 2.161 mPa.S for cross flow MF) with other properties remaining almost similar. Thus, it is apparent that the microfiltration operation achieved the desired objective to retain nutrition content and sugars in the permeate samples and minimize or omit pectin (AIS) compounds. Further, it is interesting to note that

only when ETCJ feed samples were considered, the pectin content in the permeate samples reduced to negligible value. Thus the MF of ETCJ feed samples provided high quality clarified pineapple juice that can be subjected to long term storage without further deterioration.

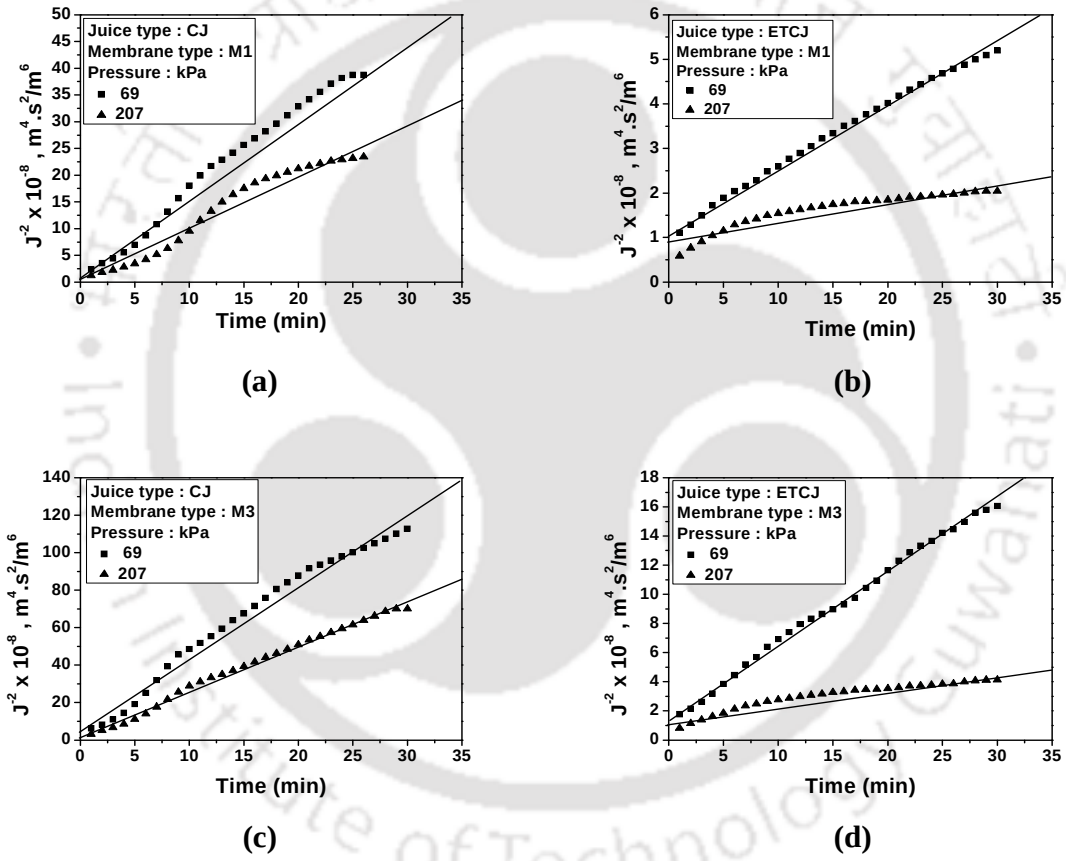

Figure 5.6: Fitness plots for cake filtration model to represent pineapple juice dead end MF flux data: (a) M1 membrane and CJ; (b) M1 membrane and ETCJ; (b) M3 membrane and CJ; (d) M3 membrane and ETCJ.

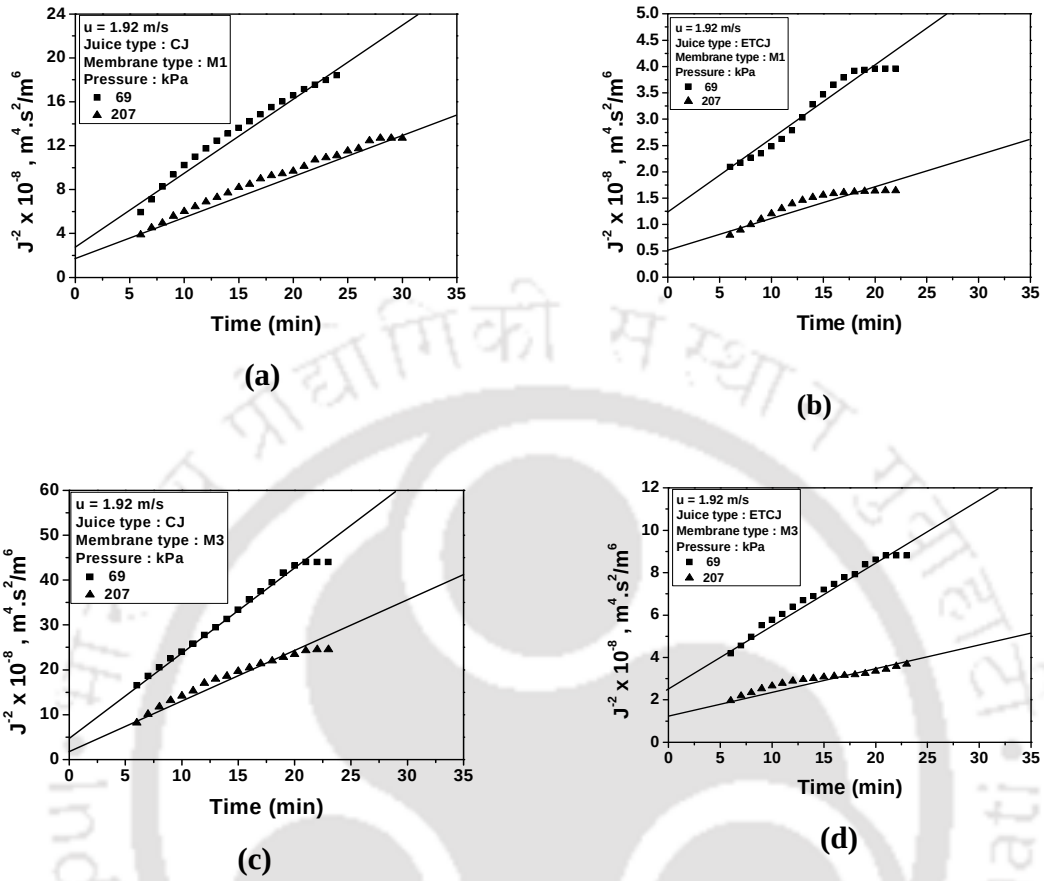

Figure 5.7: Fitness of cake filtration model to represent pineapple juice cross flow MF flux data at a cross flow velocity of 1.92 m/s: (a) M1 membrane and CJ; (b) M1 membrane and ETCJ; (b) M3 membrane and CJ; (d) M3 membrane and ETCJ.

5.2.5 Fouling models fitness

For all cases of dead end of pineapple juice samples (both CJ and ETCJ), it was evaluated that amongst all fouling models, cake filtration model fit well to represent experimentally measured flux data. Figure 5.6 a – 5.6 d present the fitness of cake filtration model for the flux decline data obtained for M1 and M3 membranes at various values of ΔP.

Corresponding coefficient of correlation (R^2), slope and intercept parameters obtained from the fitness plots of various fouling models for the dead end MF of CJ and ETCJ using M1 and M3 membranes is presented in Table 5.4. As presented in Figure 5.6 a – 5.6 d, a good fitness of cake filtration model is apparent for all cases, even though it can be observed that minor deviations exist either at the start of the run or at intermediate time periods. This indicates that combination fitness models might fit better than single fouling models. Thus, it is apparent that the pertinent fouling mechanisms are strongly governed by the time dependent variation of the parameters associated to polarization and cake layers during the MF. This confirms that the membrane morphology had significant interaction with the pectin content in the juice which significantly contributed to the additional permeation resistances during the MF runs. For the cross flow microfiltration case, similar experimental trends were obtained for various cases of cross flow velocities and ΔP.

Figure 5.7 a – 5.7 d present the fitness of cake filtration model at a cross flow velocity of 1.92 m/s for both M1 and M3 membranes. Corresponding coefficient of correlation (R^2), slope and intercept parameters obtained from the fitness plots for various fouling models during the cross flow MF of CJ and ETCJ for both M1 and M3 membranes is presented in Table 5.5. As shown in Figure 5.7 a – 5.7 d, minor variations from the cake filtration model exist either at the start or during the intermediate time periods of the MF runs. A critical comparison between the dead end and cross flow MF cake filtration constants indicates that for CJ case, k_c varied from $0.2 - 0.4 \times 10^7$ $s.m^{-2}$ for dead end MF and $0.1 - 0.2 \times 10^7$ $s.m^{-2}$ for cross flow MF with the M3 membrane. Corresponding J_0^{-2} varied from $2 - 6 \times 10^8$ for dead end MF and $5 - 7 \times 10^8$ for cross flow MF. Similarly, for ETCJ case, k_c varied from $1 - 5 \times 10^7$ $s.m^{-2}$ for dead end MF and $0.9 - 3 \times 10^7$ $s.m^{-2}$ for cross flow MF for the M3 membrane.

Table 5.4: A summary of fouling model fitness parameters (Coefficient of correlation, slope and intercept) to represent dead end pineapple juice microfiltration flux data.

Membrane name	Juice type	Pressure (kPa)	Models	Regression coefficient (R^2)	Slope	Intercept
M1	CJ	69	CPB	0.86	$k_b = 0.049\ s^{-1}$	$\ln(J_0^{-1}) = 9.97$
			SPB	0.91	$k_s = 4.774\ m^{-0.5}\ s^{-0.5}$	$J_0^{-0.5} = 143.6$
			IPB	0.95	$k_i = 1889\ m^{-1}$	$J_0^{-1} = 19197$
			CF	0.99	$k_c = 0.20 \times 10^7\ s.m^{-2}$	$J_0^{-2} = 0.80 \times 10^8$
		207	CPB	0.86	$k_b = 0.055\ s^{-1}$	$\ln(J_0^{-1}) = 9.62$
			SPB	0.90	$k_s = 4.653\ m^{-0.5}\ s^{-0.5}$	$J_0^{-0.5} = 119.8$
			IPB	0.93	$k_i = 1608\ m^{-1}$	$J_0^{-1} = 13001$
			CF	0.96	$k_c = 0.10 \times 10^7\ s.m^{-2}$	$J_0^{-2} = 0.40 \times 10^8$
	ETCJ	69	CPB	0.93	$k_b = 0.023\ s^{-1}$	$\ln(J_0^{-1}) = 9.404$
			SPB	0.96	$k_s = 1.539\ m^{-0.5}\ s^{-0.5}$	$J_0^{-0.5} = 109.3$
			IPB	0.98	$k_i = 402.3\ m^{-1}$	$J_0^{-1} = 11699$
			CF	0.99	$k_c = 1.00 \times 10^7\ s.m^{-2}$	$J_0^{-2} = 1.00 \times 10^8$
		207	CPB	0.74	$k_b = 0.015\ s^{-1}$	$\ln(J_0^{-1}) = 9.199$
			SPB	0.78	$k_s = 0.810\ m^{-0.5}\ s^{-0.5}$	$J_0^{-0.5} = 99.52$
			IPB	0.81	$k_i = 175.5\ m^{-1}$	$J_0^{-1} = 9905$
			CF	0.86	$k_c = 0.40 \times 10^7\ s.m^{-2}$	$J_0^{-2} = 1.00 \times 10^8$
M3	CJ	69	CPB	0.82	$k_b = 0.041\ s^{-1}$	$\ln(J_0^{-1}) = 10.53$
			SPB	0.88	$k_s = 5.248\ m^{-0.5}\ s^{-0.5}$	$J_0^{-0.5} = 192.1$
			IPB	0.93	$k_i = 2701\ m^{-1}$	$J_0^{-1} = 35297$
			CF	0.98	$k_c = 0.40 \times 10^7\ s.m^{-2}$	$J_0^{-2} = 6.00 \times 10^8$
		207	CPB	0.84	$k_b = 0.043\ s^{-1}$	$\ln(J_0^{-1}) = 10.25$
			SPB	0.90	$k_s = 4.789\ m^{-0.5}\ s^{-0.5}$	$J_0^{-0.5} = 165.8$

Membrane name	Juice type	Pressure (kPa)	Models	Regression coefficient (R^2)	Slope	Intercept
			IPB	0.95	$k_i = 2174\ m^{-1}$	$J_0^{-1} = 25846$
			CF	0.99	$k_c = 0.20 \times 10^7\ s.m^{-2}$	$J_0^{-2} = 2.00 \times 10^8$
	ETCJ	69	CPB	0.90	$k_b = 0.033\ s^{-1}$	$\ln(J_0^{-1}) = 9.730$
			SPB	0.94	$k_s = 2.706\ m^{-0.5}\ s^{-0.5}$	$J_0^{-0.5} = 127.9$
			IPB	0.97	$k_i = 890.7\ m^{-1}$	$J_0^{-1} = 15653$
			CF	0.99	$k_c = 5.00 \times 10^7\ s.m^{-2}$	$J_0^{-2} = 1.00 \times 10^8$
		207	CPB	0.77	$k_b = 0.020\ s^{-1}$	$\ln(J_0^{-1}) = 9.419$
			SPB	0.81	$k_s = 1.250\ m^{-0.5}\ s^{-0.5}$	$J_0^{-0.5} = 111.0$
			IPB	0.85	$k_i = 313.1\ m^{-1}$	$J_0^{-1} = 12294$
			CF	0.91	$k_c = 1.00 \times 10^7\ s.m^{-2}$	$J_0^{-2} = 1.00 \times 10^8$

Table 5.5: A summary of fouling model fitness parameters (Coefficient of correlation, slope and intercept) to represent cross flow pineapple juice microfiltration flux data (measured at a cross flow velocity of 1.92 m/s).

Membrane name	Juice type	Pressure (kPa)	Models	Regression coefficient (R^2)	Slope	Intercept
M1	CJ	69	CPB	0.92	$k_b = 0.027\ s^{-1}$	$\ln(J_0^{-1}) = 10.06$
			SPB	0.94	$k_s = 2.568\ m^{-0.5}\ s^{-0.5}$	$J^{-0.5} = 150.5$
			IPB	0.96	$k_i = 953.9\ m^{-1}$	$J_0^{-1} = 21644$
			CF	0.98	$k_c = 7.00 \times 10^7\ s.m^{-2}$	$J_0^{-2} = 3.00 \times 10^8$
		207	CPB	0.94	$k_b = 0.022\ s^{-1}$	$\ln(J_0^{-1}) = 9.874$
			SPB	0.96	$k_s = 1.896\ m^{-0.5}\ s^{-0.5}$	$J^{-0.5} = 137.2$
			IPB	0.97	$k_i = 640\ m^{-1}$	$J_0^{-1} = 18052$
			CF	0.99	$k_c = 4.00 \times 10^7\ s.m^{-2}$	$J_0^{-2} = 2.00 \times 10^8$

Membrane name	Juice type	Pressure (kPa)	Models	Regression coefficient (R^2)	Slope	Intercept
	ETCJ	69	CPB	0.95	$k_b = 0.023\ s^{-1}$	$\ln(J_0^{-1}) = 9.449$
			SPB	0.95	$k_s = 1.518\ m^{-0.5} s^{-0.5}$	$J^{-0.5} = 111.4$
			IPB	0.96	$k_i = 400.0\ m^{-1}$	$J_0^{-1} = 12066$
			CF	0.96	$k_c = 1.00 \times 10^7\ s.m^{-2}$	$J_0^{-2} = 1.00 \times 10^8$
		207	CPB	0.82	$k_b = 0.020\ s^{-1}$	$\ln(J_0^{-1}) = 9.07$
			SPB	0.84	$k_s = 1.104\ m^{-0.5} s^{-0.5}$	$J^{-0.5} = 92.62$
			IPB	0.85	$k_i = 233.7\ m^{-1}$	$J_0^{-1} = 8445$
			CF	0.87	$k_c = 0.50 \times 10^7\ s.m^{-2}$	$J_0^{-2} = 0.70 \times 10^8$
M3	CJ	69	CPB	0.97	$k_b = 0.029\ s^{-1}$	$\ln(J_0^{-1}) = 10.5$
			SPB	0.97	$k_s = 3.402\ m^{-0.5} s^{-0.5}$	$J^{-0.5} = 186.8$
			IPB	0.98	$k_i = 1591\ m^{-1}$	$J_0^{-1} = 33055$
			CF	0.99	$k_c = 0.20 \times 10^7\ s.m^{-2}$	$J_0^{-2} = 7.00 \times 10^8$
		207	CPB	0.90	$k_b = 0.028\ s^{-1}$	$\ln(J_0^{-1}) = 10.22$
			SPB	0.92	$k_s = 2.889\ m^{-0.5} s^{-0.5}$	$J^{-0.5} = 163.3$
			IPB	0.94	$k_i = 1162\ m^{-1}$	$J_0^{-1} = 25502$
			CF	0.97	$k_c = 0.10 \times 10^7\ s.m^{-2}$	$J_0^{-2} = 5.00 \times 10^8$
	ETCJ	69	CPB	0.95	$k_b = 0.021\ s^{-1}$	$\ln(J_0^{-1}) = 9.856$
			SPB	0.96	$k_s = 1.704\ m^{-0.5} s^{-0.5}$	$J^{-0.5} = 136.8$
			IPB	0.97	$k_i = 545.2\ m^{-1}$	$J_0^{-1} = 18270$
			CF	0.98	$k_c = 3.00 \times 10^7\ s.m^{-2}$	$J_0^{-2} = 3.00 \times 10^8$
		207	CPB	0.91	$k_b = 0.015\ s^{-1}$	$\ln(J_0^{-1}) = 9.524$
			SPB	0.92	$k_s = 0.988\ m^{-0.5} s^{-0.5}$	$J^{-0.5} = 116.5$
			IPB	0.93	$k_i = 256.2\ m^{-1}$	$J_0^{-1} = 13432$
			CF	0.95	$k_c = 0.90 \times 10^7\ s.m^{-2}$	$J_0^{-2} = 2.00 \times 10^8$

Corresponding J_0^{-2} was 1×10^8 for dead end MF and was $2 - 3 \times 10^8$ for cross flow MF. Thus, it is apparent that significant deviations exist between the cake filtration constants obtained for both dead end and cross flow MF and an assumption to relate both dead end and cross flow MF is not valid.

Also, it can be observed that for cross flow MF, the J_o values for CJ were significantly lower ($38 - 45 \times 10^{-6}$ $m^3/m^2.s$) than those obtained for the ETCJ ($58 - 71 \times 10^{-6}$ $m^3/m^2.s$), thus indicating that instantaneous fouling of the M3 membrane is significantly high for the CJ case due to greater quantity of colloidal and pectin material in the feed juice. Also, the cake filtration constant for CJ was significantly lower ($0.1 - 0.2 \times 10^7$ $s.m^{-2}$) than that obtained for the ETCJ ($0.9 - 3 \times 10^7$ $s.m^{-2}$). This also indicates that flux enhancement with time was significant for the case of ETCJ when compared to the CJ. These analytical observations are in good agreement with the experimental trends presented in the earlier sub - sections.

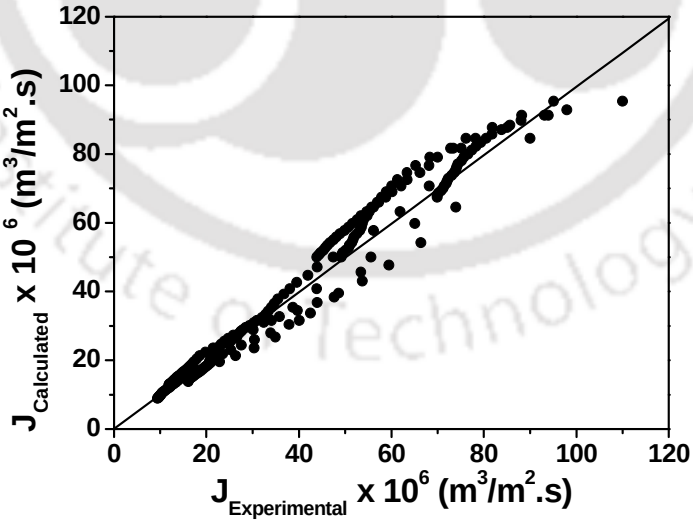

(a)

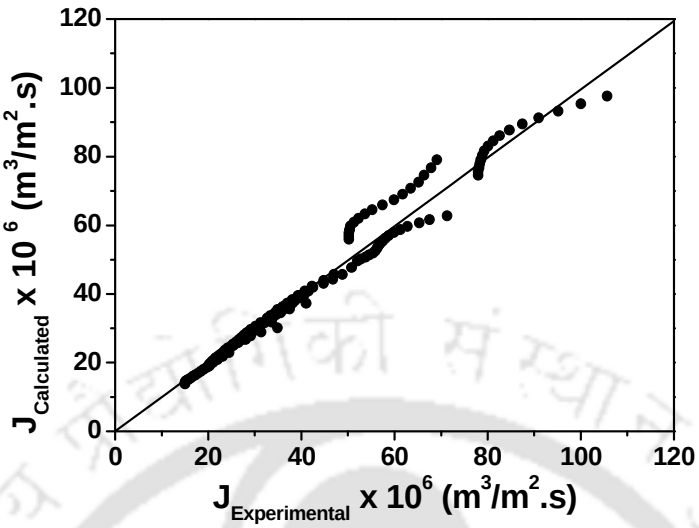

(b)

Figure 5.8: Parity plots for best fit pore blocking models to represent CJ and ETCJ (pineapple juice) MF flux data for (a) dead end and (b) cross flow microfiltration.

Figure 5.8 a and 5.8 b present the parity plots for the predicted and measured experimental flux data in the dead end and cross flow MF, respectively. Both CJ and ETCJ cases have been included in each plot. It can be observed that for both cases of dead end and cross flow MF, the fitness of cake filtration is good but not excellent. This is possibly due to the variation of dynamic cake filtration layer in due course of time period for the MF runs. Thus, to achieve a more accurate prediction, combination models need to be considered in the modelling approach. The RMS error for the experimental data for dead end and cross flow MF is 9.92 and 6.32 % respectively.

Cross flow Microfiltration Studies with Mosambi and Orange Juices

In chapter 4, the results obtained from the dead end MF of mosambi juice using membranes M1 – M3 have been presented. Among the membranes, M1 and M3 provided higher and lower fluxes and satisfactory dead end MF performance. For all membranes, the fouling index for ETCJ is lower than that of CJ. Considering these aspects, it will be interesting to carry out cross flow MF of ETCJ mosambi juice. On the other hand, orange juice dead end MF has been reported in the literature for ETCJ samples. In addition, few cases have also reported the cross flow MF of orange juice. Cross flow MF studies for orange juice samples with low cost ceramic membranes has not been reported till date. Therefore, it is interesting to carry out such studies using orange juice. Also, the cross flow MF of orange juice is conducted so as to compare the flux and separation factors obtained for the mosambi juice.

6.1 Experimental

This chapter addresses the cross flow MF of ETCJ (mosambi and orange) juices using membranes M1 – M3 (average pore size of 1.69 – 0.72 μm). The microfiltration procedures, adopted analytical methods and experimental set up for cross flow microfiltration have been presented in chapters 3 and 4, respectively in the thesis. The analytical methods refer to the estimation of colour, clarity, TSS, citric acid, pH, density, viscosity, AIS and vitamin C for both feed and permeate samples. The operating parameters for MF operation are ΔP of 69 - 207 kPa and cross flow velocity of 1.92 – 5.76 m/s. For all membranes, the fouling indices

have been evaluated procedures are presented in section 2.1.6 of the thesis. Standard fouling models (complete, standard, intermediate pore blocking and cake filtration) have been evaluated for their fitness to represent cross flow MF flux data. Further details with respect to fouling models and the associated procedures have been presented in chapter 2 of the thesis. Since Pagliero *et al.* [54] applied resistance in series model, similar efforts have been considered in this work to compare the steady state total permeation resistances with those reported in their work. Further details are presented in the subsequent section.

6.2 Evaluation of fouling resistances

The total fouling resistance R_t during a cross MF run is expressed as the sum of hydraulic resistance R_m, reversible fouling resistance R_r and irreversible fouling resistance R_i:

$$R_t = R_i + R_m + R_r \qquad (6.1)$$

In the above expressions, R_r corresponds to the permeation resistance caused by reversible adsorption, concentration polarization and cake or gel layer resistance. Similarly, R_i corresponds to the permeation resistance caused by irreversible adsorption and internal pore blocking. The hydraulic permeation resistance has been evaluated using the pure water flux obtained for the fresh membrane after compaction and is expressed as:

$$R_m = \frac{\Delta P}{\eta_w J_w} \qquad (6.2)$$

The irreversible fouling resistance has been evaluated using the pure water flux of the cleaned membrane after cross flow MF operation and is expressed as:

$$R_i = \frac{\Delta P}{\eta_w J_w^{clean}} - R_m \qquad (6.3)$$

The total permeation resistance has been evaluated using the expression

$$R_t = \frac{\Delta P}{\eta_{permeate} J_{juice}} \qquad (6.4)$$

Using evaluated R_t, R_i and R_m, R_r is determined using the expression:

$$R_r = R_t - R_i - R_m \qquad (6.5)$$

With low fouling index values, $\frac{R_i}{R_r}$ will be insignificant. Therefore, it will be interesting to evaluate the contributions of R_i, R_m and R_r to R_t for various cases. The next section presents in detail the results obtained from the cross flow MF studies.

6.3 Results and discussion

6.3.1 Effect of ΔP on flux decline

For membranes M1 – M3, at a cross flow velocity u = 1.92 m/s, Figure 6.1 (a, c and e) respectively present the flux decline with time at various ΔP (69, 138 and 207) kPa. The time dependent flux variation with ΔP (69 and 207) kPa ETCJ (orange) is being presented in Figure 6.1 (b, d and f) for membranes M1 – M3 respectively. For all cases, flux increased with increasing ΔP and highest flux profiles have been obtained at ΔP = 207 kPa. For membrane M1 and ETCJ feed (mosambi), the flux varied from 91 – 43, 101 – 49 and 111 – 54 × 10^{-6} m^3/m^2.s at a ΔP of 69, 138 and 207 kPa respectively. These flux profiles reduced to 78 – 27, 89 – 36 and 101 – 44 × 10^{-6} m^3/m^2.s for M2 membrane and 71 – 19, 81 – 26 and 91 – 34 × 10^{-6} m^3/m^2.s for M3 membrane, for corresponding variation in ΔP. Similar flux

profiles have been obtained for the cross flow MF of ETCJ samples prepared with orange juice.

For the orange juice case, the time dependent flux varied from 111 – 44 and 151 – 63 × 10^{-6} $m^3/m^2.s$ for M1 membrane, 91 – 32 and 126 – 55 × 10^{-6} $m^3/m^2.s$ for M2 membrane and 71 – 25 and 101 – 35 × 10^{-6} $m^3/m^2.s$ for M3 membrane at ΔP of 69 and 207 kPa respectively. The increasing in membrane flux with ΔP is due to an increase in the driving force across the membrane. Also, the membrane flux decreased with reducing average pore size of the membrane i.e. highest fluxes have been obtained for M1 membrane and lowest fluxes for the M3 membrane.

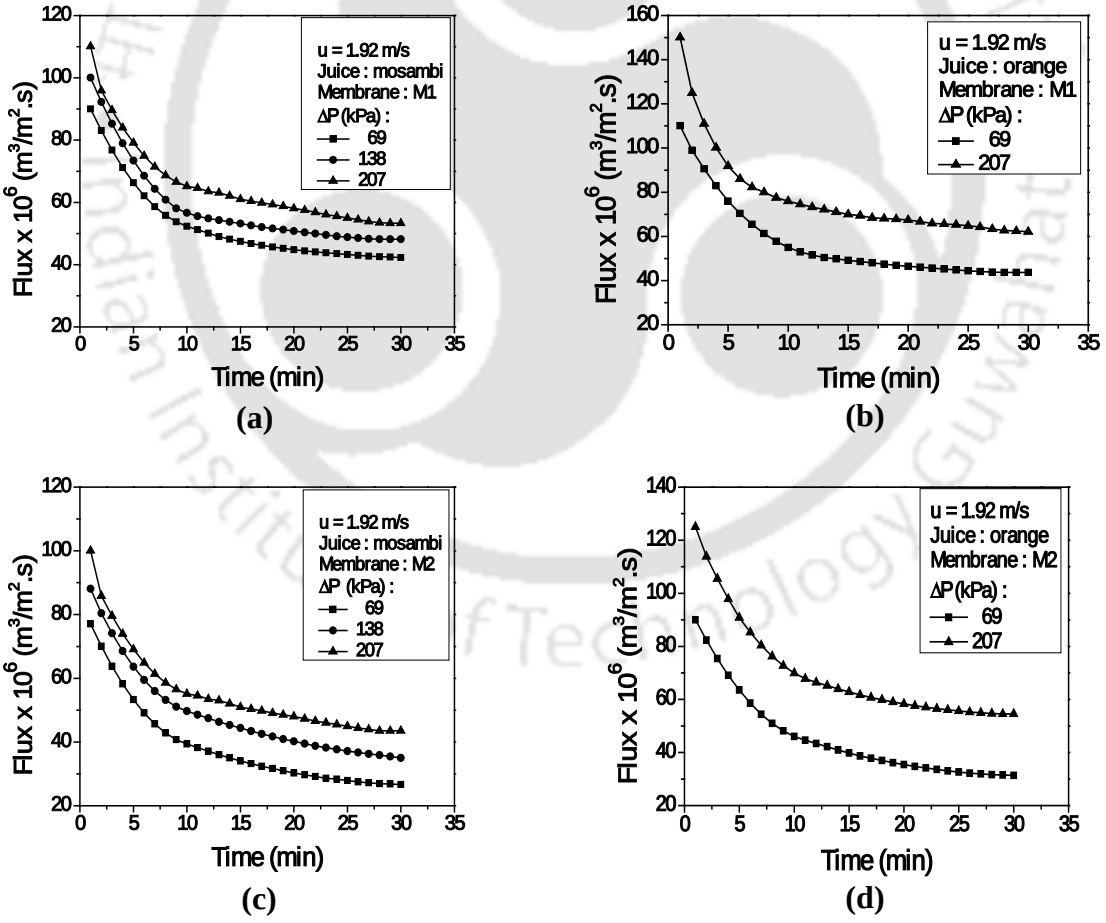

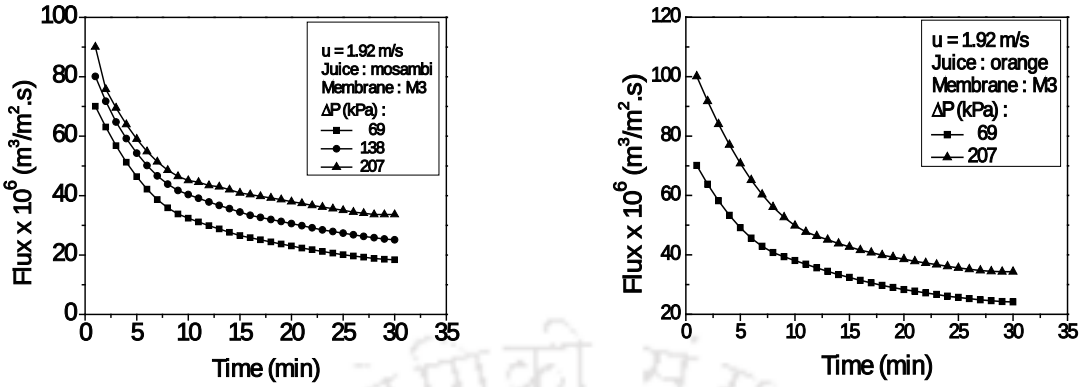

Figure 6.1: Variation of time dependent membrane flux with ΔP at u = 1.92 m/s for various membranes using ETCJ: (a) M1 membrane, mosambi juice (b) M1 membrane, orange juice (c) M2 membrane, mosambi juice (d) M2 membrane, orange juice (e) M3 membrane, mosambi juice (f) M3 membrane, orange juice.

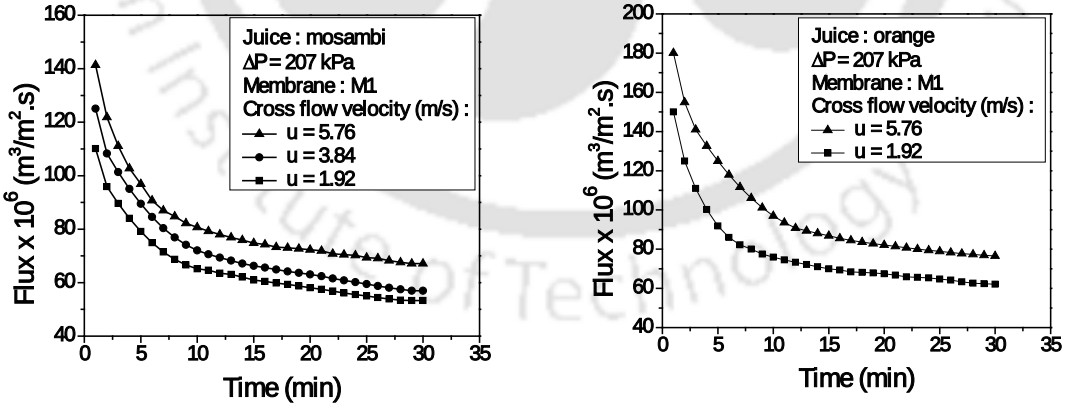

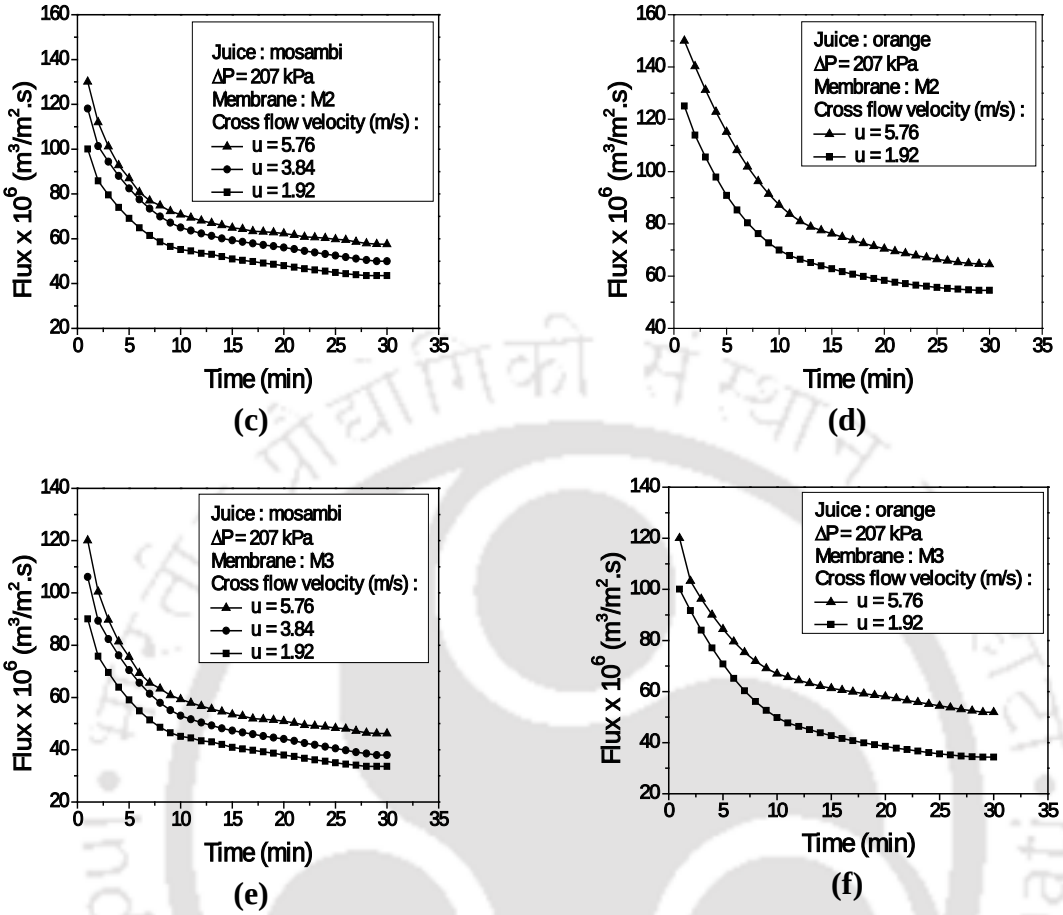

Figure 6.2: Variation of time dependent membrane flux with cross flow velocity for membranes M1 – M3 using ETCJ at ΔP = 207 kPa: (a) M1 membrane, mosambi juice (b) M1 membrane, orange juice (c) M2 membrane, mosambi juice (d) M2 membrane, orange juice (e) M3 membrane, mosambi juice (f) M3 membrane, orange juice.

6.3.2 Effect of cross flow velocity on flux decline

At a ΔP of 207 kPa, Figure 6.2 (a, c and e) illustrates the variation in mosambi juice (ETCJ) time dependent membrane flux with variation in cross flow velocity for the membranes M1 – M3 respectively. It can be observed that for M1 membrane (Figure 6.2 a) the flux varied from 142 – 68, 126 – 57 and 111 – 54 × 10^{-6} m^3/m^2.s for cross flow velocities of 5.76, 3.84 and

1.92 m/s respectively. Similarily for the M2 membrane (Figure 6.2 c), the membrane flux varied from 131 – 58 (u = 5.76 m/s), 119 – 50 (u = 3.84 m/s) and 101 – 44 × 10^{-6} m^3/m^2.s (u = 1.92 m/s). For the variation in time from 1 to 30 minutes, for M3 membrane (Figure 6.2 e), lower membrane fluxes have been obtained (121 – 47 at u = 5.76 m/s, 107 – 38 at u = 3.84 m/s and 91 – 34 × 10^{-6} m^3/m^2.s at u = 1.92 m/s). Thus, the membrane flux increased with increasing cross flow velocity and decreasing average membrane pore size. From Figure 6.2 (a, c and e), it can be also evaluated that steady state membrane flux has been obtained at a time of 30 minutes for all cases.

A similar variation in orange juice (ETCJ) membrane flux profiles can be observed in Figure 6.2 (b, d and f) for membranes M1 – M3. As shown, at a ΔP of 207 kPa, the time dependent orange juice (ETCJ) flux varied from 181 – 77 × 10^{-6} m^3/m^2.s for u = 5.76 m/s, 151 – 63 × 10^{-6} m^3/m^2.s for u = 1.92 m/s (Figure 6.2 b). For membrane M2, corresponding membrane fluxes varied from 151 – 65 × 10^{-6} m^3/m^2.s for u = 5.76 m/s and 126 – 55 × 10^{-6} m^3/m^2.s at u = 1.92 m/s (Figure 6.2 d). Similarily, for M3 membrane the lower membrane flux of 121 – 52 × 10^{-6} m^3/m^2.s at u = 5.76 m/s, 101 – 35 × 10^{-6} m^3/m^2.s for u = 1.92 m/s have been obtained (Figure 6.2 f). For the orange juice, steady state flux was obtained at 30 minutes for all cases. The enhancement in mosambi and orange juice (ETCJ) membrane fluxes with increasing cross flow velocities is due to the reason that higher cross flow velocities induce higher shear effects which in turn enhance the porosity of the dynamic cake filtration layer that gets formed during the cross flow MF operation. Higher shear effects facilitate significant variation in the morphology (pore size, porosity and thickness) of the dynamic cake filtration

layer. Higher cross flow velocities tend to reduce thickness and increase the pore size and porosity of the dynamic layer. This reduces the pore blocking and membrane fouling.

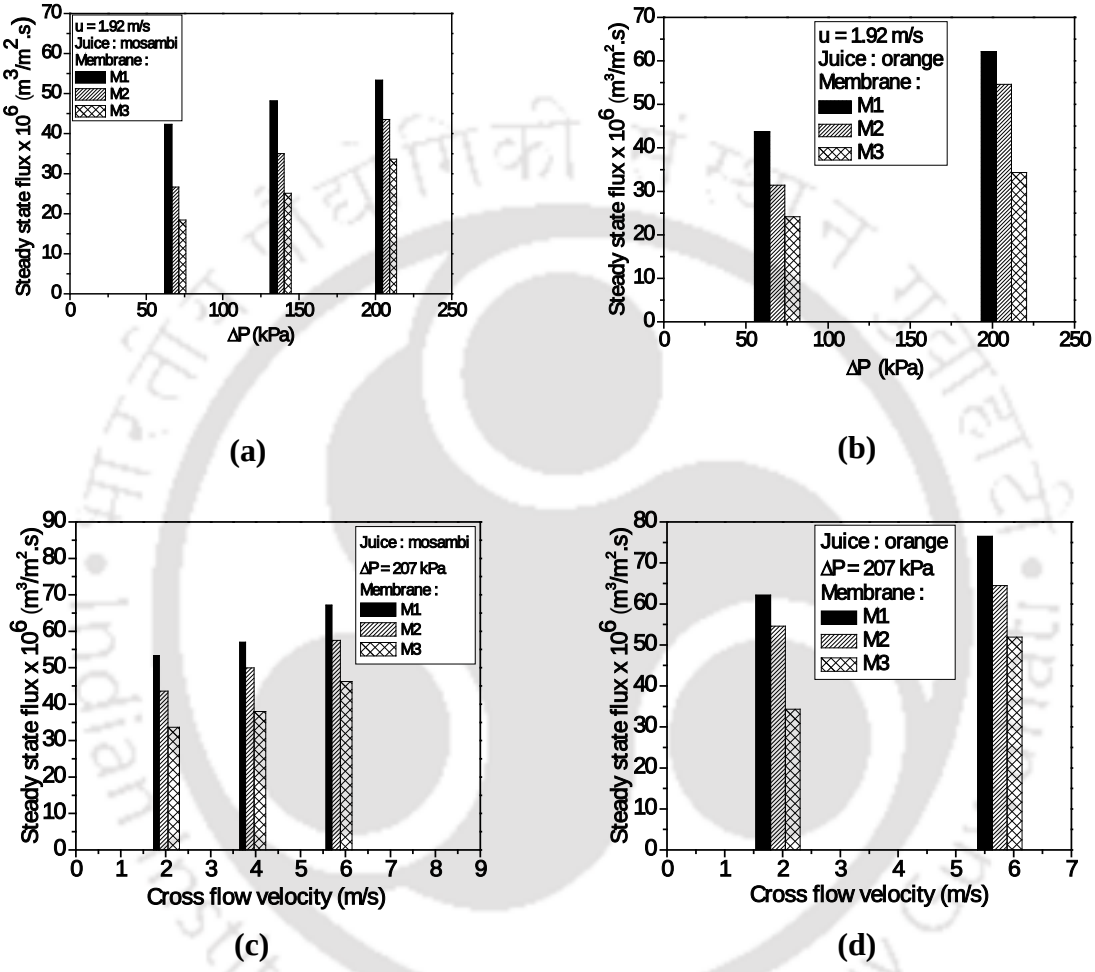

Figure 6.3: Variation of steady state membrane flux with ΔP and u for membranes M1 – M3 and ETCJ samples: (a) Effect of ΔP for mosambi juice at u = 1.92 m/s (b) Effect of ΔP for orange juice at u = 1.92 m/s (c) Effect of u for mosambi juice at ΔP = 207 kPa (d) Effect of u for orange juice at ΔP = 207 kPa.

6.3.3 Effect of operating parameters on steady state flux

The effectiveness of membrane technology for industrial application is typically expressed in terms of the steady state flux variation with operating (ΔP and u) and membrane (average pore size) parameters. Figure 6.3 (a – d) presents the variation of steady state membrane flux with operating membrane parameters during mosambi and orange juice cross flow MF. At a cross flow velocity of 1.92 m/s for ETCJ (mosambi), Figure 6.3 a presents the effect of ΔP on steady state flux for membranes M1 – M3. For these cases, the steady state flux varied from 43 – 54, 27 – 44 and 19 – 34 × 10^{-6} m^3/m^2.s for a ΔP of 69, 138 and 207 kPa for membranes M1, M2 and M3 respectively.

For an increase in ΔP from 69 – 207 kPa, this corresponds to an increase of 26, 63 and 89 % in steady state flux for membranes M1, M2 and M3 respectively. Similar steady state flux trends were obtained for orange juice cross flow MF (Figure 6.3 (b)). For these cases, with an increase in ΔP from 69 to 207 kPa, the steady state flux increased from 44 – 63, 32 – 55 and 25 – 35 × 10^{-6} m^3/m^2.s for membranes M1, M2 and M3 membranes respectively. These correspond to 44, 72 and 40 % increase in steady state flux for membranes M1, M2 and M3 respectively for a similar enhancement in ΔP (69 – 207 kPa). The effect of cross flow velocity on the steady state flux at ΔP = 207 kPa is illustrated in Figure 6.3 c and Figure 6.3 d for ETCJ (mosambi) and ETCJ (orange) feed samples respectively. During mosambi juice cross flow MF, for a variation in u from 1.92 – 5.76 m/s, it can be observed that the steady state flux varied from 54 – 68, 44 – 58 and 34 – 47 × 10^{-6} m^3/m^2.s for membranes M1, M2 and M3 respectively. For an enhancement in cross flow velocity from 1.92 – 5.76 m/s, this corresponds to 26, 32 and 39 % enhancement in steady state flux for membranes M1, M2 and

M3 respectively. Similar steady state flux trends have been obtained for orange juice cross flow MF. For an increase in cross flow velocity from 1.92 – 5.76 m/s, the corresponding steady state flux values varied from 63 – 77, 55 – 65 and 35 – 52 × 10^{-6} $m^3/m^2.s$ for membranes M1, M2 and M3 respectively. Thus, for an increase in cross flow velocity from 1.92 – 5.76 m/s, this refers to an increase in steady state flux by 23, 19 and 49 % for membranes M1, M2 and M3 respectively.

6.3.4 Comparison with literature flux data

A comparative summary of the MF and UF flux data obtained till date for mosambi juice clarification is presented in Table 6.1. From the table, it can be observed that, except this work, there is no data with respect to the cross flow MF of mosambi juice. Compared to the earlier work of Nandi *et al.* [9], higher dead end and cross flow MF data have been obtained in this work. Further, it is to be noted that the cross flow MF data for membranes M1 (average pore size 1.69 µm) and M3 (average pore size 0.72 µm) are lower than the dead end MF flux reported in the earlier work [18]. This is possibly due to the variation in the membrane morphology during cross flow MF in the earlier stages of compaction. Further research in this direction would be beneficial to understand the issues related to membrane morphology and flux dependence of the same. Table 6.2 presents a summary of the orange juice MF flux data that has been reported till date. It can be observed that only the earlier work of Nandi *et al.* [40] (dead end MF) is comparable the early fluxes reported in this work. For membrane M3 a higher flux of 34.3 × 10^{-6} $m^3/m^2.s$ has been obtained at a ΔP of 207 kPa and u = 1.92 m/s which is significantly higher than dead end MF flux 34 × 10^{-6} $m^3/m^2.s$ obtained at a ΔP of

Table 6.1: A summary of obtained (M1 and M3 membrane) and literature mosambi juice MF and UF flux data.

S. No.	Pre treatment	Membrane material	MWCO (kDa)/ pore size (µm)	Geometry	Mode of operation	Cross flow velocity (m/s)	Flux × 10^6 ($m^3/m^2.s$)	Pressure diffrential (kPa)	Reference
1.	Enzyme treatment + centrifugation	Kaolin	0.285	Circular disk	Dead end (MF)	-	35	344.74	[9]
	Centrifugation	Kaolin	0.285	Circular disk	Dead end (MF)	-	16	344.74	[9]
2.	Enzyme treatment + centrifugation	Kaolin	0.86	Circular disk	Dead end (MF)	-	30	82.7	[32]
	Centrifugation	Kaolin	1.08	Circular disk	Dead end (MF)	-	14	82.7	[32]
3.	Enzyme treatment + bentonite	Polyamide	50	-	Dead end (UF)	-	6.4	414	[33]
4.	-	Cellulose	0.2	-	Dead end (MF)	-	1.9	138	[34]
	-	acetate	50	-	Dead end (UF)	-	3.3	414	[34]
		Polyamide							
5.	Enzyme treatment + centrifugation	Kaolin	1.69	Circular disk	Dead end (MF)	-	70	206.70	This work
	Centrifugation	Kaolin	1.69	Circular disk	Dead end (MF)	-	20	206.70	This work
	Enzyme treatment + centrifugation	Kaolin	0.72	Circular disk	Dead end (MF)	-	44	206.70	This work
	Centrifugation	Kaolin	0.72	Circular disk	Dead end (MF)	-	9	206.70	This work
6.	Enzyme treatment + centrifugation	Kaolin	1.69	Circular disk	Cross flow (MF)	1.92	53.3	207	This work
	Enzyme treatment + centrifugation	Kaolin	0.72	Circular disk	Cross flow (MF)	1.92	33.6	207	This work

Table 6.2: A summary of obtained (M1 and M3 membrane) and literature orange juice MF flux data.

S. No.	Pre treatment	Membrane material	Pore size (µm)	Geometry	Mode of operation	Cross flow velocity (m/s)	Flux × 10^6 ($m^3/m^2.s$)	Pressure diffrential (kPa)	Reference
1.	Enzyme treatment + centrifugation	Kaolin	0.285	Circular Disk	Dead end	-	34	344.74	[40]
	Centrifugation	Kaolin	0.285	Circular Disk	Dead end	-	13	344.74	[40]
2.	-	PVDF/PMMA	0.1	-	Cross flow	1.25	13.1	100	[54]
3.	-	Alumina	0.8	Monotubular	Cross flow	6.7	10.3	70	[53]
4.	Enzyme treatment + centrifugation	Kaolin	1.69	Circular disk	Cross flow	1.92	62.1	207	This work
	Enzyme treatment + centrifugation	Kaolin	0.72	Circular disk	Cross flow	1.92	34.3	207	This work

344.7 kPa by Nandi *et al.* [40]. Thus, the fabricated membranes have provided better performance for the orange juice.

6.3.5 Fitness of fouling models

Various fouling models (complete pore blocking, standard pore blocking, intermediate pore blocking and cake filtration) have been evaluated for their fitness with the measured cross flow MF data for both mosambi and orange juice (ETCJ) feed samples. Among all models, cake filtration model provided the best fitness. Corresponding fitness plots for ΔP effect have been presented in Figure 6.4 (a – f) and cross flow velocity effect in Figure 6.5 (a – f). It can be observed that for cases corresponding to Figure 6.4 a, b and d, the deviations are

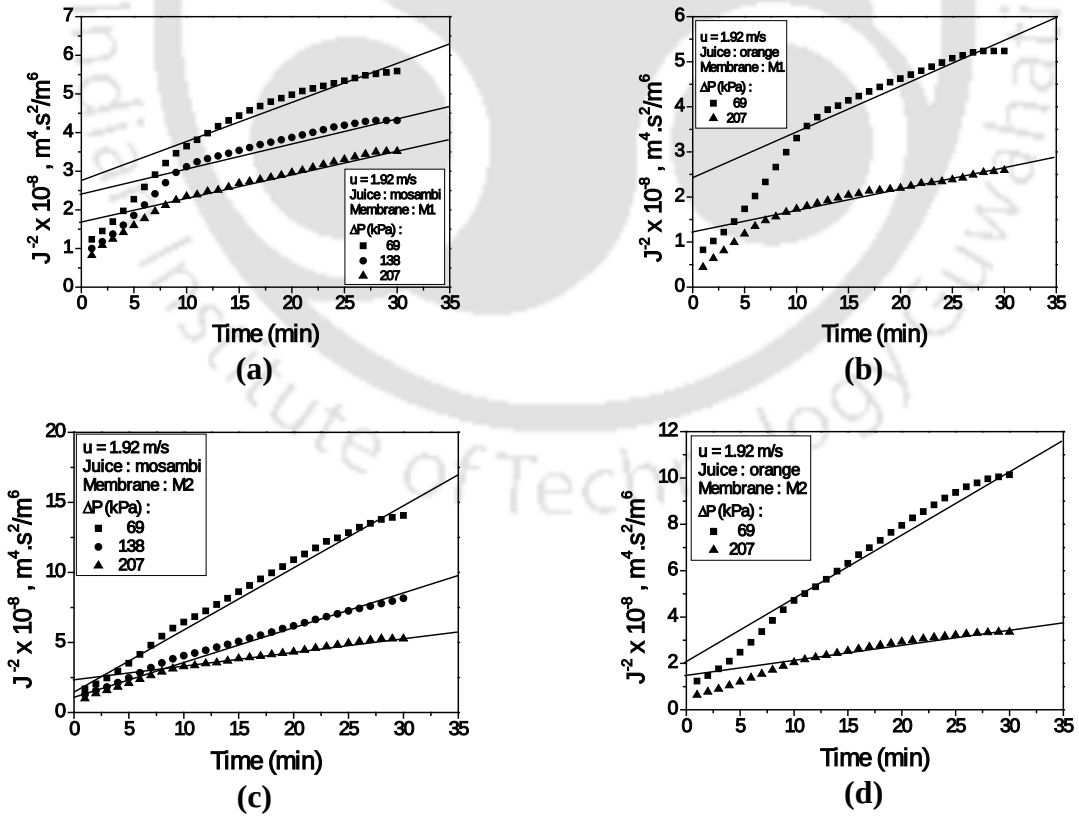

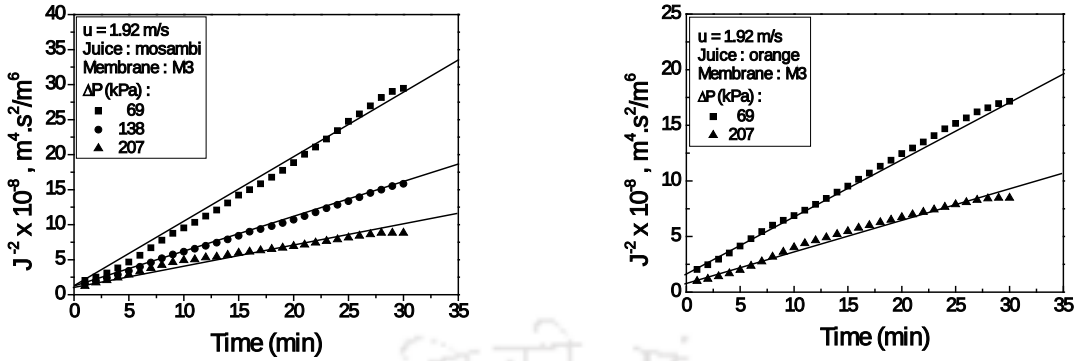

Figure 6.4: Fitness plots for cake filtration model to represent MF flux data obtained with ETCJ at u = 1.92 m/s: (a) M1 membrane, mosambi juice (b) M1 membrane, orange juice (c) M2 membrane, mosambi juice (d) M2 membrane, orange juice (e) M3 membrane, mosambi juice (f) M3 membrane, orange juice.

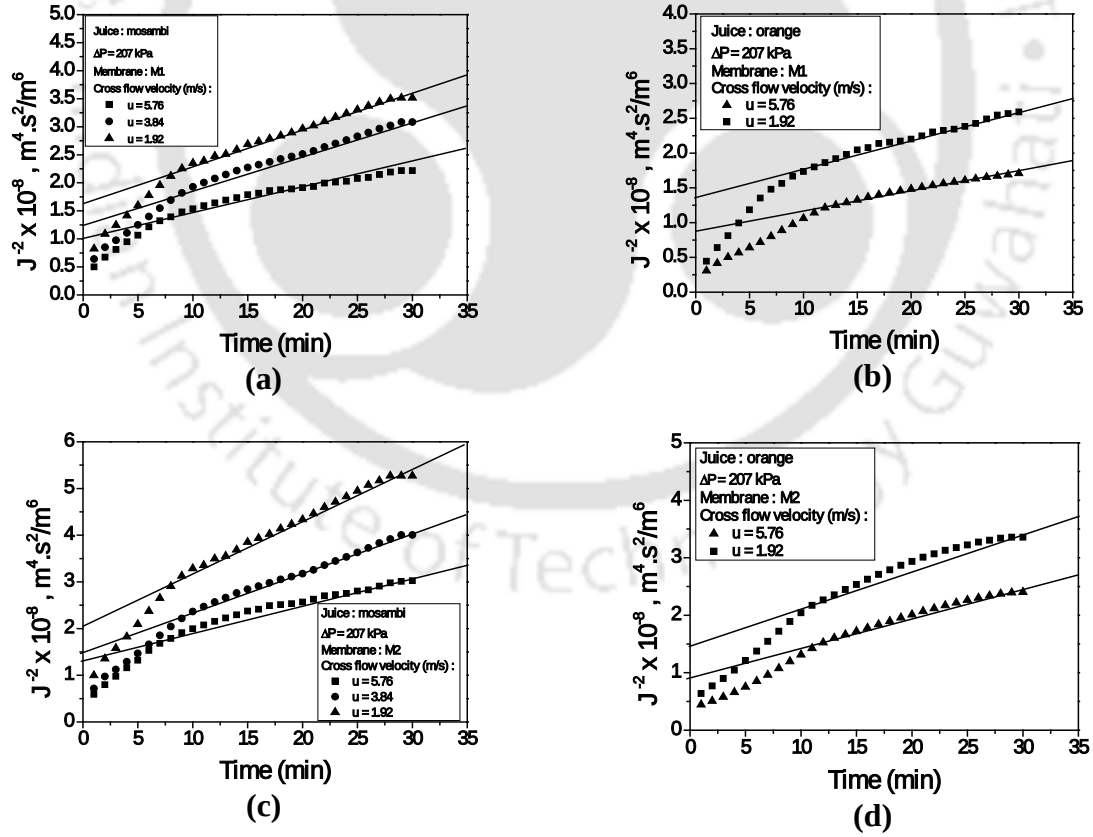

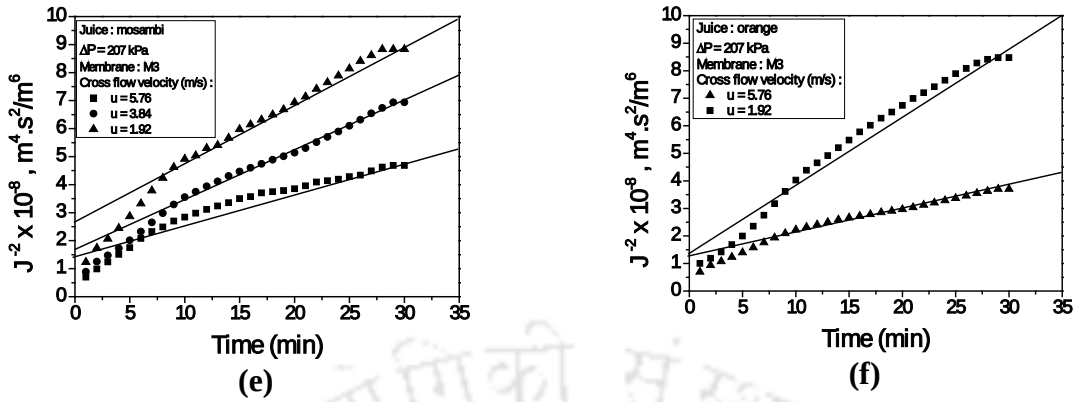

Figure 6.5: Fitness plots for cake filtration model to represent MF flux data obtained with ETCJ for various membranes at ΔP = 207 kPa: (a) M1 membrane, mosambi juice (b) M1 membrane, orange juice (c) M2 membrane, mosambi juice (d) M2 membrane, orange juice (e) M3 membrane, mosambi juice (f) M3 membrane, orange juice.

significant during the early stages of MF operation. This indicate that the early stages of MF for both mosambi and orange juice involves difficult to predict pore blocking phenomena. However, it has been also evaluated that the MF data obtained during the intial stages of operation can be modelled separately. Thus, it is apparent that the intial flux decline might be characterized with variant fouling model parameters and the later part of the flux decline could be represented by cake filtration model. For all cases, corresponding to the ΔP effect (at u = 1.92 m/s), cake filtration model can be observed to provide good fitness for the MF data measured between 10 to 30 minutes of the MF operation.

The cake filtration model fitness plots illustrating the effect of cross flow velocity at ΔP = 207 kPa are presented in Figure 6.5 (a – f). For all cases it can be observed that the cake filtration model failed to provide good fitness for the MF data measured during the intial 10 minutes MF operation. Thus, it is apparent that the intial membrane flux decline cannot be represented with the cake filtration model parameters obtained for the later stages of the MF operation.

Table 6.3: Regression coefficient (R^2) values for the fitness of various pore blocking models to represent cross flow MF of ETCJ (mosambi juice) using M3 membrane.

ΔP (kPa)	Cross flow velocity (m/s)	Complete pore blocking	Standard pore blocking	Intermediate pore blocking	Cake filtration
		R^2			
69	1.92	0.919	0.961	0.987	0.996
138	1.92	0.912	0.952	0.979	0.999
207	1.92	0.846	0.891	0.927	0.976
207	3.84	0.861	0.904	0.939	0.983
207	5.76	0.784	0.832	0.873	0.987

Once again, it is evident that the pore blocking phenomena during the intial stages of the MF are complex and combination fouling model can better represent the experimentally obtained MF flux decline data.

The regression coefficient value (R^2) for the fitness of various pore blocking models to represent the cross flow MF data of ETCJ mosambi for the M3 membrane are presented in Table 6.2. It can be observed that for very few cases R^2 value is close to 1 and in several cases poor fitness with R^2 value is in the range of 0.78 – 0.91 have been obtained. This is due to the

Table 6.4: Regression coefficient (R^2) values for the fitness of pore blocking models to represent MF flux data obtained for ETCJ (orange) juice and M1-M3 membranes.

Membrane Name	ΔP (kPa)	Cross flow velocity (m/s)	Complete pore blocking	Standard pore blocking	Intermediate pore blocking	Cake filtration
			R^2			
M1	69	1.92	0.784	0.822	0.856	0.912
	207	1.92	0.733	0.781	0.825	0.895
	69	5.76	0.810	0.842	0.870	0.915
	207	5.76	0.807	0.843	0.875	0.926
M2	69	1.92	0.883	0.922	0.952	0.988
	207	1.92	0.832	0.867	0.897	0.944
	69	5.76	0.892	0.923	0.948	0.983
	207	5.76	0.867	0.898	0.925	0.964
M3	69	1.92	0.921	0.955	0.979	0.998
	207	1.92	0.869	0.909	0.941	0.982
	69	5.76	0.900	0.932	0.958	0.989
	207	5.76	0.842	0.880	0.913	0.961

inability of the cake filtration model to represent the intial flux decline (1 – 10 minutes flux data). Similar R^2 values have been obtained for the fitness of pore blocking model to represent cross flow MF data of orange juice. These have been summarized in Table 6.3.

The RMS error for the fitness of cake filtration model to represent cross flow MF data obtained for M3 membrane and mosambi juice varied from 1.19 – 14.47 %. Significantly

Table 6.5: M3 membrane cake filtration model parameters for the representation of flux obtained during cross flow MF of (a) mosambi (ETCJ) and (b) orange juice (ETCJ) feed samples.

(a)

ΔP (kPa)	**Cross flow velocity (m/s)**	**$k_c \times 10^{-7}$ s.m^{-2}**	**$J_o^{-2} \times 10^{-8}$**
69	1.92	10.00	0.20
138	1.92	5.00	1.00
207	1.92	3.00	2.00
207	3.84	2.00	1.00
207	5.76	1.00	1.00

(b)

ΔP (kPa)	**Cross flow velocity (m/s)**	**$k_c \times 10^{-7}$ s.m^{-2}**	**$J_o^{-2} \times 10^{-8}$**
69	1.92	5.00	1.00
207	1.92	3.00	1.00
69	5.76	2.00	1.00
207	5.76	1.00	1.00

Table 6.6: Cake filtration model parameters for M1-M3 membranes at ΔP = 207 kPa and u = 1.92 m/s for (a) mosambi (ETCJ) and (b) orange juice (ETCJ) feed samples.

(a)

Membrane Name	Cake filtration		
	R^2	$J_o^{-2} \times 10^{-8}$	$k_c \times 10^{-7}$ s.m^{-2}
M1	0.941	1.00	0.80
M2	0.913	2.00	1.00
M3	0.976	2.00	3.00

(b)

Membrane Name	Cake filtration		
	R^2	$J_o^{-2} \times 10^{-8}$	$k_c \times 10^{-7}$ s.m^{-2}
M1	0.895	0.90	0.60
M2	0.944	0.90	1.00
M3	0.961	1.00	3.00

higher RMS values are due to the inability of the cake filtration model to represent the intial flux decline data (1 – 10 minutes). Similarily, high RMS error values ranging from 5.5 – 7.5 % have been obtained for the fitness of cake filtration model for the membrane orange juice cross flow MF data of M3 membrane.

For the M3 membrane, Table 6.5a and b respectively present the cake filtration model parameters for ETCJ mosambi and orange juice. It can be observed that for the mosambi case, the cake filtration constant reduced (10 – 3 × 10^7 s. m^{-2}) and J_o^{-2} increased (0.2 – 2 × 10^8)

with an increase ΔP from 69 to 207 kPa at u = 1.92 m/s. This is due to the enhancement in flux with ΔP. Also it can be analyzed that, at a ΔP of 207 kPa, k_c reduced ($3 - 1 \times 10^7$ s. m^{-2}) and J_o^{-2} reduced ($2 - 1 \times 10^8$) with an increase in u from 1.92 to 5.76 m/s. This is due to an increase in flux with increasing cross flow velocity.

Similarly, for orange juice ETCJ feed samples, at u = 1.92 m/s, the cake filtration constant reduced ($5 - 3 \times 10^7$ s.m^{-2}) and J_o^{-2} remained constant (1×10^8) for a variation in ΔP from 69 to 207 kPa. This is due to the enhancement in flux with ΔP. Also it can be analyzed that, at a ΔP of 207 kPa, for ETCJ orange juice feed samples, the cake filtration constant reduced ($3 - 1 \times 10^7$ s.m^{-2}) and J_o^{-2} increased ($1 - 2 \times 10^8$) for an increase in u from 1.92 to 5.76 m/s.

Similar variations in these parameters can be observed for variations in membrane morphology in Table 6.6 at a ΔP of 207 kPa and u of 1.92 m/s. It can be observed that for mosambi ETCJ feed juice, k_c increased ($0.8 - 3 \times 10^7$ s.m^{-2}) along with an increase in J_o^{-2} ($1 - 2 \times 10^8$) for a reduction in average membrane pore size from 1.69 (M1) to 0.72 μm (M3). However, for orange juice ETCJ feed samples, the corresponding variation in these

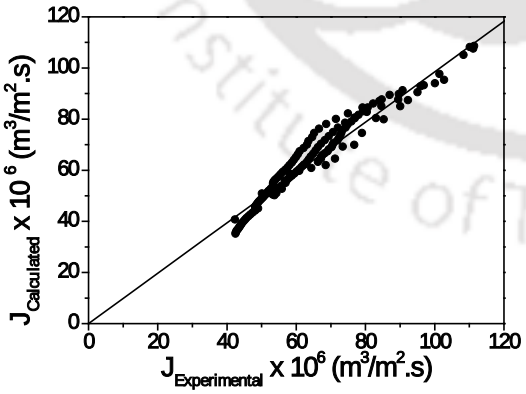

(a)

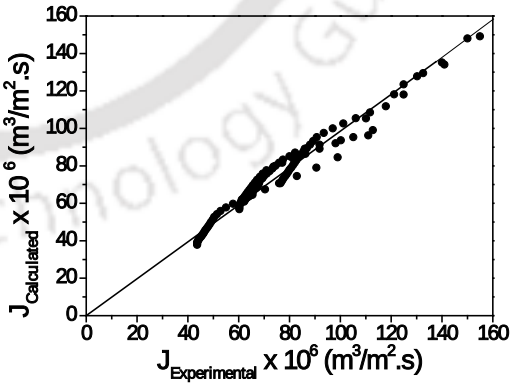

(b)

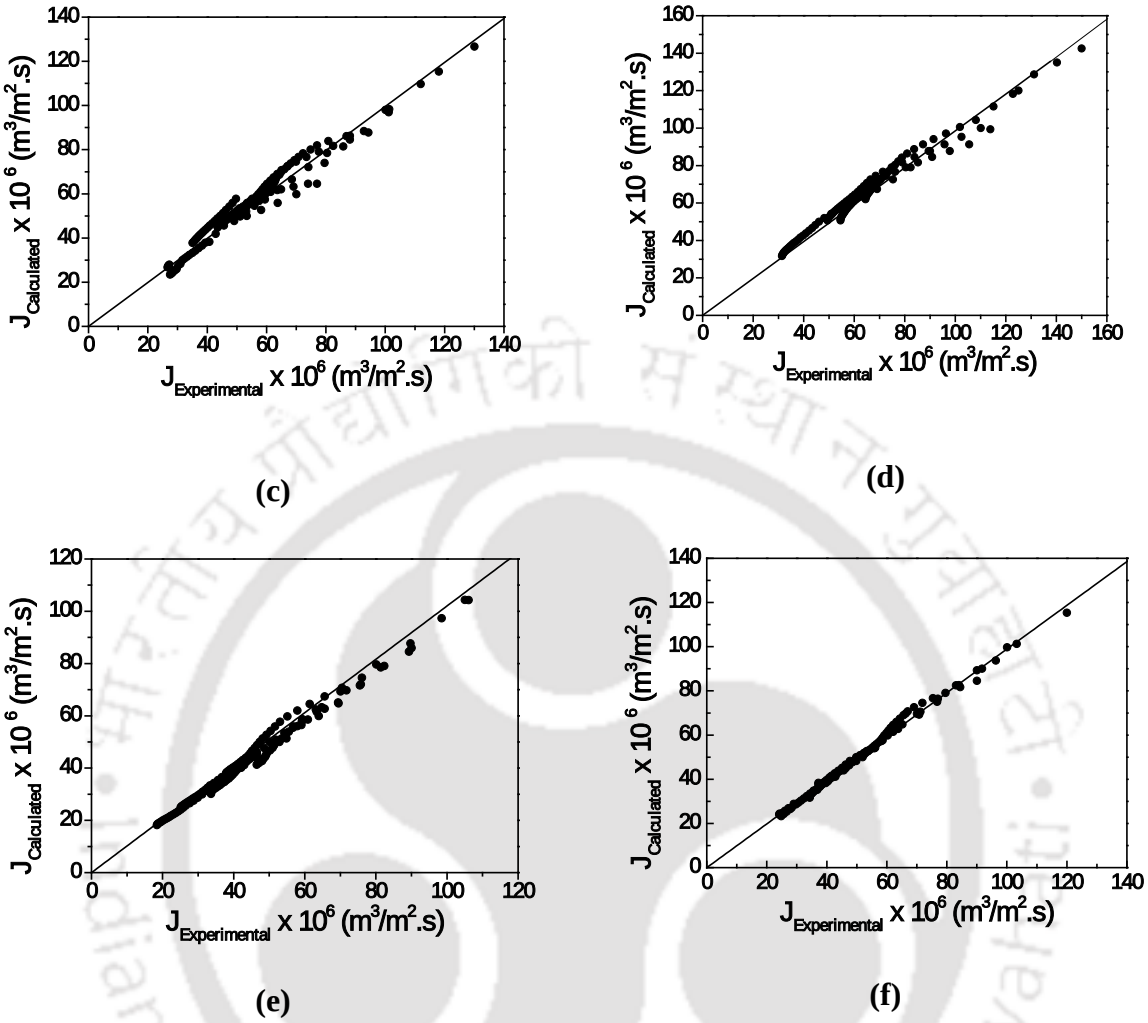

Figure 6.6: Parity plots for the fitness of cake filtration model to represent cross flow MF data obtained for ETCJ feed samples: (a) M1 membrane, mosambi juice (b) M1 membrane, orange juice (c) M2 membrane, mosambi juice (d) M2 membrane, orange juice (e) M3 membrane, mosambi juice (f) M3 membrane, orange juice.

parameters refers to an increase in k_c ($0.8 – 3 \times 10^7$ $s.m^{-2}$) along with an increase in J_o^{-2} ($0.6 – 3 \times 10^8$).

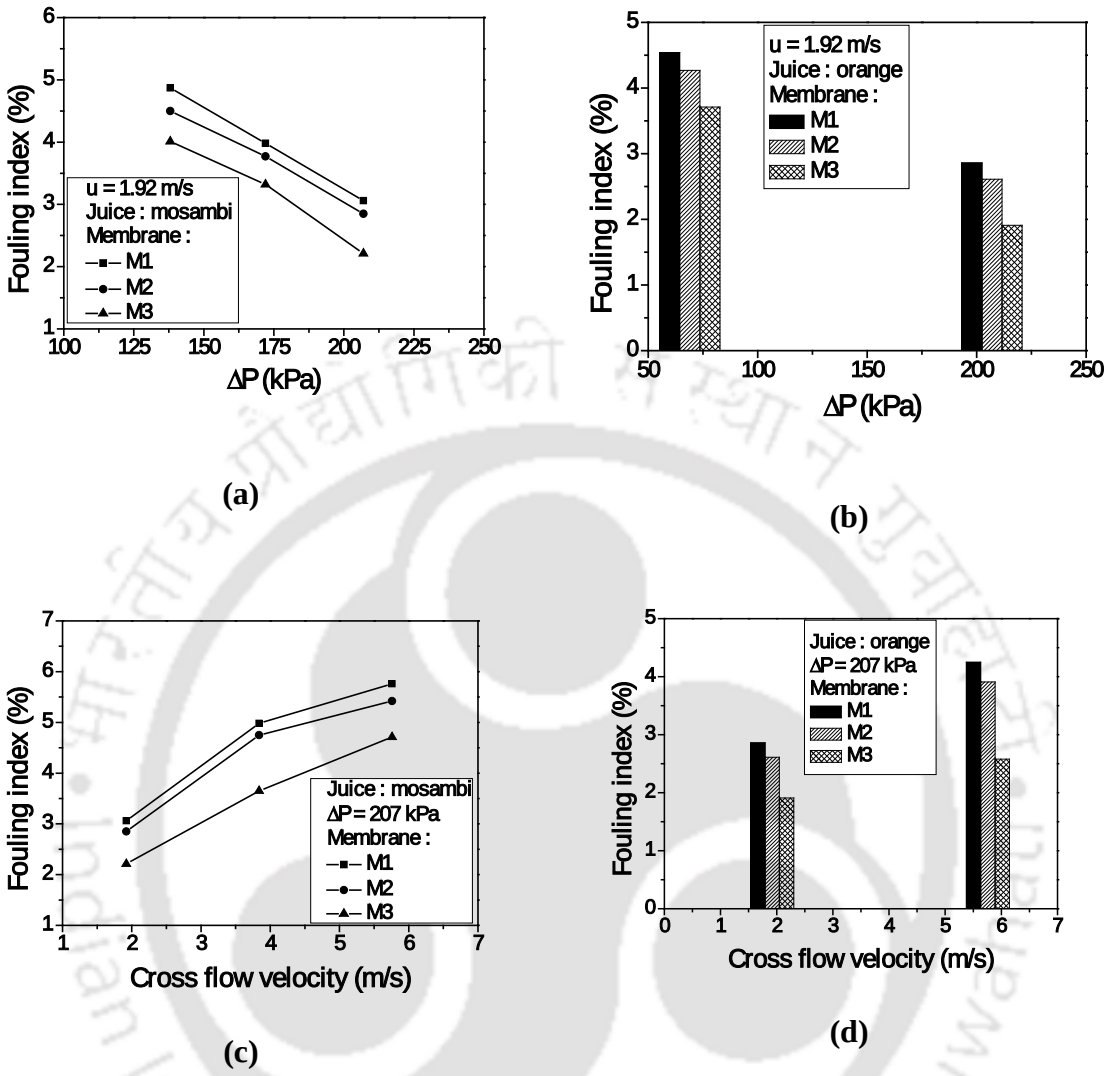

Figure 6.7: Fouling index variation with ΔP and u for ETCJ and M1 – M3 membranes: (a) Effect of ΔP for mosambi juice at u = 1.92 m/s (b) Effect of ΔP for orange juice at u = 1.92 m/s (c) Effect of u for mosambi juice at ΔP = 207 kPa (d) Effect of u for orange juice at ΔP = 207 kPa.

6.3.6 Parity plots for the fitness of cake filtration model

Figure 6.6 (a – f) presents the parity plots for the fitness of cake filtration model to represent the entire range of cross flow MF flux data. Except for Figure 6.6 (e – f), significant

deviation in parity exists for all other cases (Figure 6.6 a – d). The significant deviation in the parity for these cases is due to the inability of the cake filtration model to predict the intial flux decline (1– 10 minutes). It is opined that combination pore blocking models to represent intial (1 – 10 minutes) and later (11 – 30 minutes) flux decline data would give better parity. The parity fitness of cake filtration model, for membranes M1, M2 and M3 and ETCJ (mosambi) is about 6.46, 7.07 and 4.54 % respectively in terms of RMS error. Corresponding parity fitness for orange juice cross flow data is about 7.57, 3.84 and 3.72 % in terms of the RMS error. The overall RMS error for the entire data obtained for mosambi and orange juice MF are 6.12 and 4.77 % respectively.

6.3.7 Effect of operating parameters on fouling index

Figure 6.7 (a – d) present the effect of ΔP and u on the fouling index for the membranes M1 – M3 for mosambi and orange ETCJ feed samples. As shown in Figure 6.7 a and b, the fouling index reduced with increasing ΔP. For membranes M1 – M3 at u = 1.92 m/s and for ETCJ (mosambi) feed samples, the fouling index varied from 4.87 – 3.06, 4.5 – 2.85 and 4.01 – 2.21 % respectively for an increase ΔP from 138 – 207 kPa. Corresponding fouling index variation for orange juice feed samples varied from 4.54 – 2.86, 4.27 – 2.61 and 3.71 – 1.61 % for membranes M1, M2 and M3 respectively. It can be also observed that the membrane fouling index reduced with reducing average membrane pore size. Thus a ΔP of 207 kPa and membrane M3 provided lowest fouling index values. The reduction in fouling index with ΔP is possibly due to the dominance of cake filtration (on the membrane surface) but not internal membrane pore blocking at higher ΔP. In summary, the lower fouling index values obtained for all the membrane is promising for industrial scale clarification of

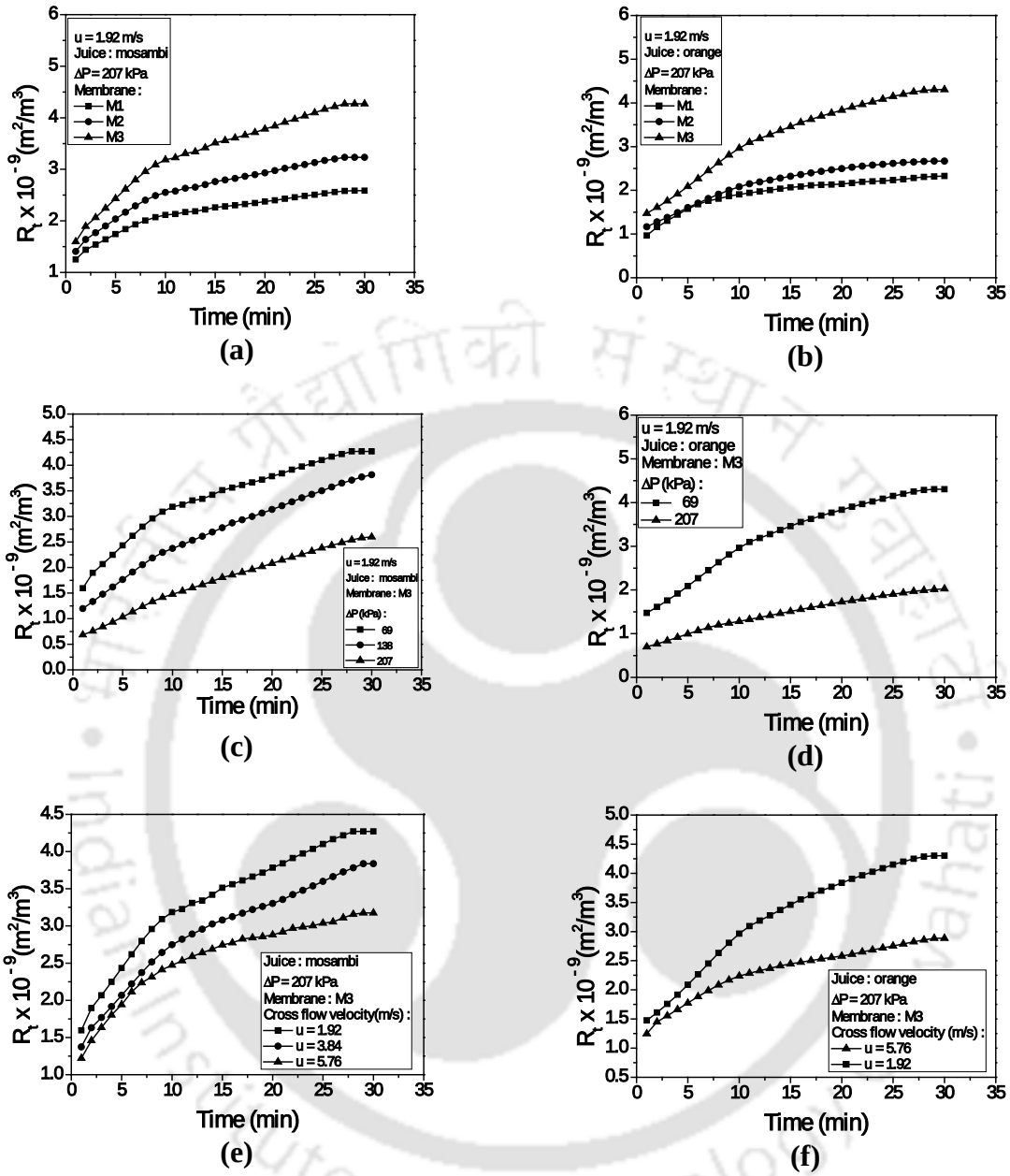

Figure 6.8: Time dependent R_t (total resistance) plots for various cases using ETCJ feed samples: (a) mosambi juice, u = 1.92 m/s and ΔP = 207 kPa (b) orange juice, u = 1.92 m/s and ΔP = 207 kPa (c) mosambi juice, u = 1.92 m/s and membrane M3 (d) orange juice, u = 1.92 m/s and M3 membrane (e) mosambi juice, ΔP = 207 kPa and M3 membrane (f) orange juice, ΔP = 207 kPa and M3 membrane.

mosambi and orange juices. In this regard it is important to note that the enzyme treatment is very important to reduce the fouling index and increase the shelf life of the membranes. On the other hand, the membrane fouling index increased with increasing cross flow velocity for both mosambi ETCJ (Figure 6.7 c) and orange ETCJ (Figure 6.7 d). For mosambi ETCJ feed samples at ΔP of 207 kPa, the membrane fouling index increased from 3.06 – 5.76, 2.85 – 5.42 and 2.21 – 4.71 % with an increase in cross flow velocity from 1.92 – 5.76 m/s for membranes M1, M2 and M3 respectively. Corresponding fouling indices for orange ETCJ feed samples increased from 2.86 – 4.25, 2.61 – 3.91 and 1.91 – 2.58 % with an increasing cross flow velocity from 1.92 – 5.76 m/s for membranes M1, M2 and M3 respectively.

An increase in fouling index with an increase in cross flow velocity is due to an enhancement in pore blocking at higher circulation rates. Typically, higher circulation rates reduce fouling index. However, since the membranes possessed wider pore size distributions, the cross flow velocity effect is adverse. Achieving the lower fouling index at lower cross flow velocity is beneficial from an operational perspective, given the fact that higher circulation rates enhance operating cost.

6.3.8 Effect of operating parameters on time dependent total permeation resistance

The pertinent MF flux decline data has also been modelled using the resistances in series model. The variation in total resistance (R_t) with time has been presented for various cases in Figure 6.8 (a – f). It can be observed that R_t increased with time for all cases. Also R_t values have been evaluated to be highest for lower membrane pore size (M3), lower ΔP (69 kPa) and lower cross flow velocity (1.92 m/s). The R_t values varied from 1.26 – 2.59,

1.41 – 3.24 and 1.6 – 4.27 × 10^9 m^2/m^3 (Figure 6.8 a) for M1, M2 and M3 membranes respectively for ETCJ mosambi feed samples at ΔP = 207 kPa and u = 1.92 m/s. Corresponding values for orange juice samples varied from 0.97 – 2.33, 1.17 – 2.67 and 1.48 – 4.31 × 10^9 m^2/m^3 (Figure 6.8 b) for M1, M2 and M3 respectively. With increasing ΔP from 69 to 207 kPa, for the M3 membrane at u = 1.92 m/s and ETCJ mosambi juice, R_t values decreased from 1.6 – 4.27 to 0.69 – 2.60 × 10^9 m^2/m^3 (Figure 6.8 c). Corresponding reduction in R_t for orange juice is from 4.31 – 2.89 × 10^9 m^2/m^3 (Figure 6.8 d). With an increase in cross flow velocity from 1.92 to 5.76 m/s, at ΔP for 207 kPa for M3 membrane for ETCJ mosambi, the R_t reduced from 1.6 – 4.27 to 1.23 – 3.18 × 10^9 m^2/m^3 (Figure 6.8 e). Corresponding variation in R_t for orange juice samples refers to a variation from 2.33 – 4.31 × 10^9 m^2/m^3 (Figure 6.8 f). In summary, R_t values for the membranes have been evaluated to be in the order of 1.25 – 4.25 × 10^9 m^2/m^3. An analysis has been carried out to evaluate the contribution of various resistances (R_m, R_r and R_i) to the overall resistance R_f for the cross flow data obtained for mosambi and orange juices. It has been evaluated that for all cases the ratio of $\frac{R_r}{R_t}$ is about 99.2 – 99.99%. This indicates that the total permeation resistance (R_t) is dominated with reversible fouling resistance (R_r).

Also, it can be observed that R_m and R_i are significantly lower than the R_t (or R_r). This is due to very low fouling index evaluated after cross flow MF. Thus, the overall permeation resistance during the cross flow operation has been fully dominated by the reversible fouling resistance (R_r). In this regard it should be noted that adsorption, concentration polarization and gel or cake layer resistances only contribute to the overall permeation resistance. This was not the case for data reported by Pagliero et al. [54] who have indicated that significant R_i

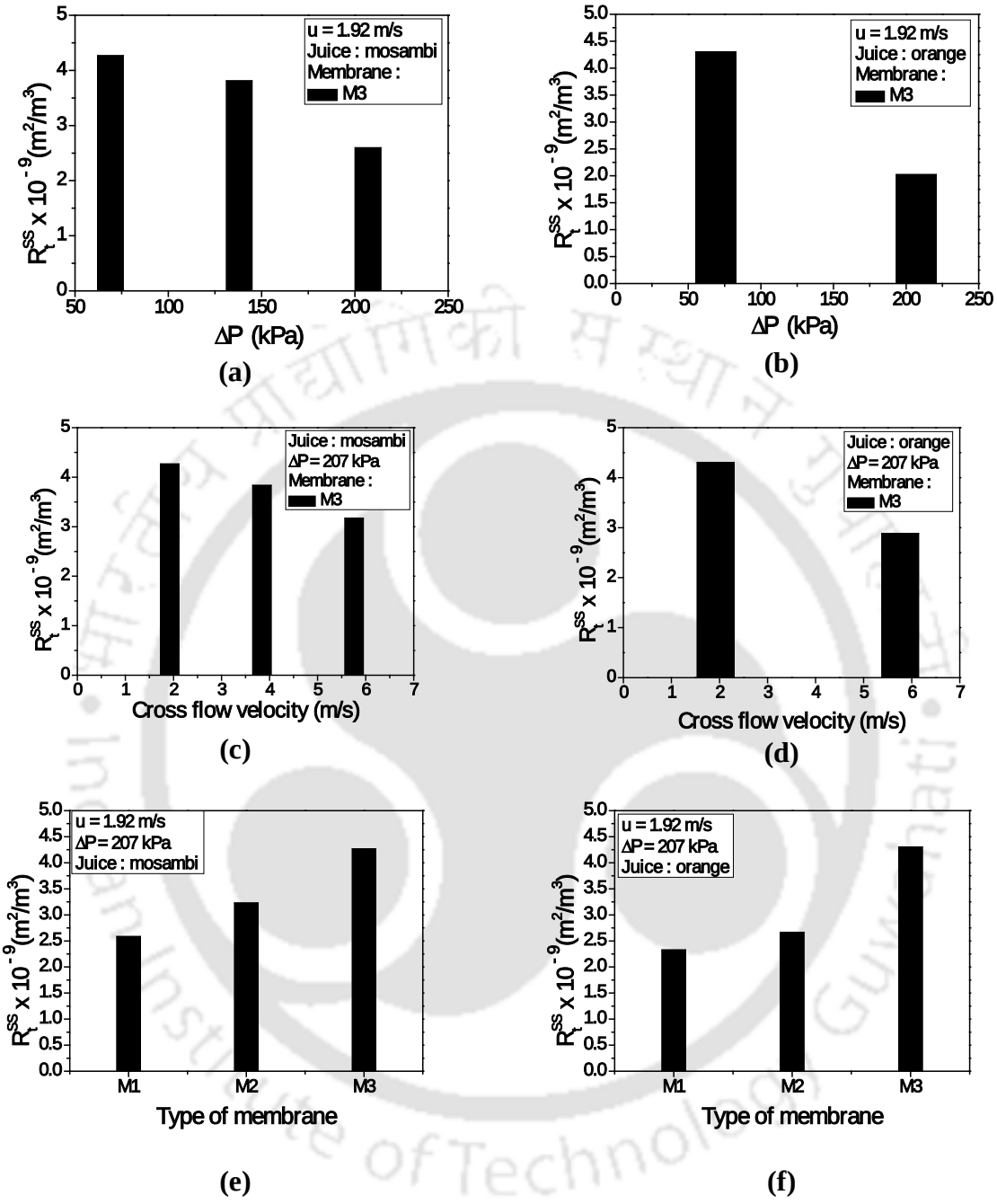

Figure 6.9: Variation of R_t^{SS} (steady state total resistance) with ΔP, u and membrane type for various cases: (a-b) Effect of ΔP for mosambi juice and orange juice respectively for membrane M3 at u = 1.92 m/s (c-d) Effect of u for mosambi juice and orange juice respectively for membrane M3 at ΔP = 207 kPa (e-f) Effect of membrane type for mosambi and orange juice respectively at u = 1.92 m/s and ΔP = 207 kPa.

(22.2 – 30.98 % of R_t) values exists during the cross flow MF of sieved orange juice. Also, the authors reported an R_t of 5.8 – 11.6 × 10^{12} m^2/m^3 which is significantly higher than the R_t values obtained in this work for orange juice clarification. This is due to the enzyme treatment followed by centrifugation which has been documented earlier (Nandi *et al.* [40]) to be effective to reduce membrane fouling and increase membrane flux.

6.3.9 Effect of operating parameters on steady state total permeation resistance

The effect of operating parameters (ΔP and u), membrane choice and juice on the steady state total resistance (R_t^{SS}) has been presented in Figure 6.9 (a – f). At u = 1.92 m/s, for M3 membrane and mosambi juice, the R_t^{SS} reduced from 4.27 – 2.60 × 10^9 m^2/m^3 (Figure 6.9 a) with an increase in ΔP from 69 to 207 kPa. Corresponding reduction in R_t^{SS} for orange juice is from 4.31 – 2.03 × 10^9 m^2/m^3 (Figure 6.9 b). These reductions corresponding to 40 and 53 % for mosambi and orange juice respectively. Similarily for the M3 membrane at ΔP = 207 kPa and mosambi juice, the R_t^{SS} reduced from 4.27 – 3.18 × 10^9 m^2/m^3 (Figure 6.9 c) with an increase in cross flow velocity from 1.92 to 5.76 m/s. Corresponding reduction in R_t^{SS} for orange juice is from 4.27 – 2.89 × 10^9 m^2/m^3 (Figure 6.9 d). These reductions correspond to about 26 and 33 % for an increase in cross flow velocity for mosambi and orange juice respectively. At ΔP = 207 kPa and u = 1.92 m/s, for mosambi juice, the R_t^{SS} increased from 2.59 to 4.27 × 10^9 m^2/m^3 for a reduction in average membrane pore size from 1.69 (M1) to 0.72 µm (M3). Corresponding variation in R_t^{SS} for orange juice refers to an increase from 2.33 – 4.31 × 10^9 m^2/m^3.

Table 6.7: Physico-chemical properties of (a) mosambi and (b) orange juice (ETCJ) feed samples considered for cross flow MF.

(a)

Membrane Name	Colour (A_{420})	Clarity (% T_{660})	TSS (^oBrix)	Citric acid (wt %)	pH	Density (g/cm^3)	Viscosity (mPa. S)	AIS (wt %)	Vitamin C (mg/100 ml)
M1	0.551 – 0.576	66.41 – 66.86	9.2	0.85	3.89	1.08	1.54 – 1.58	0.23 – 0.24	23.31 – 23.65
M2	0.582 – 0.608	71.605 – 71.655	9.2	0.84	3.93	1.08	1.52 – 1.56	0.22 – 0.23	23.21 – 23.59
M3	0.604 – 0.638	75.620 – 75.695	9.1	0.83	3.96	1.07 – 1.08	1.50 – 1.54	0.21 – 0.22	23.16 – 23.54

(b)

Membrane Name	Colour (A_{420})	Clarity (% T_{660})	TSS (^oBrix)	Citric acid (wt %)	pH	Density (g/cm^3)	Viscosity (mPa. S)	AIS (wt %)	Vitamin C (mg/100 ml)
M1	0.378 – 0.398	61.65 – 61.85	11.8	0.52	4.05	1.05	1.48 – 1.50	0.20 – 0.21	41.48 – 41.85
M2	0.405 – 0.415	63.45 – 64.75	11.8	0.51	4.05	1.05	1.46 – 1.47	0.19 – 0.20	41.42 – 41.78
M3	0.447 – 0.455	68.08 – 68.38	11.8	0.49	4.05	1.05	1.44 – 1.45	0.17 – 0.18	41.32 – 41.65

Table 6.8: Physico - chemical properties of (a) mosambi and (b) orange juice (ETCJ) permeate samples obtained during cross flow MF for M1 – M3 membranes.

(a)

Membrane Name	Colour (A_{420})	Clarity (% T_{660})	TSS (^oBrix)	Citric acid (wt %)	pH	Density (g/cm^3)	Viscosity (mPa. S)	AIS (wt %)	Vitamin C (mg/100 ml)
M1	0.0278 – 0.0328	97.654 – 98.047	9.1	0.80 – 0.82	3.90 – 3.94	1.06 – 1.07	1.48 – 1.50	Nil	22.23 – 22.65
M2	0.0308 – 0.0348	97.918 – 98.792	9.1	0.79 – 0.81	3.93 – 3.97	1.05	1.45 – 1.47	Nil	22.17 – 22.58
M3	0.0327 – 0.0395	98.568 – 99.385	9 – 9.1	0.78 – 0.80	3.95 – 4.00	1.04	1.41 – 1.44	Nil	22.11 – 22.51

(b)

Membrane Name	Colour (A_{420})	Clarity (% T_{660})	TSS (^oBrix)	Citric acid (wt %)	pH	Density (g/cm^3)	Viscosity (mPa. S)	AIS (wt %)	Vitamin C (mg/100 ml)
M1	0.054 – 0.095	91.58 – 94.76	11.6 – 11.7	0.49 – 0.50	4.10 – 4.12	1.03 – 1.04	1.42 – 1.43	Nil	35.49 – 35.85
M2	0.069 – 0.115	95.68 – 97.36	11.5 – 11.6	0.48 – 0.49	4.15 – 4.16	1.04	1.40 – 1.42	Nil	35.41 – 35.81
M3	0.098 – 0.138	97.08 – 99.27	11.3 – 11.4	0.48 – 0.49	4.17 – 4.20	1.04	1.38 – 1.41	Nil	35.36 – 35.77

6.3.10 Physico-chemical properties of feed and permeate samples

Table 6.6 a and b respectively present the physico – chemical properties of mosambi and orange ETCJ feed samples. It has been evaluated that for mosambi ETCJ feed samples, colour, clarity, TSS, citric acid, pH, density, viscosity, AIS and vitamin C are about 0.551 – 0.638, 66.41 – 75.695, 9.1 – 9.2, 0.83 – 0.85, 3.89 – 3.96, 1.07 – 1.08, 1.50 – 1.58, 0.21 – 0.24 and 23.16 – 23.65 respectively. Similarly for orange ETCJ feed samples, properties such as colour, clarity, TSS, citric acid, pH, density, viscosity, AIS and vitamin C are about 0.378 – 0.455, 61.65 – 68.38, 11.8, 0.49 – 0.52, 4.05, 1.05, 1.44 – 1.50, 0.17 – 0.21 and 41.32 – 41.85. Thus mosambi ETCJ feed samples have lower TSS, slightly lower pH and lower vitamin C content in comparison with the orange ETCJ feed samples. The objective of the MF operation is to minimize colour, clarity and AIS and achieve minimum variation in TSS, citric acid, pH, density, viscosity and vitamin C. Most important issue of the MF operation is to achieve negligible AIS content in the permeate and maximum citric acid and vitamin C content as these respectively represent pectin and nutrition content of the juice.

The physico – chemical properties of permeate samples for mosambi and orange ETCJ samples is presented Table 6.7 a and b respectively. The membranes provided desired combinations of physico – chemical properties for all cases. For mosambi and orange juice ETCJ permeate samples, colour reduced to 0.0278 – 0.0395 and 0.054 – 0.138 respectively. Corresponding variation in clarity refers to an increase in clarity to 97.654 – 99.385 and 91.58 – 99.27 respectively. The TSS, citric acid, pH, density, viscosity and vitamin C content remained fairly constant with respect to corresponding physico – chemical properties of the feed samples. The vitamin C and citric acid content of the permeate samples varied from 22.11 – 22.65 (mosambi), 35.36 – 35.85 (orange), 0.78 – 0.82 (mosambi) and 0.48 – 0.50

(orange) for permeate samples. Also, it can be noted that the AIS content in the permeate samples is negligible for all cases, which indicates negligible pectin content in the permeate samples and their long storage capability.

Conclusions and Scope of Future Work

This chapter summarizes the conclusions drawn from various chapters presented in this thesis. Also, some suggestions towards the scope for future research are also outlined.

7.1 Conclusions

This work dealt with the preparation, characterization and applications of inexpensive ceramic membranes. Morphological characterization studies including FESEM, TGA, XRD, liquid permeation studies, porosity measurement and finally acid base corrosion resistance have indicated that the prepared membranes possessed desired properties for MF applications. The prepared ceramic membranes were used for the treatment of oily wastewater and mosambi juice clarification. The prepared ceramic membranes provide higher membrane fluxes, adequate product quality and lower fouling. Morphological study by FESEM analysis, permeation characterization by water was carried out to evaluate the general characteristics of the membranes. Prepared membranes were used for batch and cross flow microfiltration of oil-water emulsions, mosambi and pine apple juices. The major conclusions obtained from this study are summarized below.

Dead end microfiltration of oil - water emulsions using low cost ceramic membranes prepared with uniaxial dry compaction method

1. It is observed that for a similar dry basis composition, uniaxial method provides wider pore size distribution and pore sizes in comparison with the membrane fabricated with the paste method. Thus it will be even more interesting to examine the role of wet

binding agents in altering the membrane morphology and pore size distributions and further experimentation.

2. The membranes fabricated using uniaxial dry compaction method at a fabrication pressure of 73 MPa with the chosen precursor formulation possessed an average pore size and porosity of 2.16 µm, and of 37.4 % respectively, and is the optimal choice to process 400 mg/L oil water emulsions.
3. The membrane provides a near steady state flux of 8×10^{-6} $m^3/m^2.s$ and a rejection of 97.9 % at a ΔP of 206.70 kPa at which minimal fouling index of 15.54 % is evaluated.
4. For all the membranes, combination model provides the best fitness in comparison with the most competent single pore blocking model. In summary, the membrane PM3 is promising for the treatment of oil water emulsion in the concentration range of 400 – 500 mg/L as a low cost ceramic membrane technology.

Cross flow microfiltration of oil-water emulsions using kaolin based low cost ceramic membranes

1. Membranes prepared with the uniaxial dry compaction method possessed higher combinations of average membrane pore size and porosity and all membranes upon cross flow microfiltration using oil water emulsions indicated that there existed significant pore blocking during the first 10 minutes of the experimental run. Thus, it is apparent that the prepared membranes do have the tendency to undergo irreversible fouling.
2. Optimal combinations of membrane morphology and operating parameters refers to the M3 membrane (with average membrane pore size and porosity of 2.16 µm and

37.4 % respectively) which provided a steady state flux and rejection of 22.14×10^{-6} $m^3/m^2.s$ and 98.52 % respectively along with a fouling index of 11.58 % at a ΔP of 207 kPa and Reynolds number (cross flow velocity) of 3417.

3. The fitness of various fouling models indicates that combination fouling models could only represent the observed flux decline data which refers to existence of one of the pore blocking phenomena (complete/intermediate/standard pore blocking) during the first 10 minutes of experimental run followed with cake filtration for the data obtained for later time periods.
4. The prepared low cost MF range ceramic membranes provided low fouling index during cross flow microfiltration, which indicates upon longer shelf life of the membrane and thus cost effective processing of industrial oil-water emulsions.
5. The experimental investigations were carried out using synthetic oil-in-water emulsions and hence the evaluated flux and rejection characteristics need not represent real time situations.
6. With real wastewater systems, the interaction of the multi-component feed with the membrane matrix could be significant and flux decline profiles could be quite different. Thus, in the near future, research shall target upon the treatment of real oily wastewater samples.

Preparation and characterization of low cost ceramic membranes for mosambi juice clarification in batch mode

1. For the first time, this work reported the fabrication of low cost ceramic membranes for juice clarification using uniaxial dry compaction method. It was observed that both mesh screen size (to obtain precursors with finer pore size) and fabrication pressure

significantly influenced the membrane morphological parameters and enabled the achievement of membranes that can be deployed for mosambi juice clarifications.

2. Several membrane characterization parameters such as hydraulic permeability and average pore diameter, porosity, chemical stability, FESEM, XRD, TGA and flexural strength are in agreement with those reported by Nandi *et al.* [4].
3. Amongst all membranes, M1 membrane provided maximum flux where as membrane M3 provided minimum fouling index for CJ and ETCJ. However, membrane M3 is recommended for further process engineering studies due to its higher mechanical strength, lower fouling and acceptable combinations of membrane flux and juice quality.
4. The prepared membranes possessed average pore size (based on FESEM) varying from 1.85 to 0.89 µm, hydraulic pore size varying from 1.69 to 0.72 µm, porosity ranging from 35.4 to 39.4 %, flexural strength ranging from 7.81 to 11 MPa. Amongst several membranes, the MF performance of M3 membrane (fabricated at 49 MPa) for mosambi juice is highly satisfactory. The M3 membrane provided a membrane flux of 90 to 44×10^{-6} $m^3/m^2.s$ at 206.7 kPa with a permeate juice quality of negligible AIS content for the enzyme treated centrifuged juice (ETCJ). Flux decline modelling analysis indicated that enzyme treatment followed by centrifugation minimizes irreversible fouling and is highly recommended before the MF.
5. The effect of pressure on the microfiltration studies for M3 membrane indicated that while flux was highly dependent on pressure, the juice quality was fairly independent of the applied pressure. Amongst CJ and ETCJ, ETCJ provided minimal fouling and clarified juice with negligible AIS content for all membranes.

6. Cake filtration has been identified to be the most competent fouling mechanism for membrane M3 operated at 206.7 kPa.

Flux decline analysis during microfiltration of pineapple juice using low cost ceramic membranes

1. For ETCJ, membrane M3 (average pore size and porosity of 0.72 µm and 39.4 %, respectively) provided optimal cross – flow microfiltration performance with a steady state flux of 53×10^{-6} $m^3/m^2.s$ at a ΔP and circulation rate of 207 kPa and 1 LPM, respectively for MF of pine apple juice.
2. Membrane M1 underwent significant fouling during both dead end and cross flow MF which infers that enhancing membrane pore size is detrimental to the shelf life of the membrane.
3. Using ETCJ feed samples, excellent separation characteristics were provided by the M3 membrane with negligible alcohol insoluble solids content in the permeate samples.
4. Both M1 and M3 membranes provided lowest fouling indices during cross flow MF using ETCJ but not CJ.
5. Amongst various fouling models, cake filtration provided the best fitness with an RMS error of 9.92 % and 6.32 % for dead end and cross flow MF, respectively.
6. For ETCJ, fouling indices have been reported to be lower than 5 – 6 % during cross flow MF which indicates the longer shelf life of the said membrane.
7. Finally, it can be concluded that the optimal performance of M3 membrane refers to higher transmembrane flux values and similar separation characteristics in comparison

with the literature data. In conclusion, prepared low cost ceramic membranes provide promising opportunities for pineapple juice microfiltration.

Cross flow microfiltration studies with mosambi and orange juices

1. The cross flow MF study using ETCJ Mosambi and Orange juice feed samples provided significant insights with respect to the effect of membrane and operating parameters on flux and separation factors. Among all membranes, membrane M3 provided lowest fouling index and this signifies that the membrane is less susceptible for internal fouling due to its lower average pore size.
2. For all experiments considered herein, the optimal cases correspond to a u = 1.92 m/s, ΔP = 207 kPa for membrane M3 where a steady state flux of 33.6×10^{-6} $m^3/m^2.s$ has been obtained. Similarly for ETCJ orange juice samples, for the membrane M3, the optimal case corresponds to u = 1.92 m/s, ΔP = 207 kPa where the steady state flux of 34.3×10^{-6} $m^3/m^2.s$ has been obtained.
3. All membranes provided excellent separation factors with respect to the complete removal of AIS (pectin), minimization of colour and clarity and maximum retention of TSS, Citric acid, pH, density, viscosity and vitamin C content.
4. The vitamin C and citric acid content of the permeate samples varied from 22.11 – 22.65 (mosambi), 35.36 – 35.85 (orange), 0.78 – 0.82 (mosambi) and 0.48 – 0.50 (orange) for permeate samples. Also it can be noted that the AIS content in the permeate samples is negligible for all cases, which indicates negligible pectin content in the permeate samples and their long storage capability.

5. The membranes provided desired combinations of physico – chemical properties for all cases. For mosambi and orange juice ETCJ permeate samples, colour reduced to 0.0278 – 0.0395 and 0.054 – 0.138 respectively. Corresponding variation in clarity refers to an increase in clarity to 97.654 – 99.385 and 91.58 – 99.27 respectively. The TSS, citric acid, pH, density, viscosity and vitamin C content remained fairly constant with respect to corresponding physico – chemical properties of the feed samples.
6. In summary, the membranes fabricated provided excellent performance characteristics towards the clarification of mosambi and orange juices. While the comparative performance with respect to dead end clarification is not significantly promising, the lower fouling indices obtained and the impact of operating parameters has been extremely useful to obtain good insights with respect to the microfiltration operation. The obtained results are promising for the large scale microfiltration based clarification of enzyme treated centrifuged citrus fruit juices.

From the perspective of thesis novelty, the following issues can be presented:

1. Identification of inorganic precursor formulation that enable the achievement of low cost ceramic membranes with wide and larger pore sizes (3.06 – 2.16 μm).
2. Higher combinations of cross flow MF flux and rejection for the large pore size membrane in comparision with literature at significantly higher feed concentration of o/w emulsions.
3. Identification of inorganic precursor formation to achieve ceramic membranes with micron range average pore size.

4. Higher combinations of flux and rejection for the micron range MF membrane during cross flow MF operation with ETCJ feed samples of pineapple, mosambi and orange juices.
5. Evaluation of fouling indices for the prepared low cost ceramic membranes which have confirmed upon their efficacy towards the treatment of oil-water emulsions and juice clarification.

In summary, the thesis outlines the efficacy of low cost ceramic membranes for the cross flow MF of o/w emulsions and fruit juices (pineapple/mosambi/orange). The obtained data is anticipated to serve as reference data for furthering research in the field of low cost ceramic membrane fabrication and application.

7.2 Recommendations for future work

Research findings in this work provided a good number of insights with respect to fabrication and applications of comparatively low cost ceramic and polymer ceramic composite membranes. Few research areas for future work are presented as follows:

Identification of efficient compositions to achieve sub-micron range MF membranes

1. In this work, using low cost ceramic precusors, an average pore size of about 100 – 200 nm could not be obtained. In many cases, higher pore size membranes underwent significant internal pore blocking. Therefore, in this regard, it will be interesting to identify compositions with low cost inorganic precursors to achieve sub-micron range (100 – 200 nm) microfiltration ceramic supports.

Preparation of tubular low cost inorganic membranes

1. Preparation and characterization of monochannel and multichannel tubular ceramic membranes using the identified compositions and extrusion method.
2. To evaluate the effect of extrusion process parameters and compositions on the morphology of tubular membranes.
3. To evaluate upon the role of binders and inorganic additives on the membrane morphological parameters.

Preparation of tubular polymer ceramic membranes using low cost precursors

1. Using dip coating and sol-gel methods, polymer-ceramic composite membranes can be fabricated with low cost precursors. Till date, while such studies are relevant for alumina supports, the utility of kaolin and other low cost ceramic supports needs to be examined thoroughly from the fabrication perspective of polymer-ceramic composite membranes.
2. Effect of dip coating and sol-gel process parameters on the structural and morphological optimality of asymmetric polymer ceramic membranes.

Microfiltration of oil water emulsions using tubular membranes

1. The efficacy of multi-channel tubular membranes for industrial oil-water emulsions need to be investigated in the context of process scale up and large scale processing scenarios. Further studies in this direction will further consolidate the applicability of low cost tubular ceramic microfiltration range membranes for industrial processing. Subsequently, the performance for industrial wastewaters shall be compared with

those obtained with simulated wastewater compositions that are often investigated in the laboratory.

2. Identification of optimal membrane morphology and process parameters for maximizing membrane performance and minimizing fouling performance.
3. Fouling studies with repetitive experimentation involving the sequential operations of microfiltration runs, membrane cleaning runs and hydraulic permeability evaluation tests.

Microfiltration of fruit juices using mono and multichannel ceramic membranes

1. The proximity of industrial scale applicability of low cost ceramic membranes can be furthered by examining their performance for the microfiltration of various fruit juices such as mosambi, orange, pineapple juices. Thus, in the near future, it is important to carry out microfiltration studies using fruit juices for mono and multichannel tubular ceramic microfiltration range membranes.
2. Fouling studies with repetitive experimentation involving the sequential operations of microfiltration runs, membrane cleaning runs and hydraulic permeability evaluation tests.

Ultrafiltration of fruit juices using polymer ceramic tubular membranes prepared with low cost ceramic supports

1. In the near future, ultrafiltration experiments can be conducted for polymer ceramic membranes that can be prepared with low cost ceramic supports. This will consolidate

the applicability of low cost ceramic supports for ultrafiltration processes associated to fruit juice clarification.

2. Fouling studies with repetitive experimentation involving the sequential operations of microfiltration runs, membrane cleaning runs and hydraulic permeability evaluation tests.

Nutrition tests and Microbial Tests

In this study, the nutrition content of the permeate samples and microbial tests of feed and permeate samples have not been carried out. These are extremely relevant for the further characterization of membrane processes and products prepared from membrane processes. Future work shall include such investigations to enhance the applicability of low cost ceramic membranes for microfiltration and ultrafiltration applications.

Rigorous Cost analysis

Furthering the conceptual cost analysis conducted in this work, a detailed cost analysis of membrane fabrication process and process cost of microfiltration and suggested ultrafiltration processes needs to be studied as well in the near future to precisely define the benchmarks associated to low cost ceramic membrane technology.

References

1. M. Mulder, Basic Principles of Membrane Technology, Kluwer Academic Publishers, Dordrecht, (1991).
2. A. J. Burggraaf and L. Cot, Fundamentals of Inorganic Membrane Science and Technology, Elsevier, Amsterdam, The Netherlands, (1996).
3. P. Monash and G. Pugazhenthi, Effect of TiO_2 addition on the fabrication of ceramic membrane supports: a study on the separation of oil droplets and bovine serum albumin (BSA) from its solution, Desalination, 279 (2011) 104 – 114.
4. P. Mittal, S. Jana, K. Mohanty, Synthesis of low-cost hydrophilic ceramic – polymeric composite membrane for treatment of oily wastewater, Desalination, 282 (2011) 54 – 62.
5. B. K. Nandi, R. Uppaluri, M. K. Purkait, Preparation and characterization of low cost ceramic membranes for micro filtration applications, Appl. Clay Sci., 42 (2008) 102 – 110.
6. B. K. Nandi, R. Uppaluri, M. K. Purkait, Treatment of oily waste water using low – cost ceramic membrane: Flux decline mechanism and economic feasibility, Sep. Sci. Technol., 44 (2009) 2840 – 2869.
7. D. Vasanth, R. Uppaluri, G. Pugazhenthi, Fabrication and Properties of low cost ceramic microfiltration membranes for separation of oil and bacteria from its solution, J. Membr. Sci., 379 (2011) 154 – 163.
8. D. Vasanth, R. Uppaluri, G. Pugazhenthi, Performance of low cost ceramic microfiltration membranes for the treatment of oil in water emulsions, Sep.

Sci. Technol., 48 (2013) 1 – 10.

9. B. K. Nandi, B. Das, R. Uppaluri, M. K. Purkait, Microfiltration of mosambi juice using low cost ceramic membrane, J. Food Eng., 95 (2009) 597 – 605.

10. D. Vasanth, R. Uppaluri, G. Pugazhenthi, Influence of sintering temperature on the properties of porous ceramic support prepared by uniaxial dry compaction method using low cost raw materials for membrane applications, Sep. Sci. Technol., 46 (2011) 1241 -1249.

11. D. Vasanth, R. Uppaluri, G. Pugazhenthi, Cross – flow microfiltration of oil – in - water emulsions using low cost ceramic membranes, Desalination, 320 (2013) 86 – 95.

12. D. Vasanth, R. Uppaluri, G. Pugazhenthi, Biomass assisted microfiltration chromium (VI) using backer's yeast by ceramic membrane prepared from low cost raw materials, Desalination, 285 (2012) 239 – 244.

13. F. L. Hua, Y. F. Tsang, Y. J. Wang, S. Y. Chan, H. Chu, S. N. Sin, Performance study of ceramic microfiltration membrane for oily wastewater treatment, Chem. Eng. J., 128 (2007) 169 – 175.

14. N. Saffaj, M. Persin, S. A. Younsi, A. Albizane, M. Cretin, A. Larbot, Removal of salts and dyes by low $ZnAl_2O_4 – TiO_2$ ultrafiltration membrane deposited on support made from clay, Sep. Purf. Technol., 47 (2005) 36 – 42.

15. M. R. Weir, E. Rutindeka, C. Detellier, C. Y. Feng, Q. Wang, T. Matsuura, R. Le Van Mao, Fabrication, characterization and preliminary testing of all inorganic ultrafiltration membranes composed entirely of a naturally occurring sepiolite clay mineral, J. Membr. Sci., 182 (2001) 41 – 50.

16. Y. Dong, S. Chen, X. Zhang, J. Yang, X. Liu, G. Meng, Fabrication and characterization of low cost tubular mineral based ceramic membranes for

microfiltration from natural zeolite, J. Membr. Sci., 281 (2006) 592 – 599.

17. M. Abbasi, M. Mirfendereski, M. Nikbakht, M. Golshenas, T. Mohammadi, Performance study of mullite and mullite – alumina ceramic MF membranes for oily wastewaters treatment, Desalination, 259 (2010) 169 – 178.

18. E. Sriharsha, R. Uppaluri, M. K. Purkait, Preparation and characterization of low cost ceramic membranes for mosambi juice clarification, Desalination, 317 (2013) 32 – 40.

19. J. Zhou, Q. Chang, Y. Wang, J. Wang, G. Meng, Separation of stable oil – water emulsion by the hydrophilic nano-sized ZrO_2 modified Al_2O_3 microfiltration membrane, Sep. Purf. Technol., 75 (2010) 243 – 248.

20. S. Abadi, M. Sebzari, M. Hemati, F. Rekabdar, T. Mohammadi, Ceramic membrane performance in microfiltration of oily wastewater, Desalination, 265 (2010) 222 – 228.

21. M. Abbasi, A. Salahi, M. Mirfendereski, T. Mohammadi, A. Pak, Dimensional analysis of permeation flux for microfiltration of oily wastewaters using mullite ceramic membranes, Desalination, 252 (2010) 113 – 119.

22. C. Psoch, B. Wendler, B. Goers, G. Wozny, B. Ruschel, Waste oil conditioning via microfiltration with ceramic membranes in crossflow, J. Membr. Sci., 245 (2004) 113 – 121.

23. R. Del Colle, C. A. Fortulan, S. R. Fontes, Manufacture of ceramic membranes for application in demulsification process for cross - flow microfiltration, Desalination, 245 (2009) 527 – 532.

24. V. Singh, M. K. Purkait, C. Das, Cross – flow microfiltration of industrial oily wastewater: experimental and theoretical consideration, Sep. Sci. Technol., 46 (2011) 1213 – 1223.

25. J. M. Foght, D. L. Gutnick and D. W. S. Westlake, Effect of emulsion on biodegradation of crude oil by pure and mixed bacterial cultures, Appl. Environ. Microbiol., 55 (1989) 36 – 42.

26. P. Canizares, F. Martinez, C. Jimenez, C. Saez, M. Rodrigo, Coagulation and electro coagulation of oil- in – water emulsions, J. Hazard. Mater., 151 (2008) 44 – 51.

27. L. J. Stack, P. A. Carney, H. B. Malone, T. K. Wessels, Factors influencing the ultrasonic separation of oil – in – water emulsions, Ultrason. Sonochem., 12 (2005) 153 – 160.

28. Regulations for all effluent guidelines and standards, United States Environmental Protection Agency (USEPA), 40 CFR Ch.1, (2013)407.82.

29. B. Hu, K. Scott, Microfiltration of water in oil emulsions and evaluation of fouling mechanism, Chem. Eng. J., 136 (2008) 210 – 220.

30. B. Chakrabarty, A. K. Ghoshal, M. K. Purkait, Ultrafiltration of stable oil – in - water emulsion by polysulfone membrane, J. Membr. Sci., 325 (2008) 325 – 427.

31. E. Sriharsha, R. Uppaluri, M. K. Purkait, Microfiltration of oil – water emulsions using low cost ceramic membranes prepared with the uniaxial dry compaction method, Ceram. Int., 40 (2014) 1155 – 1164.

32. B. K. Nandi, R. Uppaluri, M. K. Purkait, Identification of optimal membrane morphological parameters during microfiltration of mosambi juice using low cost ceramic membranes, LWT – Food Sci. Technol., 44 (2011) 214 – 223.

33. P. Rai, G. C. Majumder, G. Sharma, S. Das Gupta, S. De, Effect of various pretreatment methods on permeate flux and quality during filtration of mosambi juice, J. Food Eng., 78 (2007) 561 – 568.

34. P. Rai, G. C. Majumder, G. Sharma, S. Das Gupta, S. De, Effect of various cut – off membranes on permeate flux and quality during filtration of mosambi (citrus sinesis (l.) Osbeck) juice, Food Bio. Pro., 84 (2006) 213 – 219.

35. V. Jegatheesan, D. D. Phong, L. Shu, R. Ben, Performance of ceramic micro – and ultrafiltration membranes treating limed and partially clarified sugar cane juice, J. Membr. Sci., 327 (2009) 69 –77.

36. F. Vaillant, A. M. Perez, O. Acosta, M. Dornier, Turbidity of pulpy fruit juice: A key factor for predicting cross – flow microfiltration performance, J. Membr. Sci., 325 (2008) 404 – 412.

37. B. J. Wang, T. C. Wei, Z. R. Yu, Effect of operating temperature on component distribution of West Indian cherry juice in a microfiltration system, LWT – Food Sci. Technol., 38 (2005) 683 – 689.

38. F. S. Gomes, P. A. Costa, M. B. D. Campos, R.V. Tonon, S. Couri, L. M. C. Cabral, Watermelon juice pretreatment with microfiltration process for obtaining lycopene, Int. J. Food Sci. Technol., 48 (2013) 601 – 608.

39. J. Zhang, A. Rahman, M. Atergul, Application of microfiltration sterilizing of ceramic membrane in hami melon juice, ShipinGongyeKeji 33 (2012) 243 – 245.

40. B. K. Nandi, B. Das, R. Uppaluri, Clarification of orange juice using ceramic membrane and evalution of fouling mechanism, J. Food Pro. Eng., 35 (2012) 403 – 423.

41. L. R. Fukumoto, P. Delaquis, B. Girard, Microfiltration and ultrafiltration ceramic membranes for apple juice clarification, J. Food Sci., 63 (1998) 845 – 850.

42. L. M. J. de carvalho, C. A. Bento da silva, A. P. T. R. Pierucci, Clarification of

pineapple juice (Ananascomosus, L. Merryl) by ultrafiltration and microfiltration: Physicochemical evalution of clarified juices, soft drink formulation and sensorial evalution, J. Agric. Food Chem., 46 (1998) 2185 – 2189.

43. R. Jiraratananon, D. Uttapap, C. Tangamornsuksun, Self – forming dynamic membrane for ultrafiltration of pineapple juice, J. Membr. Sci., 129 (1997) 135 – 143.

44. S. T. D. de Barros, C. M. G. Andrade, E. S. Mendes, L. Peres, Study of fouling mechanism in pineapple juice clarification by ultrafiltration, J. Membr. Sci., 215 (2003) 213 – 224.

45. S. I. Gassaye, A. Davin, M. M. Peuhot, B. Aim, Interet des techniques a membrane dans la production de just de freuitstropicaux (cas des jus clarifies dananas). Part A. Evolution des flux de filtration au cours du procede, Fruits, 46 (1991) 251 – 258.

46. A. Laorko, Z. Li, S. Tongchitpakdee, S. Chantachum, W. Youravong, Effect of membrane property and operating conditions on phytochemical properties and permeate flux during clarification of pineapple juice, J. Food Eng., 100 (2010) 514 – 521.

47. L. M. J. de Carvalho, I. M. de Castro, C. A. B. da Silva, A study of retention of sugars in the process of clarification of pineapple juice (*Ananascomosus*, L. Meril) by micro – and ultra – filtration, J. Food Eng., 87 (2008) 447 – 454.

48. Z. Ji, Y. He, G. Zhang, Treatment of wastewater during the production of reactive dyestuff using a spiral nanofiltration membrane system, Desalination, 201 (2006) 255 – 266.

49. R. N. Haneda, R. Ikegami, C. A. Fortulan, B. M. Purquerio, E. Longo, S. R.

Fontes, Microfiltration with chemistry treating of commercial membranes and microporous tubes for retention of bacteria E. Coli on processing of wastewater of dairy products, Desalination, 200 (2006) 313 – 315.

50. X. Tan, Z. Wang, B. Meng, X. Meng, K. Li, Pilot – scale production of oxygen from air using perovskite hollow fibre membranes, J.Membr. Sci., 352 (2010) 189 – 196.

51. A. P. Echavarria, V. Falguera, C. Torras, C. Berdun, J. Pagan, A. Ibarz, Ultrafiltraand reverse osmosis for clarification and concentration of fruit juices at pilot plant scale, LWT – Food Sci. Technol., 46 (2012) 189 – 195.

52. R. C. C. Domingues, A. A. Ramos, V. L. Cardoso, M. H. M. Reis, Microfiltration of passion fruit juice using hollow fibre membranes and evaluation of fouling mechanisms, J. Food Eng., 121 (2014) 73 – 79.

53. W. G. V. Filho, M. Dornier, M. P. Belleville, Tangential microfiltration of orange juice in bench pilot, Cienc. Tecnol. Aliment, Campinas, 23 (2003) 330 – 336.

54. C. Pagliero, N. A. Ochoa, J. Marchese, Orange juice clarification by microfiltration: effect of operational variables on membrane fouling, Lat. Am. Appl. Res. 41 (2011) 279 – 284.

55. M. Cheryan, Ultrafiltration and Microfiltration Handbook, Technomic Publishing Co. Inc. Lancaster, Pennsylvania, (1998).

56. J. Hermia, Constant pressure blocking filtration laws – Application to power – law non – newtonian fluids, Trans. Inst. Chem. Eng., 60 (1982) 183 – 187.

57. S. Tennison, Current hurdles in the commercial development of inorganic membrane reactors, Membrane technology, 2000 (2000) 4 – 9.

58. Novel Polymer Membrane Process for Pre-Combustion CO_2 Capture, NETL CO_2 capture technology Meeting, Membrane Technology and Research Inc., (2011).

59. L. J. Stack, P. A. Carney, H. B. Malone, T. K. Wessels, Factors influencing the ultrasonic separation of oil – in – water emulsions, Ultrason. Sonochem., 12 (2005) 153 – 160.

60. S. S. Nielsen, Vitamin C determination by indophenol method, Food Anal. Lab. manual (2010) 55 – 60.

Appendix A: Calibration Curve for the determination of oil-water emulsion concentration in permeate samples

The determination of oil-water emulsion concentration in the permeate samples is determined by first preparing a calibration curve. To do so, standard oil-water emulsions in the concentration range of 100 – 400 mg/L were prepared using Millipore water and specific amounts of crude oil and subjecting the mixture to undergo continuous sonication for about 15 h. The obtained crude oil emulsions with varied solution concentrations were analyzed for their absorbance using UV-Visible spectrophotometer at a wavelength of 235 nm. Subsequently, the obtained absorbance values were plotted with respect to variations in emulsion solution concentration. Figure A1 presents the obtained calibration curve in this regard. It can be observed that the absorbance varied linearly with variation in emulsion solution concentration. Thus, using the obtained calibration curve, the concentration of permeate samples obtained during MF of oil-water emulsions was evaluated by measuring its absorbance.

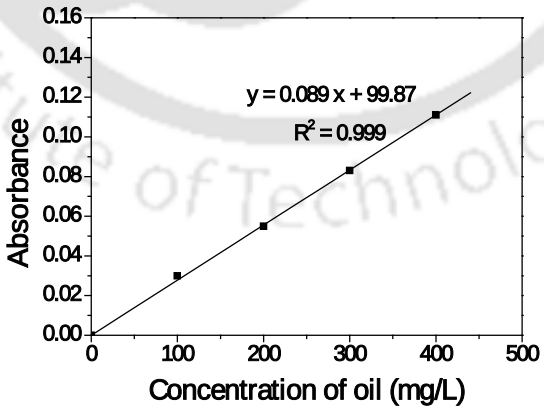

Figure A1: Calibration curve for the evaluation of oil-water emulsion concentration in permeate samples.

Appendix B: Error Analysis

Error analysis refers to the accuracy of the calculations and reliability of experimentally reported data. Despite carrying out experimental investigations with utmost care, systematic errors do occur during measurement of various parameters. Also, random errors arise due to variation in the successive measurements carried out by the experimentalist with nearly identical conditions of operating parameters.

The Ph.D. thesis involved the measurement of flux and separation characteristics for oil-water emulsions and juice clarification. The measurement maximum error for the estimation of solution concentration for oil-water emulsions is about 1.25 %. With such an error value, the maximum error in the estimation of oil-water rejection is about 0.2 %. Considering these variations in the experimental measurements, average rejection values have been reported throughout the thesis for the results reported for various oil-water emulsion related MF studies.

The maximum uncertainty in the measurement of permeate flux is about 0.8 – 1 %, which due to limitations of the instruments used (four digit precision for weighing balance and 2 digit precision for the stop watch).

For the clarification of juice samples, AIS measurements were carried out using gravimetric method. The maximum error in the estimation of AIS using gravimetric method is about 1%. Throughout the thesis, average AIS values have been reported for various feed and permeate samples. For Vitamin C content, the maximum error in its evaluation is about 1.01 %, which is due to the least count associated to the burette and measuring jar used.

International Journals:

1. E. Sriharsha, R. Uppaluri, M. K. Purkait, Preparation and characterization of low cost ceramic membranes for mosambi juice clarification, Desalination, 317 (2013) 32 - 40.
2. E. Sriharsha, R. Uppaluri, M.K. Purkait, Microfiltration of oil – water emulsions using low cost ceramic membranes prepared with uniaxial dry compaction method, Ceramic International, 40 (2014) 1155 - 1164.
3. E. Sriharsha, R. Uppaluri, M.K. Purkait, Cross flow microfiltration of oil – water emulsions using kaolin based low cost ceramic membranes, Desalination, 341 (2014) 61 - 71.

Manuscripts Communicated:

1. E. Sriharsha, R. Uppaluri, M. K. Purkait, Flux decline analysis during microfiltration of pineapple juice using low cost ceramic membranes, LWT - Food Sci. Technol., (under review, 2013).
2. E. Sriharsha, R. Uppaluri, M. K. Purkait, Cross flow microfiltration studies with Mosambi and orange juice (under preparation).

National Conference:

1. E. Sriharsha, R. Uppaluri, M.K.Purkait, “Cross flow microfiltration of crude oil in water emulsions using low cost ceramic membranes: Effect of fabrication pressure on membrane performance characteristics” Indian Chemical Engineering Congress (CHEMCON-2011), 27 – 30 December, 2011, Bangalore, India.